



TAMPEREEN TEKNILLINEN YLIOPISTO
TAMPERE UNIVERSITY OF TECHNOLOGY

Ville-Pekka Seppä
**Development and Clinical Application of
Impedance Pneumography Technique**



Julkaisu 1253 • Publication 1253

Tampereen teknillinen yliopisto. Julkaisu 1253
Tampere University of Technology. Publication 1253

Ville-Pekka Seppä

Development and Clinical Application of Impedance Pneumography Technique

Thesis for the degree of Doctor of Science in Technology to be presented with due permission for public examination and criticism in Rakennustalo Building, Auditorium RG202, at Tampere University of Technology, on the 27th of November 2014, at 12 noon.

Tampereen teknillinen yliopisto - Tampere University of Technology
Tampere 2014

ISBN 978-952-15-3388-4 (printed)
ISBN 978-952-15-3437-9 (PDF)
ISSN 1459-2045

Abstract

Assessment of the lung function is essential in the diagnosis and management of respiratory disease such as asthma. However, conventional spirometry requires difficult manoeuvres from the subject and is thus unsuitable for young children and infants. This renders the diagnosis of childhood asthma often qualitative, time-consuming and clinically challenging. However, information relating to the lung function can be derived from restful tidal breathing (TB) as well. Traditionally TB has been recorded in short intervals in laboratory conditions with obtrusive instrumentation using a face mask or a mouth piece. The principal aim of this thesis was to develop a noninvasive and convenient, yet highly accurate method for recording TB over extended time periods for clinical purposes, especially in young children.

The measurement methodology developed within this thesis is based on impedance pneumography (IP), where breathing is recorded through the respiratory variations of the electrical impedance of the thorax. This is established by placing four skin electrodes on the upper body and connecting them to a recording device. The main focus was in ensuring the accuracy of the IP-derived tidal flow recording as compared to direct measurement from the mouth. This was established by attenuating the distortive cardiac oscillations (CGO) of the impedance signal and by optimising the locations of the skin electrodes. The complete method was then validated in healthy adults during respiratory loading (n=17) and in preschool children with wheezing disorder (n=20).

The CGO attenuation was realised through an ensemble averaging based signal processing algorithm. The algorithm takes into account the respiratory modulation of the CGO waveform thus enabling efficient CGO attenuation while preserving the respiratory component of the signal unchanged. The newly proposed electrode configuration provides consistently more linear impedance to lung volume ratio than those previously established in the literature. The complete method integrating these developments provided highly accurate TB flow signal during normal and altered respiratory mechanics (loading) in adults and during induced bronchoconstriction in young children.

It may be concluded that in this thesis significant improvements were realised with the IP technique. These improvements were experimentally validated in two studies and the integrated system was found to consistently provide an accurate respiratory flow signal. The method may have clinical implications for the diagnosis of respiratory diseases especially in non-cooperative subjects, such as young children.

Acknowledgements

Firstly, I wish to thank professor Jari Hyttinen for offering me the first position in the department as an research assistant in 2006. At the time I had an option to take a basic engineering job, but now I could not be more happy for choosing research career.

I encountered professor Jari Viik first during a research project as a student. When Jari refused to accept my project report for the fourth time, I realised that he is serious about academic research and writing. Later as I steered more towards physiological measurement, I found myself consulting Jari more often. Jari has taught me the skills and tradition of academic work on many levels. Most importantly, however, I thank him for supporting me and believing in my success during times when I have faced research problems so tough that I have felt like there is no way forward.

For a biomedical engineer in my field, only clinicians can validate the relevance of a research idea. I wish to thank Pekka Malmberg, Mika Mäkelä, Anna Pelkonen, and Anne Kotaniemi-Syrjänen at HUCS Skin and Allergy Hospital, Helsinki for giving me the opportunity to take my work into clinical setting. It has been very motivating for me to work with highly dedicated, ambitious and skilled people and I wish our collaboration will be a long and prosperous one.

I have found innovative research work to be such a delicate flower that it can only flourish in optimal conditions. My wife, Mari, and our two sons, Jaakko and Hannu, have provided me with wonderful counterbalance from research and reminded me that there is more to life than work. It has also been important to me that Mari has shown interest in my work and, to my slight surprise, given comments that would be exceptionally insightful even from peers. Thank you for everything. I also wish to thank my parents and parents-in-law for supporting us in many ways.

Finally, I wish to express my gratitude to the pre-examiners, Kors van der Ent from Utrecht and Tapio Seppänen from Oulu, and to the instances who have financially supported my work. These include Finnish Cultural Foundation, Ella and Georg Ehrnrooth Foundation, Jalmari and Rauha Ahokas Foundation, Finnish Society of Allergology and Immunology, Tampere Tuberculosis Foundation, Instrumentarium Science Foundation, and Tekes.

Tampere, November 2014

A handwritten signature in blue ink, consisting of a stylized 'J' followed by a horizontal line that extends to the right and then curves downwards.

Contents

Abstract	iii
Acknowledgements	v
Contents	v
List of publications	ix
Author's contribution	x
Abbreviations	xi
Symbols	xiv
1 Introduction	1
2 Aims of the thesis	5
3 Background	7
3.1 Impedance pneumography	7
3.1.1 History	7
3.1.2 Bioimpedance basics	9
3.1.3 Origin of the respiratory impedance signal	12
3.1.4 Electrode locations	17
3.1.5 Deriving absolute measures of respired volume	18
3.1.6 Motion artefact rejection	19
3.1.7 Cardiogenic oscillations	20
3.2 Tidal breathing analysis	24
3.2.1 Quantification of tidal breathing	24
3.2.2 Physiological relevance of the tidal flow curve shape	28
3.2.3 Technical aspects of tidal breathing measurement	30
3.2.4 Cross-sectional and intervention studies on tidal breathing	33
3.2.5 Longitudinal studies in tidal breathing analysis	40
4 Materials and methods	43
4.1 Concept of flow measurement with impedance pneumography	44
4.2 Method for suppressing cardiogenic oscillations	44
4.3 Novel electrode placement strategy	45
4.4 Accuracy during respiratory loading	45

4.5	Accuracy in wheezy preschool children	45
5	Results	47
5.1	Concept of flow measurement with impedance pneumography	47
5.2	Method for suppressing cardiogenic oscillations	48
5.3	Novel electrode placement strategy	49
5.4	Accuracy during respiratory loading	50
5.5	Accuracy in wheezy preschool children	50
6	Discussion	53
6.1	Cardiogenic oscillations	53
6.1.1	Considerations on the proposed filtering algorithm	55
6.2	Linearity between lung volume and impedance	57
6.2.1	Considerations on achieving maximal linearity	57
6.2.2	Our findings on the linearity of impedance measurement	58
6.2.3	On comparing two measurement modalities	61
6.3	Clinical potential and feasibility	62
6.4	Limitations of the studies	63
7	Conclusions	65
	Bibliography	65
	Publications	85

List of publications

- I Seppä V.-P., Viik J., Hyttinen J. 2010. Assessment of pulmonary flow using impedance pneumography. *IEEE Transactions on Biomedical Engineering*, 57(9), 2277-2285.
- II Seppä, V.-P., Hyttinen, J., & Viik, J. 2011. A method for suppressing cardio-genic oscillations in impedance pneumography. *Physiological Measurement*, 32(3), 337–345.
- III Seppä, V.-P., Hyttinen, J., Uitto, M., Chrapek, W., & Viik, J. 2013. Novel electrode configuration for highly linear impedance pneumography. *Biomedizinische Technik (Berl)*, 58(1), 35–38.
- IV Seppä V.-P., Uitto M., Viik J. 2013. Tidal Breathing Flow-Volume Curves with Impedance Pneumography During Expiratory Loading. In: *Proceedings of the 35th Annual International IEEE EMBS Conference*, 2437-2440.
- V Seppä, V.-P., Pelkonen, A. S., Kotaniemi-Syrjänen, A., Mäkelä, M. J., Viik, J., & Malmberg, L. P. 2013. Tidal breathing flow measurement in awake young children by using impedance pneumography. *Journal of Applied Physiology*, 115(11), 1725–1731.

The permissions of the copyright holders of the original publications to reprint them in this thesis are hereby acknowledged.

Author's contribution

The author was the main author of all five publication of this thesis, although all named authors approved and made contributions to the writing.

In Publication I the author designed study protocol, conducted part of measurements, analysed measured signals and produced statistical analysis.

In Publication II the author designed and implemented the presented signal processing algorithm and a protocol to validate it. He conducted all measurements, analysed measured signals and produced statistical analysis.

In Publication III the author designed study protocol, conducted part of the measurements, and produced statistical analysis.

In Publication IV the author designed study protocol, analysed measured signals and produced statistical analysis.

In Publication V the author took part in designing study protocol, analysed measured signals and produced statistical analysis.

Abbreviations

AAA aortic arch anomaly

ATS American Thoracic Society

BD bronchodilation

BL baseline

BMI body mass index

BP bronchial provocation

BPD bronchopulmonary dysplasia

BRD bronchodilation

CF cystic fibrosis

CGO cardiogenic oscillation

CLD chronic lung disease

COPD chronic obstructive pulmonary disease

CPAP continuous positive airway pressure

DAAA double aortic arch anomaly

EA ensemble average

ECG electrocardiogram

EER extrathoracic expiratory resistance

EIP electromagnetic inductance plethysmography

EIT electrical impedance tomography

ERS European Respiratory Society

FRC functional residual capacity

FTT flow-through technique

FVC flow-volume curve

FVL flow-volume loop

FEV1 forced expired volume in one second

ICA independent component analysis

ICG impedance cardiography

ICS inhaled corticosteroid

ICU intensive care unit

IEEE Institute of Electrical and Electronics Engineers

IP impedance pneumography

LCI lung clearance index

LRI lower respiratory tract illness

MIB methacholine-induced bronchoconstriction

NASA National Aeronautics and Space Administration

NCPAP nasal continuous positive airway pressure

PEF peak expiratory flow

PNT pneumotachograph

PPV positive prediction value

RAAA right aortic arch anomaly

rBO recurrent bronchial obstruction

RIP respiratory inductive plethysmography

RR respiratory rate

RSV respiratory syncytial virus

RV residual volume

SAR signal to artefact ratio

SEM standard error of measurement

TB tidal breathing

TBFVL tidal breathing flow-volume loop

TD thoracic diameter

VCM vital capacity manoeuvre

Symbols

V	volume	L
\dot{V}	flow rate	L/s
U	voltage	V
I	current	A
Z	impedance	Ω
$\Delta Z/\Delta V$	ratio of lung volume change to impedance change	Ω/L
\mathbf{J}_{LE}	voltage lead field (for reciprocal current of 1)	$1/m^2$
\mathbf{J}_{LI}	current lead field (for current of 1)	$1/m^2$
σ	conductivity	$S/m = 1/(\Omega \bullet m)$
R^2	coefficient of the determination (linearity)	1
d_{\max}	maximal distance between curves	1
D_{SS}	absolute sample-by-sample difference between signals	1
D_L	absolute mean value of linearity bins between signals	1

Chapter 1

Introduction

Narrowing of the lower airways of the respiratory system is a common source of shortness of breath and a typical feature of diseases such as chronic obstructive pulmonary disease (COPD) and asthma. Conventionally, the narrowing, or obstruction, is assessed in a lung function laboratory with a spirometer. In spirometry the subject conducts a forced exhaling manoeuvre and the resulting air flow at the mouth is measured. There are, however, patient groups such as the elderly, disabled, intensive care patients and young children and infants who cannot adequately perform the required manoeuvres. For instance, the diagnosis of childhood asthma is often qualitative, time-consuming and difficult due to the limited methods for paediatric lung function assessment.

However, as it is intuitive, the air flow limitation in the lungs is also manifested in the tidal breathing (TB) air flow profile, not only in forced breathing. The measurement of TB is suitable for practically any patient regardless of age or condition. Considerable effort has been put into finding indices from the tidal air flow that would reliably tell about the presence or severity of airway obstruction. This has proven difficult, due to the multitude of mechanical, neurological, physiological, psychological and instrumentation-related factors that affect TB. Especially conventional measurement equipment using a mouthpiece or a face mask has been shown to alter respiratory control through increased dead space (Emralino & Steele, 1997) and facial nerve stimulus (Dolfin *et al.*, 1983). These problems and the cognitive factors could be removed if TB was measured at normal living conditions with noninvasive methods. Moreover, noninvasive equipment could allow TB measurement over extended periods of time, revealing the spontaneously occurring nocturnal obstruction of asthma (Greenberg & Cohen, 2012) and enable analysis of the fractal (Thamrin *et al.*, 2010a) and chaotic features of respiration (Teulier *et al.*, 2013) in a natural setting.

There is a wide selection of noninvasive respiration measurement instruments for research and clinical purposes. However, the techniques have been used for, and are usually only capable of, monitoring the respiratory rate (RR) or tidal volume instead of the respiratory air flow profile. This deficit in accuracy may be attributed to the measurement principle of most methods, which is based on assessing the movement of the chest wall. One of the earliest methods, impedance pneumography (IP), is, however, based on measuring the respiration-induced changes of electrical conductivity (or impedance) *within* the chest using electrodes placed on the skin surface.

Two of the earliest investigators to describe the phenomenon of respiration-induced impedance changes were Atzler & Lehmann (1932). They analysed the impedance variations of cardiac origin, cardiogenic oscillation (CGO), and discovered that respiration distorted their measurements. Nearly three decades later, the first paper to quantitatively describe the respiratory variation, IP, was published by Goldensohn & Zablow (1959). In their seminal work they presented two key concepts that have remained at the center of IP research. Firstly, the need to obtain a linear relationship between the lung volume and the measured impedance, and secondly, the need to attenuate the CGO.

Linearity between lung volume and impedance depends heavily on placement of the skin electrodes (Logic *et al.*, 1967). The general agreement has been that when the electrodes are placed on the sides of the thorax, a higher placement closer to the axilla yields a more linear relationship. There is evidence that this is because at higher location the impedance variations stem from variation in the lung tissue aeration, as desired, whereas in the lower locations other factors such as the movement of the diaphragm contribute to the signal (Kawakami *et al.*, 1974, Petro, 1969).

Attenuation of the CGO needs to be done efficiently, but without distorting the respiratory part of the impedance signal. This is difficult due to several features of the signals, most prominently their nonstationarity and overlap in the frequency spectrum. Several signal processing methods to decompose the respiratory and cardiac part have been proposed (Krivoshei *et al.*, 2008, Ouyang *et al.*, 1998, Pandey *et al.*, 2011), but thus far the results have been either unsatisfactory or lack proper clinical validation.

Finally, in order to provide the reader with an understanding of the phases and motivation of this thesis, an informal chronological outline of my work and studies is presented in Figure 1.1.

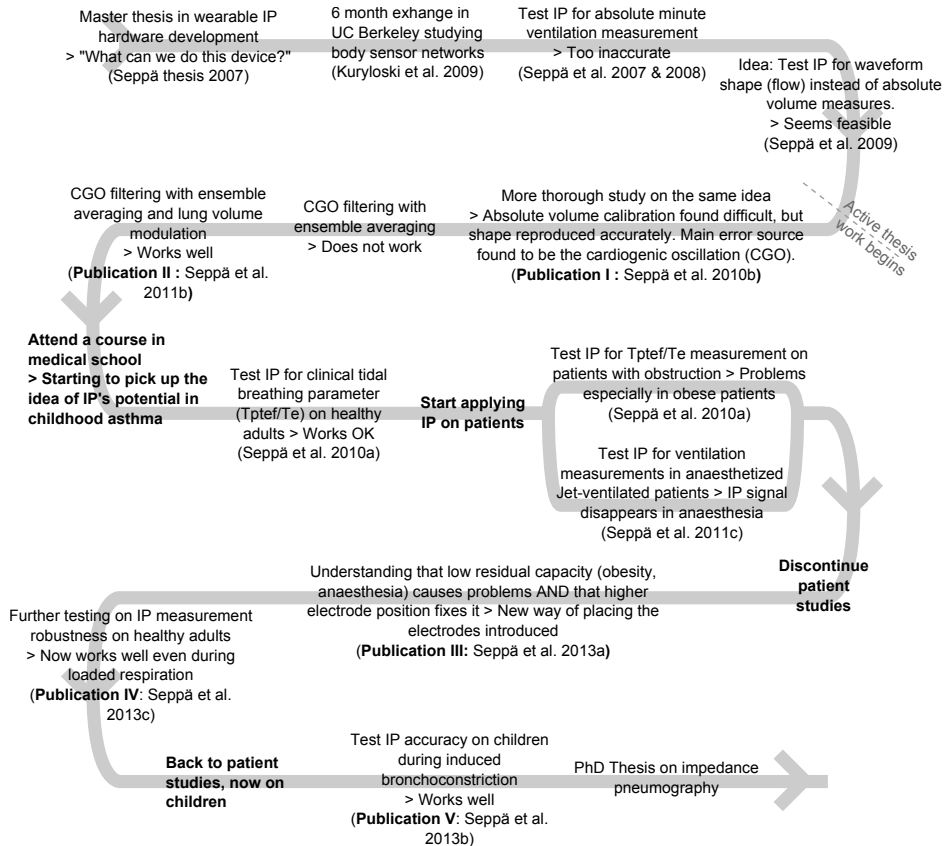


FIGURE 1.1: Informal outline on the research activities before and during the thesis work.

Chapter 2

Aims of the thesis

The general objective of this thesis was to develop and validate a highly accurate non-invasive respiration measurement technique based on IP.

The first part of the work focuses on the methodological development of IP, with the specific aims of

- demonstrating the concept of deriving respiratory flow signal from the IP measurement (I)
- developing a signal processing method that attenuates the CGO efficiently while presenting minimal distortion to the respiratory impedance signal (II)
- finding an optimal electrode placement strategy which results in a linear lung volume to impedance relationship (I, III)

Although some experimental test results were presented with each of the method development studies above, the latter part of the thesis presents a more rigorous clinical validation of the integrated measurement concept. The specific aims were

- to introduce the concept of deriving clinically relevant tidal breathing flow-volume loops (TBFVLs) and numeric TB parameters from the IP signal
- to assess the accuracy of IP in supine position during normal and altered respiration as induced by intense expiratory loading in healthy subjects (IV)
- to assess the accuracy of IP in preschool children with wheezing disorder during methacholine-induced bronchoconstriction (MIB) (V)

Chapter 3

Background

3.1 Impedance pneumography

In this section a short background and literature review on bioimpedance and IP is presented. Although the text touches on impedance cardiography (ICG), it mainly focuses on IP and does not cover other thoracic bioimpedance-based assessments such as electrical impedance tomography (EIT), other multielectrode IP measurements for ventilation distribution, thoracic fluid amount or body composition measurements. The referenced literature may seem rather old, but it is only because the majority of the most seminal work on IP was done in the 1960s and 70s and the research interest has declined since then.

3.1.1 History

Atzler & Lehmann (1932) investigated how cardiac activity induces changes in thoracic electrical impedance through a capacitive measurement (Figure 3.1). They noticed that respiration also changes impedance, but they did not investigate it further. Later, Nyboer (1959) found that the thoracic impedance signal recorded by skin electrodes followed that of a volume spirometer. Goldensohn & Zablow (1959) were the first to directly investigate the respiration associated impedance changes, but Geddes *et al.* (1962) soon realized its first practical application by enabling noninvasive respiratory monitoring and telemetry in National Aeronautics and Space Administration (NASA) astronauts.



FIGURE 3.1: Young subject in an early experimental ICG setup of Atzler & Lehmann (1932). Printed with permission from the publisher.

In an Institute of Electrical and Electronics Engineers (IEEE) History Center interview¹ in 2000, Geddes described his background with IP: *"Respiration was detected by the cooling of a heated thermistor on the microphone in the helmet when the astronaut exhaled. ... But there was a problem because the respiration signal was lost when the astronaut turned his head away from the microphone. At this point NASA contacted me and asked if I could devise a more reliable method of detecting respiration. On a Saturday afternoon at Baylor, I went into the lab, placed two electrodes across my chest at the xiphoid level and measured the 20 kHz impedance changes that occurred with respiration. The method was described later in Aerospace Medicine in 1962 and we used it in the medical student physiology laboratory; the method becomes known as impedance pneumography"*

In their pioneering paper, Goldensohn & Zablow (1959) raised the two important issues relating to IP that this thesis research tries to resolve. Firstly, how to remove the cardiogenic signal contribution without compromising the respiratory part, and secondly, the question of linearity between lung volume change ΔV and impedance change ΔZ . They implemented an electrocardiogram (ECG)-triggered electronic filter that was manually adjusted to subtract a waveform matching that of a cardiac oscillation at each heart

¹Leslie A. Geddes, an oral history conducted 13 October 2000 by Frederik Nebeker, IEEE History Center, Hoboken, NJ, U.S.A.

contraction. They also realized that when using a configuration where the electrodes are placed on the arms, the $\Delta Z/\Delta V$ ratio was not linear in all patients.

Currently, the only established clinical application of IP is respiratory rate monitoring in integrated intensive care unit (ICU) patient monitors.

3.1.2 Bioimpedance basics

Electrical impedance refers to the properties of a physical object that oppose (impede) the flow of electrical current through it. Bioimpedance refers to the electrical impedance of biological matter, such as living human tissues. The measurement of the bioimpedance of human tissues, organs or body parts gives information on their state or function. Bioimpedance measurement has attracted wide and long-lasting research interest because of its noninvasiveness and apparent simplicity.

Generally, the bioimpedance measurement is based on Ohm's law relating the imaginary quantities of impedance Z , current I and voltage U as $Z = U/I$. In practice, an alternating current is generated and led through the tissues by the measurement instrument while measuring the voltage generated by the current. The measurement instrument is connected to the tissues by electrodes, which are essentially transducers transforming the electron-carried current in the cables and electronics into a ion-carried one in the biological substance, and vice versa. Most measurement solutions feature two or four electrodes and are referred to as bipolar or tetrapolar, respectively. Regarding the current feeding, the most obvious and most used approach is to construct an electric circuit, a current source, that aims to provide as stable as possible current into the tissue. An example of such circuitry is the Howland current pump (Franco, 2002). However, depending on the application, the requirements for the stability of the current source under varying loads (impedances) may be rather strict and difficult to fulfil. Thus, an approach where the current source is actually a simpler voltage source and the generated current is measured, is gaining more of a foothold (Min *et al.*, 2012). Either way, the basic principle of $Z=U/I$ prevails.

Bioimpedance measurements can be divided into categories of frequency domain and time domain assessments. In the first one the current is fed at several different frequencies, often referred to as impedance spectroscopy. This can be realised by applying consecutively sinusoidal currents of different frequency or by feeding a composite signal consisting of several frequencies that is then decomposed by means of signal processing (Min *et al.*, 2012). In the bioimpedance context, impedance spectroscopy has been used in a variety of in vivo and in vitro applications such as stem cell growth (Onnela *et al.*, 2012), patient hydration status and body composition (Kyle *et al.*, 2004), biopsy needle

guiding through tissue type recognition (Mishra *et al.*, 2012), and wound healing monitoring (Kekonen, 2013). In the time domain, impedance is assessed at a single frequency but continuously over time in order to capture temporal impedance variations stemming from physiological functions. Modern instrumentation allows the combining of both domains (Min *et al.*, 2012) and also conducting multiple non-interfering bioimpedance measurements simultaneously in the same body (Gracia *et al.*, 2012), but their applications are still very few. Most efforts in the time domain have been directed towards ICG, where haemodynamic parameters such as stroke volume are determined from thoracic impedance signals (Woltjer *et al.*, 1997). The other main application of time domain impedance measurement is in assessing the respiration, impedance pneumography, as in this thesis. Both IP and ICG have been deployed in a wearable format as well in several projects (Ulbrich *et al.*, 2014, Vuorela *et al.*, 2010). According to the Thomson-Reuters Web of Science database as of 2014, there were more than ten times more indexed journal articles on impedance cardiography than on impedance pneumography (over 1800 vs. 140, respectively).

Defining the components that contribute to a measured impedance in an electronic circuit is rather unambiguous, whereas in a homogeneous biological volume conductor it is not. One cannot model the thorax as a series or parallel connected circuit consisting of the lungs, heart, bones, etc. Instead, in a volume conductor the current forms a distribution, a vector field, that is called the *lead field*. The current forms a spatial distribution that avoids any regions of higher impedance and favours ones of lower impedance. The same applies for the lead field of the voltage measurement according to the principle of reciprocity (Malmivuo & Plonsey, 1995). In fact, interchanging the current and the voltage lead fields has no effect on the measured impedance, apart from the effects that stem from non-idealities in the measurement instruments. As shown by Geselowitz (1971) and Lehr (1972), the current lead field \mathbf{J}_{LI} and the voltage lead field \mathbf{J}_{LE} combined form the *sensitivity field* \mathbf{S} of the impedance measurement as $\mathbf{S} = \mathbf{J}_{LE} \bullet \mathbf{J}_{LI}$. The measured impedance of a volume conductor V is thus obtained by integrating the inverse of conductivity σ and the product of the sensitivity field at each point within the volume as

$$Z = \int_V \frac{1}{\sigma} \mathbf{S} = \int_V \frac{1}{\sigma} \mathbf{J}_{LE} \bullet \mathbf{J}_{LI}.$$

It is worth noting that the lead fields are vector fields, whereas the sensitivity field is a scalar field.

There are important aspects to consider in how the lead fields interact to form the sensitivity field as their dot product. In a bipolar measurement, the current and the voltage are applied through the same pair of electrodes, which implies that their lead

fields are uniform and the sensitivity field (dot product of the lead fields) is always positive. In a tetrapolar setting the situation is not as straightforward. As illustrated in Figure 3.2 and Table 3.1, the sensitivity field may form areas of zero sensitivity and even negative sensitivity. In the areas of negative sensitivity an increase in impedance contributes as a decrease in the total measured impedance. In areas where the fields are perpendicular or only either field is present, the sensitivity is zero. However, this complexity of the tetrapolar measurement brings important advantages over the bipolar one. Firstly, it allows focusing the sensitivity field spatially in a more elegant way when used correctly. For instance, one may exclude the tissues close to the surface of the body. Secondly, perhaps as a more widely recognised feature, because the two lead fields do not meet in the connectors, cables, electrodes or electrode-tissue interfaces, these unwanted distortive components of the system will not contribute to the measured impedance.

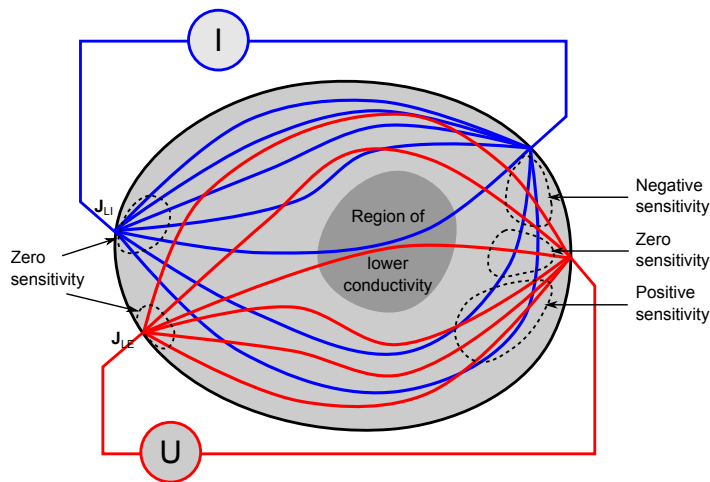


FIGURE 3.2: A tetrapolar bioimpedance measurement illustrating the paths of the current \mathbf{J}_{LI} and voltage \mathbf{J}_{LE} lead fields and example areas of negative, zero and positive measurement sensitivity (see Table 3.1).

TABLE 3.1: Effect of the angle of the current \mathbf{J}_{LI} and voltage \mathbf{J}_{LE} lead fields on the sensitivity field

Angle of \mathbf{J}_{LI} and \mathbf{J}_{LE}	Sensitivity
$< 90^\circ$	Negative
0°	Zero
$> 90^\circ$	Positive
Only other field present	Zero

3.1.3 Origin of the respiratory impedance signal

The thoracic impedance signal consists of a cardiac and a respiratory component (Figure 3.3). In order to acknowledge the benefits and limitations of IP, it is important to understand what creates the measured respiratory impedance signal. Unfortunately, an exact answer seems to elude the investigators, but there have been many notable attempts to shed light on the origins of the signal. A major question has been whether the respiratory impedance changes reflect only chest wall movement and thoracic expansion or whether they reflect the aeration of the lung tissue. The literature on this issue is discussed in the following.

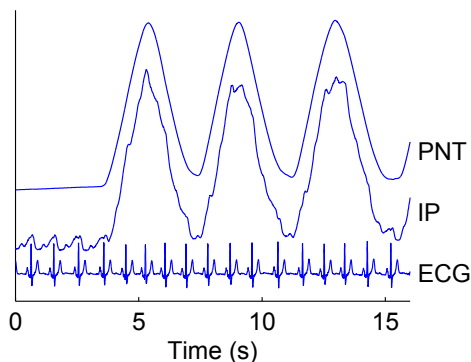


FIGURE 3.3: Simultaneous recordings of integrated PNT (lung volume), IP, and ECG in a healthy supine adult subject. During the apneic period only the cardiac component of the thoracic impedance signal is seen in the IP signal.

Baker & Geddes (1966) measured the change in transthoracic impedance changes in mechanically ventilated dead dogs using a bilateral electrode configuration at the xiphoid level as various current pathways were interrupted by the gross dissection of tissue. According to their findings most of the current was conducted by the posterior thoracic pathway (79.9 %), some through the diaphragm, liver and anterior chest wall, and only 4.7 % through the lungs.

Baker *et al.* (1966) also studied the $\Delta Z/\Delta V$ ratio with respect to the thoracic diameter (TD) in 10 anaesthetised dogs with sectioned phrenic nerves to enable external control of the diaphragm. The electrodes were inserted subcutaneously on various rib levels on the midaxillary lines to remove the impedance changes due to electrode sliding over ribs and due to loose tissue. Intratracheal pressure and respired volume were recorded. Perhaps the most important finding was that when the diaphragm was externally tetanised, resulting in a considerable increase in the lung volume, without thoracic movement a consistent increase was seen in the spirometer volume and in the impedance, but not in the TD, strongly suggesting that IP measurement reflects lung aeration and not chest wall movement. Baker *et al.* were mostly interested in the location of the source of the

respiratory impedance variations. They concluded that in a bilateral electrode placement the signal amplitude was strongest at the height of the 8th rib, regardless of whether respiration occurred normally or solely by diaphragmatic movement. This led them to conduct another study in dogs in order to determine whether respiratory impedance changes could be produced by the movement of the diaphragm-liver mass alone in the absence of lung aeration (Baker & Geddes, 1967). They employed a pneumothorax by inserting plastic tubes into the thorax, which were connected to a spirometer bell. They could thus introduce and reverse the pneumothorax manually. They found a large sustained increase in both TD and impedance when pneumothorax was initiated while the diaphragm and liver moved caudally, and the lungs, being exposed to the atmosphere, collapsed. They then closed the trachea to prevent lung volume changes. Operating the spirometer bell then caused a corresponding change in TD and a small motion of the diaphragm and liver. They found that the impedance change corresponding to change in the intrapleural volume had the same ratio as impedance and lung volume change during normal respiration before pneumothorax. They also discovered that the strongest impedance change was still localised at the 8th rib. The paradigm at that time seemed to be that there was a single localised source of respiratory impedance variations in the thorax, and whichever electrode placement produced the strongest impedance changes was the one that they sought. Unfortunately, they neglected a more important feature of the signal, namely, how linear the change is with the lung volume change. They concluded that the impedance changes recorded at all rib levels had their source at or near the xiphoid level and were tightly associated with changes in the TD and motion of the diaphragm-liver mass. In addition they concluded that TD change and diaphragm motion alone can account for impedance changes without lung aeration. This conclusion in particular must be criticised because the measurements were made in a situation where the lungs have collapsed, and thus have no contact with the chest wall (or the electrodes) and thus obviously cannot be part of the impedance sensitivity field.

Logic *et al.* (1967) investigated the contribution of the TD change to respiratory impedance changes in man and paid more attention to the linearity of the relationship between impedance and volume change, instead of focusing only on the strength of the impedance signal. They reasoned that, according to the findings of Baker & Geddes (1966), the current paths would reside predominantly in the chest wall, and the impedance changes should thus follow TD changes. They placed the electrodes at various levels bilaterally on the midaxillary lines. Higher electrode placements closer to the axilla yielded a linear $\Delta Z/\Delta V$, whereas the lower ones were less linear. Moreover, TD measured at the electrode level was linear with the impedance change at high locations, but not at low locations. These findings were considered to support the concept that TD change cannot be the sole factor responsible for respiratory impedance changes. Their measurement

procedure also included having the subjects wear a rigid cast that prevented respiratory deformation of the lower thorax. Wearing the cast significantly increased the linearity between impedance and volume at low electrode placements, where the relationship had been found to be rather nonlinear without the cast.

Hill *et al.* (1967) reported that observed impedance fluctuations sense pressure-volume changes produced by small motions at the thoracic electrode-tissue interface, rather than impedance-volume changes caused by physiological events within the conducting volume. This claim that the mechanical respiratory movement of the skin electrodes was the source of the IP signal had been shown as false by Goldensohn & Zablow (1959) already over 10 years earlier by successful IP recordings with electrodes in the arms instead of the thorax. A successful between-arms measurement was also conducted by Weltman & Ukkestad (1969) soon after.

Baker's student Petro (1969) continued on the same path in his master's thesis, in trying to understand the role of lung aeration in the respiratory impedance signal. He again confirmed that the strongest respiratory impedance signal originates at the 8th rib level. He then insulated the intact lungs of a dog with thin plastic to prevent electrical current flow, but allowing normal respiratory movement. After insulation, the impedance signal amplitude at higher locations, the 4th and 6th rib level, decreased, but at the 8th remained almost unchanged and slightly increased at the 10th level. He confirmed the location of the diaphragm with X-ray imaging during the various measurements and concluded that at lower electrode locations the respiratory impedance signal is dominated by the diaphragm, but at higher locations lung aeration assumes a more important role. Although conclusions along these lines have been corroborated by others since then, this study should be criticised for the same reasons as the pneumothorax study of Baker & Geddes (1967): removing the lungs from the electrical pathway will naturally influence the total current distribution in the thorax (Section 3.1.2) and the results from such a condition cannot be generalised to the normal condition.

Kawakami *et al.* (1974) conducted an extensive series of experiments on dogs to investigate the relation between thoracic impedance changes and TD changes. Some of the most interesting findings were: 1) Injection of hypertonic (electrically highly conductive) saline to the vena cava produced an increment in the thoracic dimension TD due to small increase in thoracic volume and a decrement in the thoracic impedance Z . The time delay between the Z decrement and the injection increased as the injection site moved further away from the pulmonary circulation in the venous system. Such an effect was not noticed in TD. Moreover, increasing the concentration of the saline (making it more conductive) augmented the effect in Z , but not in TD. 2) Occlusion of the vena cava, which presumably causes a slow decrease in the blood volume of the pulmonary

circulation, resulted in somewhat constant increase in Z and a decrease in TD. On the release of the occlusion, TD increased rapidly to the pre-occlusion level, preceded by a noticeable overshoot, and the Z declined slowly to the pre-occlusion level. The duration of the change in Z was similar to the duration of aortic pressure normalization; thus, the impedance change was considered to reflect the pulmonary blood volume, whereas TD change was a result of a combination of blood volume shifts. 3) Finally, ventilating the lung with saline instead of air caused the Z to behave in an inverted manner, but caused no change in TD compared to air ventilation. In addition, they injected ether into the vena cava, which evaporated in the lung, causing a sudden increase in the alveolar gas volume. This caused a clear impedance increase with electrodes at the 6th rib level, but not at all at the 8th, even though normal respiration was seen in both. These experiments opposed earlier understanding of that changes in impedance would mostly reflect changes in TD, and instead favoured the lung aeration paradigm.

Using a simplistic geometrical model, Albisser & Carmichael (1974) stated that the geometrical factors of TD and interelectrode distance made significantly larger contributions to thoracic impedance change than changes in lung resistivity (Kawakami *et al.*, 1974). However, only a quite modest research effort has been made towards understanding the electrical conductivity of the lung tissue itself. Witsoe & Kinnen (1967) experimented on seven dogs with the lungs intact, but accessed the lung surface through incision between the ribs. They made an assumption that although the lung tissue at a microscopic level is highly heterogeneous, at a macroscopic level the lung represents a semi-infinite, homogeneous, isotropic, resistive medium. This allowed them to use a tetrapolar impedance measurement to analyse tissue conductivity at 100 kHz, while keeping the lung intact using the theoretical analytical approaches presented by Stefanescu *et al.* (1930) and Valdes (1954). The lungs were manually inflated in the anaesthetised dogs to control and record the lung volume. They found the lung volume to be highly linear with tissue resistivity with a volume range from full expiration (lung collapse) to full inspiration. There was approximately 30 % interindividual variation in the volume-resistivity ratio, but no intraindividual variation between lung lobes. Later, in two studies Nopp *et al.* (1993, 1997) used an electrical impedance tomographic spectroscopy system (Brown *et al.*, 1994), and corroborated that lung resistivity is linear with volume change, and proposed a model explaining the dielectric behaviour of the lung tissue. From their model they concluded that with inspiration the volume of electrically conductive condensed matter per unity volume of lung tissue decreases, which leads to increasing resistivity (Figure 3.4).

The general conclusions from the literature on the source of respiratory impedance signal are that 1) the lung tissue itself has linear volume-impedance relationship, and 2) the thoracic respiratory impedance changes can be seen with both low and high bilateral midaxillary electrode placements, but the low ones may reflect respiratory sources other

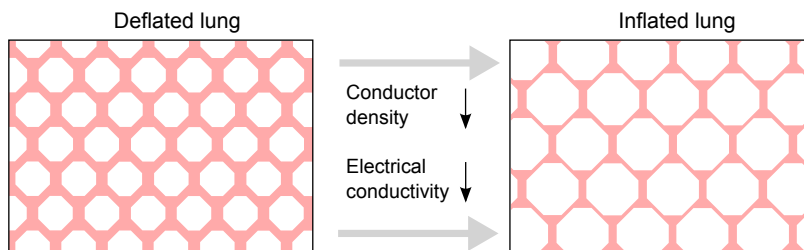


FIGURE 3.4: A simplified conceptual drawing on the principle of IP. Stretching of the lung due to inspiration renders the tissue (conductor) sparser, which decreases the electrical conductivity (increases impedance).

than lung tissue aeration and are thus less linear with lung volume changes than the high ones.

3.1.3.1 Computer simulation of the sensitivity distribution

For deeper understanding of how the impedance measurement relates to the physiological function, it would be desirable to have at least an estimate of how the sensitivity field of the measurement is distributed within the body and even how it behaves dynamically with respiration or cardiac action. Computer modelling of the lead fields could potentially yield this information. The most used data set has come from the U.S. National Library of Medicine Visible Human Project (Ackerman, 1998). The male and female models are anatomically relatively detailed and several groups have used the data to create impedance models by segmenting the tissue types and assigning conductivities (Kauppinen *et al.*, 1998). However, the models lack realistic dynamic motion. This is obviously a serious shortcoming for understanding respiration-induced impedance changes that stem from the macroscopic and microscopic geometry changes of the thorax and the lungs. A detailed dynamic model has been introduced by Segars *et al.* (2010). Although this model has not yet been used for impedance modelling, it may significantly improve the benefits of computer simulation in IP. However, even for this advanced dynamic model the spatial resolution is in the millimetre scale, whereas the smallest lung structures such as the alveolus are roughly two decades smaller.

Computer modelling has thus far produced only limited information as to what is the real source (and what is not) of the thoracic respiratory signal, but with the accuracy of the models constantly increasing, it is likely that they will enable a comprehensive investigation of thoracic impedance in the future.

3.1.4 Electrode locations

The location of the electrodes on the body affects the magnitude of the respiratory, cardiac, and motion artefact signals and, importantly, the linearity of the $\Delta Z/\Delta V$ ratio. Depending on the application, different features are favoured. For instance, in ICG, one naturally would prefer a strong cardiac component and negligible respiratory component, whereas for IP the preference is obviously the opposite. Usually the most important feature is linearity with the physiological phenomenon of interest. In IP this means linearity with lung volume changes. Electrode placement is the main determinant of this linearity.

In one of the first papers on IP, Goldensohn & Zablow (1959) placed the electrodes on the arms. However, most researchers have placed them on the thorax, perhaps as an intuitive choice. Possibly the first paper investigating the effect of different electrode locations was published by Geddes *et al.* (1962). Using a bipolar impedance measurement with the electrodes on the opposite sides of the chest (bilaterally) on the midaxillary line, they found that the $\Delta Z/\Delta V$ ratio in man was highest at the level of the sixth rib. This was corroborated by Baker *et al.* (1966) in subjects of low body mass, but they found the electrode location to be less sensitive in subjects with high body mass. This finding is rather logical, considering that a thick subcutaneous fat layer distributes the measurement sensitivity field to a wider area (Grimnes & Martinsen, 2008). Importantly, both papers describe that the location of the highest $\Delta Z/\Delta V$ ratio is not the one with highest linearity, but placing the electrodes higher on the midaxillary line achieves a more linear $\Delta Z/\Delta V$ ratio. Soon Logic *et al.* (1967) published a paper focusing entirely on the linearity and they corroborated the earlier findings that favour high placement. They also found that when the electrodes are placed below the most linear location of 4th intercostal space, the nonlinearity is such that the $\Delta Z/\Delta V$ ratio increases with inhaled volume. A similar finding was produced by Hamilton *et al.* (1965) in adults and later in infants by Hamilton & Bruns (1973). These studies did include some variation in the depth of breathing, but, importantly, no deepened exhalation which would have lowered the lung volume below functional residual capacity (FRC). Allison *et al.* (1964) used a tetrapolar measurement, with other electrode locations than those on the midaxillary line and including some vital capacity manoeuvres (VCMs) that reduce the lung volume to residual volume (RV). They found that the electrode positions involving the wrists or shoulders were too sensitive to motion during forced respiratory manoeuvres. Instead they concluded that the best configuration regarding linearity even for deep exhalations was having the current electrodes on the neck and below the diaphragm on the posterior thorax and the voltage recording electrodes on the back, 30 cm apart. However, even with this placement, they found nonlinearity at the

highest and lowest lung volumes. In a study in anaesthetised dogs, Kawakami *et al.* (1974) injected ether into the vena cava, which evaporated in the lung, causing a sudden increase in the alveolar gas volume without notable thoracic expansion. This caused a clear impedance increase with electrodes at the 6th rib level, but not at all at the 8th, even though spontaneous normal respiration could be seen at both locations. Kawakami *et al.* concluded that in a lower placement the respiratory impedance signal may be due to the movement of diaphragm, liver and other organs, whereas a higher placement reflects change in the lung.

Since the early investigations of the 1960s and 70s, this topic of IP electrode locations has received little interest, until recently when Seppä *et al.* (2013a) studied similar electrode placements regarding their linearity during more demanding respiratory manoeuvres. They found that even a high midaxillary electrode placing is not very linear when the test manoeuvre includes also deep exhalations. Instead, in a tetrapolar setting, placing one electrode pair high on the midaxillary line and the other electrode pair on the arms, opposing the first pair, yields a highly linear $\Delta Z/\Delta V$ at all lung volumes during a VCM. This electrode configuration was further validated in three body positions by Młyńczak *et al.* (2015).

3.1.5 Deriving absolute measures of respired volume

An obvious aim for IP research has been to obtain absolute ventilation volume values such as tidal volume and minute ventilation in a noninvasive and even ambulatory manner. As the $\Delta Z/\Delta V$ ratio is known to have a high intersubject variation (Kubicek *et al.*, 1964), there are two potential ways to achieve absolute measures. Firstly, to find a regression equation that uses a priori information such as body geometry and tissue conductivities to convert impedance changes to volume changes, or secondly, to calibrate impedance measurement by breathing at a known volume.

The first approach would often be more beneficial, but has proven difficult to establish. The challenges include variation in the human anatomy, and difficulty in determining the measurement sensitivity field and tissue conductivities. Allison *et al.* (1964) determined a $\Delta Z/\Delta V$ equation which included tissue conductivities, electrode distance (fixed) and the measured base resistance. In their boldly named paper “Law of impedance pneumography” Valentinuzzi, Geddes and Baker determined a very simple equation as $\log(\Delta Z/\Delta V) = 2.656 - 1.08 \log(W)$ where W was the body mass in kilograms (Valentinuzzi *et al.*, 1971). Curiously, in order to verify the equation on high body masses, they conducted a test on a living elephant. Various similar experiments were conducted, with diverse results, but often in a very limited test settings.

The second approach for obtaining the $\Delta Z/\Delta V$ ratio would be to simply measure the respired volume during a calibration period. For subjects in a static position such as patients in an ICU this could be feasible at least for limited time periods, but in mobile subjects the postural changes cause changes in the $\Delta Z/\Delta V$ ratio, often in a rather unpredictable manner (Adams *et al.*, 1993, Hamilton *et al.*, 1965, Houtveen *et al.*, 2006, Logic *et al.*, 1967, Seppä *et al.*, 2010b). Even in ICU patients the $\Delta Z/\Delta V$ may be likely to change due to, for instance, edemic fluid accumulation (Fein *et al.*, 1979).

Albisser & Carmichael (1974) stated that there are too many factors that affect the absolute impedance readings to establish a reliable $\Delta Z/\Delta V$ equation and that IP has clinical value only in the monitoring of respiratory rate and apnoeas. Their statement on the clinical use of IP has been correct so far.

3.1.6 Motion artefact rejection

Thoracic impedance recording is susceptible to motion artefacts created by, for example, walking or arm movement. The artefacts can be rather strong, masking the signal of interest. In certain applications, such as apnoea monitoring, it would be important to remove the artefact or at least reliably detect between the artefact and the physiological event of interest. Various approaches have been studied to solve this problem.

Graham (1965) introduced the idea of using of a guard electrode to better focus the sensitivity field of the IP measurement. In bipolar impedance measurement the electrode used for excitation and voltage measurement is surrounded by a larger circular guarding electrode that is kept at the same potential as the excitation electrode. The voltage, however, is measured only at the middle electrode. This approach creates a wider lead field so that the lead field of the middle electrode may have a narrower, more homogeneous field. This technique was also adopted for attempts to increase the signal to artefact ratio (SAR). Cooley & Longini (1968) studied a bipolar system with guard electrode and found it not only significantly more sensitive to respiratory impedance changes, but also more immune towards motion artefact. However, soon after, Plonsey & Collin (1977) showed that the theoretical basis for using a guard electrode in IP is questionable. Nevertheless, Sahakian *et al.* (1985) found that guarding increases the SAR of a bipolar measurement to the level of non-guarded tetrapolar measurement. They also introduced a guarding scheme for tetrapolar measurement, but it did not provide substantial improvement. In addition, they concluded that a larger electrode area increased SAR.

An obvious approach in studying motion artefact reduction is investigating the effect of electrode locations. Luo *et al.* (1992) measured SAR of 171 different bipolar electrode

configurations in 10 healthy subjects during various bodily movements. They found an anteroposterior configuration on the 3rd intercostal space on the sagittal plane to have the highest mean SAR. They also discovered that subcutaneous fat decreases SAR and that the electrode size was not proportional with SAR, as suggested by Sahakian *et al.* (1985). However, they experimented with a larger electrode consisting of a matrix of smaller interconnected electrodes and found that to increase SAR. A major limitation of their study is the lack of assessment of the linearity of $\Delta Z/\Delta V$ ratio of the tested configurations. For most clinical applications, the lack of motion artefact is of little interest if the respiratory impedance change is nonlinear with lung volume in the first place. They also suggested that combining the signals from multiple simultaneous measurements could be successful in artefact rejection, and indeed Khambete *et al.* (2000) proposed using six strategically placed electrodes in concert. They found in a small experimental setup (4 subjects) a significant reduction in motion artefact when the individually measured signals were appropriately multiplied and summed.

Another approach to the problem was taken by Rosell & Webster (1995). Based on their finding that the signal amplitude of breathing increases and that of motion artefact decreases with increasing excitation frequency, they proposed a filtering scheme where impedance was measured simultaneously at two frequencies, 57 kHz and 185 kHz. They found that the amplitude ratio between the two measurements differed between breathing and motion signals and were able to devise an adaptive filter based on that. They discovered more than two-fold increases in SAR for motion and a 34 % increase for artefact created by simulated obstructive apnoea. Another adaptive filter scheme was employed by Ansari *et al.* (2014).

Despite the aforementioned attempts, no method for movement artefact rejection has been established as the standard method in IP.

3.1.7 Cardiogenic oscillations

The cyclic pumping action of the heart muscle moves blood within the thorax. This creates a pulsatile measurable impedance signal (Figure 3.3). This signal can be either desired as in ICG or distortive as in IP. In the following the cardiac impedance signal is discussed from the IP standpoint.

3.1.7.1 Origin of cardiac oscillations

Although cardiogenic impedance variations have been studied thoroughly by researchers of ICG, they have received little attention from IP researchers. Unfortunately, the electrode placements that have been used in ICG studies are fundamentally different from those used in IP studies. This greatly limits the usefulness of ICG studies in understanding the cardiogenic impedance signal present in IP. One reason for IP researchers to put so little effort into understanding CGO could be that firstly, obviously, IP focuses on the lungs, not the heart, but secondly, the applications of IP have so far been rather unambitious, permitting the use of heavily distortive filtering methods in the removal of CGO or even simply ignoring it.

One of the main questions in understanding CGO within the IP context is the relative contribution of the systemic and pulmonary circulation to the signal. This can be studied by injecting highly conductive saline solutions into the circulatory system at different locations and observing the resulting impedance changes. Hukushima (1970) measured thoracic impedance variations in dogs using an unconventional electrode placement with a narrow sensitivity field that putatively focuses on a single lung. He found that saline injections to the inferior vena cava resulted in an anticipated impulse in the impedance signal after a short delay, whereas injection to the left atrium showed no distinct impulse. He concluded that in using that particular narrow-focusing electrode placement, the cardiogenic impedance variations stem solely from the pulmonary circulation. Geddes & Baker (1972) carried out similar saline injection experiments in dogs, but using a wide band electrode configuration similar to that used in ICG research at the time. They found that with this configuration the saline injections to both pulmonary and systemic circulations produced an impedance response. Injections to the right atrium had a slower impedance response, reaching the maximum typically after four to five cardiac cycles, whereas injections to the left atrium had a faster and shorter effect. However, according to a review by Patterson (1989) there have been studies supporting also a sole contribution from the pulmonary circulation and sole contribution from systemic circulation when using traditional ICG band electrodes. To the best of my knowledge, the only paper on this topic that used a bilateral midaxillary electrode configuration that is conventionally used in IP was published by Kawakami *et al.* (1974). They injected saline at three different locations in the vascular system before the pulmonary circulation. They found a clear impedance impulse due to the injection. The delay between the injection time and the resulting impedance impulse was proportional to the vascular path distance to the lungs. Unfortunately, they did not include injections to the systemic circulation. They do, however, discuss that the cardiac oscillations may have components associated with the mechanical movements of large vessels in the thorax and of the heart.

Kira *et al.* (1970) complemented these findings using the same narrow electrode configuration as Hukushima (1970) and Kawakami *et al.* (1974), but intervening through vessel occlusion instead of saline injection. They performed simultaneous measurement of the blood flow rate at the right and left pulmonary trunk. While manipulating the blood flow with partial occlusion, a clear correlation between the blood flow signal and first time derivative of the impedance signal was found.

To summarize, the following observations can be made. Most of the results, except for those of Kawakami *et al.* (1974), are of limited applicability regarding the most widely used bilateral configuration IP measurement due to the use of unconventional or ICG-oriented electrode configurations. It is, however, clear that, depending on the electrode placement, the origin of the cardiac impedance signal may stem solely from the pulmonary circulation (Hukushima, 1970, Kira *et al.*, 1970) or from both pulmonary and systemic circulation (Geddes & Baker, 1972).

3.1.7.2 Attenuating the cardiogenic oscillations

The effective attenuation of the cardiogenic impedance part is essential if respiratory variables more sophisticated than tidal volume or respiratory rate are to be derived from the signal. Furthermore, it is highly important that the method of attenuation does not deteriorate the respiratory part of the impedance signal.

The problem is not a trivial one, mainly for two reasons: 1) Even though the main power band of the respiratory signal component is clearly at a lower frequency than the cardiac signal, the respiratory signal contains harmonics that overlap with the cardiac signal frequency. 2) Neither of the signal components are stationary, meaning they change over time. Despite the variety of methods proposed for solving the problem, most papers lack objective clinical evidence regarding their performance, or they are assessed only from the cardiology standpoint, leaving their applicability to IP unknown.

The need for attenuating the CGO was realised by Goldensohn and Zablow already in 1959 in one of the earliest papers describing the use of impedance to measure respiration (Goldensohn & Zablow, 1959). They devised an electronic filter to which the individual CGO waveform was manually programmed. The system then subtracted the programmed waveform from the raw impedance signal at times triggered by the ECG R-wave. Finally, the remaining cardiac signal was removed by a low pass filter with a 2.5 Hz cutoff frequency, which was considered not to distort the respiratory part. Very limited analysis on the efficacy of this approach is presented, but the authors mention that the waveforms can occasionally be rather complicated and that they are not stable

over time in an individual. A similar approach was taken by Wilson *et al.* (1982) using a separate averaging device that was triggered by ECG. They found this approach to be unsatisfactory because the oscillation waveform depends on the geometry of the thorax and therefore varies with the phase of respiratory cycle at which it occurs. They also experimented on a feature filter (Lynn, 1977) and a notch filter but found them inadequate as well.

The infant tidal volume monitor of Hamilton *et al.* in 1973 employed a simplistic electric circuit to account for the cardiac distortion (Hamilton & Bruns, 1973). The operation of the circuit is described in a cursory manner and no results on its efficacy are presented.

A different approach was presented in 1990 by Pfützner *et al.* (Pfützner *et al.*, 1990) and slightly refined for the digital domain by Nakesch, Pfützner *et al.* (Nakesch *et al.*, 1994) four years later. The principal idea was to add a fifth electrode to a normal tetrapolar impedance pneumograph in order to attenuate cardiac signal and other artefacts as well. With respect to the cardiac attenuation, the basic operating principle was as follows. The excitation current was fed between two electrodes, 1 and 2, close to the axilla and three voltage measurement electrodes were placed so that electrodes 3 and 4 were close to 1 and 2, and the fifth approximately at the sternum. All the electrodes resided on the plane of the 4th intercostal space. Voltage measurements were taken between 1 and 2 and 1 and 3. Thus, two thoracic impedance signals from two different sensitivity fields were received. Both signals contain the respiratory and cardiac components, but with different weight factors. Through determination of the weight factors the components can be separated through signal subtraction. The authors do not refer to independent component analysis (ICA) (Hyvärinen *et al.*, 2001), but their approach is in practice very close to ICA. This approach, however, suffered from an overly simplistic assumption of how the cardiac and respiratory components are seen by the two sensitivity fields. Namely, the approach assumed that the two components only differ in gain between the two signals, but in reality they differ also in timing and, more severely, in the waveform morphology of the components. This was acknowledged by the authors and considered a major drawback despite a somewhat adequate operation of the approach in general.

Most cardiorespiratory impedance signal decomposition work has been directed towards the application of ICG. The efficacy of these approaches is usually reported from the cardiographic standpoint such as accuracy for stroke volume estimation, and it is thus difficult to assess their performance regarding IP. Some of the approaches include ensemble average (EA) (Miyamoto *et al.*, 1981, Muzi *et al.*, 1986, Wang *et al.*, 1995, Zhang *et al.*, 1986), fitting and subtracting a regression line over the cardiac oscillations (Eiken & Segerhammar, 1988), spline fitting on the cardiac oscillations (Pandey *et al.*, 2011), adaptive frequency (Barros *et al.*, 1995, Yamamoto *et al.*, 1988) or wavelet

domain (Ouyang *et al.*, 1998, Pandey *et al.*, 2011) filtering, empirical mode decomposition (Abdulhay *et al.*, 2009), and model based approach with an application-specific orthonormal basis (Krivoshei *et al.*, 2008).

Unfortunately, the proposed methods are commonly flawed with unrealistic or overly simplistic assumptions of the underlying physiological and bioelectrical properties. For instance, it is clear from the medical literature that cardiac and respiratory impedance signals are non-stationary and mutually dependent (Section 6.1). Nor can it be assumed that the impedance measurement sensitivity distribution would not change with respiration (Section 6.1). Moreover, the cardiac or respiratory part of the impedance signal measured simultaneously at two distinct locations of the thorax or the body are not simply linear combinations of each other. Instead, it should be intuitively clear that there is a likely time delay and waveform shape difference between the two simultaneous measurements at distinct body regions.

3.2 Tidal breathing analysis

Conventional lung function assessment methods, spirometry and peak expiratory flow (PEF) meter, require that the subject performs demanding respiratory manoeuvres in a repeatable manner. This hinders or prevents their use in patients with limited cooperation such as infants, preschool children, elderly or disabled people and subjects for whom deep inspiration causes pain, such as thoracic surgery patients. Nevertheless, measurements of restful spontaneous TB are feasible even in such patient groups. Close analysis of respiratory flow within each breath and from breath-to-breath yields useful information on the lung health condition of the subject, especially in the presence of airway obstruction.

3.2.1 Quantification of tidal breathing

Although the early observations on clinical relevance of TB analysis were rather descriptive or subjective, the need for numerical indices to describe TB was soon realised. Several quantification methods and their clinical relevance have been described. Most of the work has been directed towards simple indices that relate to the shape of the tidal flow curve (Section 3.2.1.1) much like in conventional forced spirometry. Another analysis approach is based on assessing the time dynamics or complexity of respiratory flow signals or other lung function measurements over time (Section 3.2.1.2).

3.2.1.1 Analysis of the tidal flow curve shape

A list covering most of the TB parameters that have been studied in a clinical setting is presented in Table 3.2 with clarifying illustrations in Figure 3.5.

TABLE 3.2: Definitions of TB parameters. See Figure 3.5 for illustration.

Name / Abbreviation	Unit	Description	Example study
Tptef/Te	1	Ratio of time to reach tidal peak expiratory flow to total expiration time	Bouhuys (1957)
Tptif/Ti	1	Ratio of time to reach tidal peak expiratory flow to total inspiration time	Seddon <i>et al.</i> (1996)
Vptef/Ve	1	Ratio of volume at peak expiratory flow to total expired volume	Bouhuys (1957)
ptef	L/s	Peak expiratory tidal flow	Benoist <i>et al.</i> (1994)
S	1	Slope of a line fitted to the post-peak part of the expiratory flow-time curve	Williams <i>et al.</i> (1998)
EV	L	Extrapolated volume that is obtained by fitting a line in the linear portion of the expiratory flow-volume curve (FVC) (Note: no unambiguous mathematical definition)	Morris <i>et al.</i> (1998)
Trs	s	Time constant of the respiratory system. The slope of a line fitted to the linear portion of the expiratory FV curve defined as $Trs = \tan(a)$. (Note: no unambiguous mathematical definition)	Morris <i>et al.</i> (1998)
Dtr/Te	1	Ratio of time from beginning of exhalation until beginning of the linear part of the FV curve to total expiratory time	Morris <i>et al.</i> (1995)
$\dot{V}b-o$	L/s	Expiratory flow at the point of end-expiratory flow break-off (premature onset of inspiration). Defined as the point of maximal change in the descent of the TBFVL in the transition from expiration to inspiration	Schmalisch <i>et al.</i> (2003)
ptef/Tptef	L/s ²	Mean initial expiratory gas acceleration	Schmalisch <i>et al.</i> (2003)
(ptif+ptef)/Vt	1/s	Axis ratio of the TBflow-volume loop (FVL)	Schmalisch <i>et al.</i> (2005)
Sphericity, triangularity, rectangularity	1	Parameters that describe the shape of expiratory or inspiratory FVL as to how closely it resembles a sphere, a triangle or a rectangle.	Leonhardt <i>et al.</i> (2010)
Polynomial fit coefficients	1	The coefficients of a first or second order equation fitted on the normalized expiratory or inspiratory FVC	Leonhardt <i>et al.</i> (2010)
tef50	L/s	Tidal expiratory flow at 50 % of total exhaled volume. Similarly for other percentages or inspiratory flows (tif)	Lødrup Carlsen <i>et al.</i> (1992)

tef25/ptef, tef50/ptef	1	Ratio of tidal flow at 25 % or 50 % of total exhaled volume to PEF	Lødrup Carlsen <i>et al.</i> (1994)
Ti/Te and Te/Ti	1	Ratio of duration of inspiration to duration of expiration or vice versa	Asai <i>et al.</i> (1991)
Ti/Ttot	1	Ratio of duration of inspiration to duration of complete respiratory cycle	Benoist <i>et al.</i> (1994)
Vt/Ti	L/s	Mean inspiratory flow	Schmalisch <i>et al.</i> (2003)
s	1	Exponential of the power law	Frey <i>et al.</i> (2001)
kd	1	Harmonic distortion in the frequency spectrum of the respiratory flow signal, i.e. the square root of the ratio of the sum of the squares of the higher harmonic amplitudes above the fundamental frequency and the sum of the squares of all amplitudes	Frey <i>et al.</i> (2001)
Appef20		Angle of a regression line passing through four points in the post PEF-time profile at point of 20 % of expiratory time	Colasanti <i>et al.</i> (2004)
Appef80		Angle of a regression line passing through four points in the post PEF-time profile at point of 80 % of expiratory time	Colasanti <i>et al.</i> (2004)
Ippef		Integral of post-PEF-time profile	Colasanti <i>et al.</i> (2004)
Vt	L	Tidal volume	
RR	1/min	Respiratory rate	
MV	L/min	Minute ventilation	

3.2.1.2 Analysis of the respiratory time dynamics

Consider some imaginary TB parameter assessed at nine moments in time. For patients A and B this series would yield values of $\{1, 3, 3, 1, 2, 1, 3, 2, 2\}$ and $\{1, 2, 3, 1, 2, 3, 1, 2, 3\}$, respectively. Assessed by conventional descriptive statistics, these two series both have a mean of 2.00 and variance of 0.75, yet it can be seen that the series of patient B is obviously periodic, whereas that of patient A is not. Differentiating between these two patients requires analysing the time dynamics of the series.

The time dynamics analysis includes several overlapping concepts such as entropy, chaos, fluctuations, fractality, nonlinearity, and complexity. Techniques based on these concepts have been applied widely in the analysis of physiological phenomena, but have yet to reach clinical approval in most cases. In pulmonology the time dynamics analysis has been applied at least in the measurements of PEF (Donaldson *et al.*, 2012, Frey *et al.*,

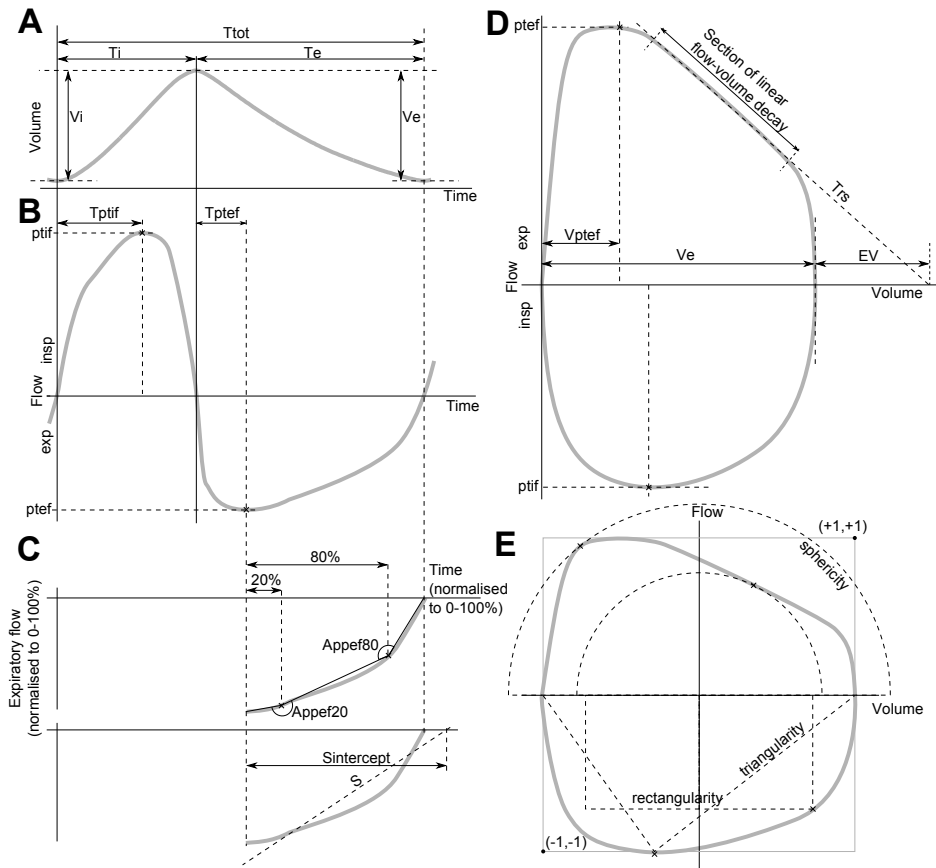


FIGURE 3.5: Illustration of definitions of various TB parameters (see Table 3.2). A: Volume-time curve B: Flow-time curve C: Post-peak part of the expiratory flow-time curve normalised in time and flow D: FVL E: Normalised FVL

2005, Thamrin *et al.*, 2009, 2010b, 2011), airway mechanical impedance (Gonem *et al.*, 2012, Muskulus *et al.*, 2010, Veiga *et al.*, 2012) and tidal air flow (Dames *et al.*, 2014, Fiamma *et al.*, 2007a,b, Frey *et al.*, 2001, Habib *et al.*, 2003, Mangin *et al.*, 2011, Minetti *et al.*, 1987, Samara *et al.*, 2009, Veiga *et al.*, 2011, Wysocki *et al.*, 2006). Analysis of the tidal air flow is the most relevant of these applications from the standpoint of this thesis.

Most of the time dynamics studies have been cross-sectional or interventional (typically, bronchodilation (BD) or MIB), but there are some longitudinal ones as well and, interestingly, some prospective ones. For instance, Frey *et al.* (2005) discovered that the presence of long-range correlations (detrended fluctuation analysis) in the PEF time series is associated with a decreased risk of asthma exacerbation within one month, regardless of the present PEF value. Indeed, it has been postulated that the analysis of time dynamics of pulmonary measurements could yield information on the presence of

an underlying respiratory disease, and of its severity and course, regardless of its current clinical symptom presence.

At a very general level, it can be said that living organisms require a delicate balance between stability (order) and variability (chaos) in their physiological functions. Diseases are characterised by either overly stable or overly variable functions. (Macklem, 2008)

3.2.2 Physiological relevance of the tidal flow curve shape

Clinical studies assessing the diagnostic value of the TB parameters derived from the flow curve are presented in Sections 3.2.4 and 3.2.5, but in the following, literature on the physiological and neurological functions underlying the changes in the TB parameters is presented.

In European Respiratory Journal editorial Bates (1998) presented the following thoughts on the clinical and physiological relevance of TB analysis. During spontaneous respiration the neural feedback system controls the muscles to overcome the mechanical impedance of the airways and to achieve ventilation at the alveolar level. An increase in the mechanical impedance, such as bronchial obstruction, will affect the neural control, which, again, should be witnessed as a change in the TB flow pattern. It should not be surprising that this leads to characteristic response in respiration. However, one must acknowledge that the TB parameters are not direct surrogates of measures of mechanical impedance of the airways. The measurable TB flow signal is a synthesis of multiple interacting factors such as the passive mechanical impedance, respiratory neural control, and glottic aperture (one could complement the list with the effects of the measurement equipment and cognitive state of the subject). Bates concluded that despite the subtle nature of TB analysis, as more sophisticated signal processing methods are applied, TB may reveal itself to be useful in the diagnosis of pulmonary diseases. In the following the relevance of selected TB parameters is discussed from the standpoint of clinical physiology and respiratory mechanics.

T_{ptef}/T_e and highly correlated V_{ptef}/V_e have been studied extensively with respect to their physiological origin and clinical meaning. From the physiology standpoint it has been established that expiratory braking is an important determinant of T_{ptef}/T_e . In normal subjects the activation of the inspiratory muscles continues well into the expiration. Shee *et al.* (1985) found that the mean time for muscle activity to reduce to 50 % and 0 % amounted, respectively, 23 % and 79 % of the expiratory time. Van der Ent *et al.* (1998) showed in an animal model that T_{ptef}/T_e can be controlled by inhibiting or exciting the inspiratory muscles during expiration. Moreover, Morris *et al.* (1990)

demonstrated that expiratory braking diminishes in the presence of airway obstruction. These findings are considered to explain why $T_{p\text{tef}}/T_e$ is reduced with obstruction.

As $T_{p\text{tef}}/T_e$ and $V_{p\text{tef}}/V_e$ are only involved at the beginning of the expiration, Morris *et al.* (1998) addressed this lack by presenting the parameters of respiratory time constant (Trs) and extrapolated volume (EV) (Figure 3.5). They rationalised these two parameters in the following way. According to the basic model of lung mechanics having constant compliance and resistance (Otis *et al.*, 1950), in a relaxed expiration there is a linear flow-volume relationship. This slope is Trs , and by analogy with an electrical model it is equal to resistance times compliance of the total respiratory system. Thus, if they were able to correctly identify the section of relaxed expiration (linear decay in flow-volume plot), that part should give information about the severity of airway obstruction. Indeed, in their study on 112 adult patients they received correlations between EV and $FRC\%_{\text{pred}}$ ($r=0.68$, $p < 0.001$), and Trs and airway resistance ($r=0.65$, $p < 0.001$). However, as they admitted, a limitation of this method is the ambiguous manual identification of the linear part of the expiratory FVC. In patients with airway obstruction the whole expiration may be a passive, relaxed event (Citterio *et al.*, 1981, Morris *et al.*, 1990), but in healthy subjects the inspiratory neuronal drive continues in the exhalation (Morris *et al.*, 1990, Shee *et al.*, 1985). Aston *et al.* (1994) circumvented manual identification by setting a fixed region between 60 % and 90 % of expired volume on which the Trs line was fitted. They excluded breaths where the correlation coefficient between the line and the flow-volume-loop section was below 0.80 or if $T_{p\text{tef}}/T_e$ was above 40 %.

The parameter S and its intercept with the zero flow as proposed by Williams *et al.* (1998), rely on a similar physiological rationale as Trs and EV. The major difference between S and Trs is that S is defined in the flow-time curve, whereas Trs is defined in the flow-volume curve. In addition, S is defined mathematically unambiguously, whereas Trs needs manual identification of the linear portion of the FVC. This benefit of exact mathematical definition could, however, be considered deceptive, as Williams *et al.* (1998) manually divided the patients into three groups according to the basic shape of their flow-time curve (convex, concave, linear). Parameter S has been studied only in the initial study of Williams *et al.* and that of Seppä *et al.* (2013b).

Tidal PEF ($p\text{tef}$) has been studied by Lonky & Tisi (1980) in adults during isoproterenol-BD and in infants by Benoist *et al.* (1994) during MIB test. The results were somewhat conflicting as both studies reported a significant increase in $p\text{tef}$ despite the presumably opposing effects of BD and MIB. This contradiction could be attributed to the difference in the study populations and to the unspecificity of isoproterenol as a bronchodilating agent, having influence, for instance, on the the respiratory control (Heistad *et al.*,

1972). Neither study presented potential physiological contributors to the ptef change, but Lonky & Tisi did conclude that bronchodilation caused a simultaneous increase in ptef despite a decrease in the driving transpulmonary pressure. Furthermore, they witnessed ptef change in patients for whom the bronchodilatory effect was not seen in conventional forced spirometric indices.

Colasanti *et al.* (2004) presented a linear regression model which used patient descriptive characteristics and various TB indices to successfully predict spirometric forced expired volume in one second (FEV1) in healthy adults and in adults with cystic fibrosis (CF) or COPD. On the general nature of the TB analysis they commented that as the tidal flow profile is rather variable in normal subjects, its interpretation may be more useful as a monitoring tool in subjects with an obstructive lung disease already diagnosed. A similar observation was made by van der Ent *et al.* (1996a) as a reduced variability of Tptef/Te in obstructed patients. A more sophisticated analysis on the variability is discussed in Section 3.2.1.2.

3.2.3 Technical aspects of tidal breathing measurement

3.2.3.1 Conventional measurement equipment

The European Respiratory Society (ERS)/American Thoracic Society (ATS) task force on infant TB analysis states that the standard equipment for clinical TB measurement is a face mask connected to a PNT (Bates *et al.*, 2000). It is, however, necessary to be aware of the effects that the most commonly used face mask and PNT equipment may have on the results. Dolfin *et al.* (1983) and Emralino & Steele (1997) compared VT and Tptef/Te values and their variation between immediate placing of the face mask and a few minutes later. They found that VT was initially significantly smaller and Tptef/Te more variable as compared to the later moment. Schmalisch *et al.* (2001a) corroborated this finding with the same equipment, but found that this effect was not seen with flow-through technique (FTT) equipment that does not increase the respiratory dead space. A similar finding with FTT was made by Patzak *et al.* (2001), but they noticed that even with FTT the Tptef/Te values were less variable a few minutes later than immediately after placing the mask. Earlier, Dolfin *et al.* (1983) and Fleming *et al.* (1982) had discovered that the placement of the mere rim of a face mask without any dead space addition significantly affects the TB pattern, supposedly through trigeminal nerve stimulation.

These effects could be entirely removed by noninvasive measurement techniques such as respiratory inductive plethysmography (RIP), electromagnetic inductance plethysmography (EIP) or IP (Section 3.2.3.2). However, thus far most work on these methods has been directed towards their validation instead of their clinical application.

3.2.3.2 Noninvasive measurement equipment

Some sort of respiration-related measurement signal can be obtained with a variety of mechanical, acoustic, optical or electromagnetic instruments. However, if breath-to-breath tidal respiratory flow, instead of respiratory rate or other trivial measures, is to be analysed, the equipment selection is much narrower. Most TB studies with a clinical interest have used equipment that needs direct access at the airway opening, namely, a PNT with a face mask or mouth piece (Section 3.2.3.1). PNT is considered the gold standard method and other less intrusive types of equipment are typically compared with PNT when their validity for tidal flow measurement is assessed.

The most studied alternative for PNT is RIP. In RIP two elastic belts with sewn-in electrical conductive coils are placed on the rib cage and abdomen to account for upper and lower chest wall movement, respectively. The electrical inductance of each belt is proportional to their varying length and is determined with electrical oscillation circuitry connected to each belt. RIP as well as IP enable measurements in mobile subjects, whereas another noninvasive option, EIP, only permits measurements at the bedside with rather sizeable external instrumentation. There is evidence that on healthy adults, RIP-derived chest wall movement signal may be linear with the lung volume signal (Seppänen *et al.*, 2013).

Studies comparing the accuracy of noninvasive techniques in deriving the most cited TB parameter, T_{ptef}/T_e , are presented in Table 3.3. The comparison of mere T_{ptef}/T_e value, however, gives a somewhat limited picture on the linearity of the methods, as discussed in Section 6.2.3.

TABLE 3.3: Studies assessing the agreement of noninvasive respiration measurement techniques and PNT in the measurement of T_{ptef}/T_e . Agreement presented as mean and 95 % confidence interval of the difference (New method)-PNT. ¹: The results in the paper should be questioned as there are four subjects missing from the Bland-Altman-plot without any mention and a different 95 % confidence interval is obtained if calculated from the plotted values. ²: There are only 27 successful measurements and the electrode configuration used is not that presented in Publication III.

Author	Subject characteristics	Method	T_{ptef}/T_e agreement
Stick <i>et al.</i> (1992) ¹	Healthy neonates aged < 5d (n=19)	RIP	-0.01 (-0.07...-0.04) corrected -0.01 (-0.10... 0.07)

Jackson <i>et al.</i> (1995)	Healthy neonates aged 0-3 w (n=32), healthy infants aged 5-82 w (n=35), infants with recurrent wheeze aged 15-94 w (n=28)	RIP	-0.06 (-0.14...0.03), 0.00 (-0.14...0.15), -0.03 (-0.23...0.18)
Manczur <i>et al.</i> (1999)	Wheezy/asthmatic children aged 1m - 10 y (n=47) + < 1 y (n=6) + 1-2 y (n=8) + 2-5 y (n=15) + 5-10 y (n=8)	RIP	-0.07 (-0.21...0.06), 0.12 (-0.32...0.08), -0.02 (-0.10...0.06), -0.08 (-0.21...0.05), -0.08 (-0.17...0.02)
Olden <i>et al.</i> (2010)	Healthy infants aged < 1w (n=10)	EIP	-0.01 (-0.35...0.32)
Williams <i>et al.</i> (2011)	Infants with continuous positive airway pressure (CPAP) support aged 23-32 w (n=23) and without support (n=20) combined	EIP	0.03 (-0.18...0.17)
Petrus <i>et al.</i> (2014)	Healthy infants (n=19) and infants with chronic lung disease (CLD) (n=18) aged 39 and 30 w (mean), respectively	EIP	0.03 (-0.00...0.06)
Seppä <i>et al.</i> (2011a) ²	Adults with varying degree of airway obstruction (n=35)	IP	0.00 (-0.10...0.10)
Seppä <i>et al.</i> (2013b)	Wheezy children aged 3 to 7 years (n=21) including MIB	IP	0.00 (-0.10...0.09)

There are also some studies on TB analysis using noninvasive methods in infants as such without validation (Black *et al.*, 2004, Mayer *et al.*, 2003, 2008, Pickerd *et al.*, 2013).

3.2.3.3 Breath averaging techniques

Individual breaths of TB are not considered representative of how the subject breathes. Instead, TB is recorded over a period of time and an averaged result is presented (Beydon *et al.*, 2007). There are two approaches to this: 1) deriving TB parameters from each breath and presenting an average of these, or 2) averaging the respiratory waveforms and presenting the TB parameters derived from the averaged waveform. The first approach is more straightforward and is more widely adopted in the clinical literature. Typically, the mean of the TB parameter is presented. This approach is also endorsed by the ATS/ERS guideline (Beydon *et al.*, 2007). The second approach of waveform averaging is less trivial, but is potentially more beneficial with noisy respiratory signals.

When averaging parameters, the majority of researchers have selected cycles for averaging manually. This has been done by an experienced operator by visually examining the

recorded TB traces for sections of stable respiration. Van der Ent *et al.* (1996a) demonstrated that computer selection of the cycles could, however, yield more reliable results. Their approach was in practice very close to taking the trimmed mean of T_{ptef}/T_e or other parameters from all breaths. Another computer selection scheme was employed by Colasanti *et al.* (2004).

Several ways of waveform averaging have been described. Benchetrit *et al.* (1989) extracted the first four Fourier components of the flow signal from each breath. The amplitude and phase lag of each component of each breath was averaged and the flow waveform was reconstructed from the averaged amplitude and phase lag. This approach was criticised and shown to produce questionable results by Sato and Robbins (Sato & Robbins, 2001). The main shortcomings stem from the phase-time differences between individual breaths and the use of only four first frequency components that are not enough to describe the complex shape of a flow waveform. Sato and Robbins proposed a method where flow and volume waveforms are averaged with respect to their phase in the FVL. This avoids the problems of the method of Benchetrit *et al.*. Its most apparent shortcoming is that it is not well defined if the phase angle does not increase monotonously. This may happen in FVLs with noisy recordings or when averaging for instance pressure-flow loops. Schmalisch *et al.* (2001b) presented a method in which the FVL is divided into segments of equal length. This method does not require the loops to have monotonous phase angle information as in the Sato and Robbins approach. They claim that the major pitfall of the method is that short noise impulses in the loop may spread over extended length.

General ATS/ERS guidelines on other aspects of the TB signal conditioning can be found in Frey *et al.* (2000).

3.2.4 Cross-sectional and intervention studies on tidal breathing

Most clinical studies in TB have been either cross-sectional or interventional. A brief review of such investigations is presented in Table 3.4.

TABLE 3.4: Cross-sectional or interventional clinical studies on TB parameters in chronological order, excluding longitudinal (Section 3.2.5) and equipment comparison studies (Section 3.2.3.2). All studies used PNT to measure flow.

Authors	Subject description	n	Age	TB parameters	Intervention	Results
Adults or adolescents						
Lonky & Tisi (1980)	Normal + suspected reversible airway obstruction	48 + 16	18-45 y	ptef	BD	In all diseased subjects ptef increased due to BD more than 2*SD of the increase in the healthy group
Morris & Lane (1981)	Normal + obstruction + restriction	15 + 51 + 24	Children and adults	Tptef/Te, Vptef/Ve, ptef	None	Tptef/Te and Vptef/Ve correlated and ptef did not correlate with FEV1%pred, FEV1/FVC and SGaw
Cutreana <i>et al.</i> (1991)	Normal + asthmatic	24 + 60	5.3-17.5 y	Vptef/Ve	bronchial provocation (BP)	Multiple spirometric indices including FEV1 and plethysmographic FRC correlated with Vptef/Ve as such and as change induced by BP
Morris <i>et al.</i> (1995)	Asthma	20	29-71 y	Tptef/Te, dtr/Te, Trs, EV	BP	BP induced significant changes in all parameters except Tptef/Te
Morris <i>et al.</i> (1998)	Suspected airway obstruction	118	7-85 y	Trs, EV	None	Trs and Raw correlated and EV and FRC%pred correlated
Williams <i>et al.</i> (1998)	Normal + chronic obstructive airway disease	32+34	18-80 y	S, Sintercept, Tptef/Te	None	Tptef/Te and S correlated with FEV1 and S intercept with FRC%pred. Note: some manual exclusion of subjects based on their flow curve shape.

Colasanti <i>et al.</i> (2004)	Normal + CF + COPD	35 + 71 + 21	6 – 77 y	Appef20, Appef80, tpfif, tpef, Tptif, Tptef, Tptef/Te, Vt, ippef, RR, Te, Ti, Ttot	None	In normal subjects the variability of TB was higher, but diseased subjects showed more stable and characteristic TB profiles. FEV1 was successfully predicted with a linear regression equation using age, height, weight and TB parameters.
Young children (predominantly age 2-7 y)						
Carlsen & Lødrup (1994)	Normal + asthmatic	26 + 26	3-85 m	Tptef/Te, Vptef/Ve, tef25/ptef	BD	In the asthma group BD induced significant increase in all parameters, in the control group Tptef/Te and Vptef/Ve decreased significantly, not tef25/ptef.
van der Ent <i>et al.</i> (1996b)	Normal + asthma + CF	228 + 64 + 12	3 – 11 y	Tptef/Te	BD	High within-subject repeatability for Tptef/Te. Tptef/Te in asthma and CF groups different from controls. Significant BD-induced change in Tptef/Te in asthma but not in CF group. Asthma group patients with FEV1/FVC below 0.8 different in Tptef/Te than those with FEV1/FVC above 0.8.
Infants (predominantly age below 1 y)						
Hughes <i>et al.</i> (1987)	Bronchiolitis	17	8-50 wk	Trs	BD	BD-induced change in Trs
Turner <i>et al.</i> (1990)	Normal	27	6-50 wk	Trs, RR, Vt	Chloral hydrate sedation + BD	Significant change from natural sleep to sedated sleep only in Vt. BD did not cause changes in any parameter.
Lødrup Carlsen <i>et al.</i> (1992)	Normal, but with family risk factors for asthma	19	1-5 days	Tptef/Te, tef50	Awake/sleep + occlusion test during sleep	Tptef/Te and tef50 higher during sleep than awake, but not after occlusion (while sleeping)

Aston <i>et al.</i> (1994)	BP responders and non-responders	19 + 18	6-12 m	Trs, Tptef/Te, Ti/Te, RR	BP	In responders BP increased RR increased with non-significant change in Ti/Te and Trs decreased. No change on Tptef/Te.
Benoist <i>et al.</i> (1994)	Recurrent wheezing history, now asymptomatic	55	Mean 16.04 (SD 5.29) m	ptef, Tptef/Te, Ti/Ttot, RR, Vt	BP	BP-induced change exceeded 1.96 * baseline (BL) SD in ptef, Tptef/Te and RR, but not in Ti/Ttot or Vt. ptef (increase) was most sensitive.
Banovcin <i>et al.</i> (1995)	Various obstructive diseases	21	6 – 14 m	Tptef/Te, Vptef/Ve	None	Both Tptef/Te and Vptef/Ve correlated well with VmaxFRC, but not with Raw
Lødrup Carlsen <i>et al.</i> (1995)	Normal + wheezing	38 + 41	2-26 m	Tptef/Te, Vptef/Ve, RR	BD	Tptef/Te and Vptef/Ve lower in wheezing than controls before but not after BD. Response to BD larger in wheezing than in controls. RR higher in wheezing both before and after BD. No BD-induced difference in RR in either group. Serum ECP (but not s-MPO) correlated with BD-induced change in Tptef/Te, but not with BL Tptef/Te.
Seddon <i>et al.</i> (1996)	Premature infants intubated + non-intubated	21 + 21	32 – 48 wk (post-conception)	Tptef/Te, Tptef, Tptif/Ti, Ti/Ttot	None	No difference in Tptef/Te between groups. Tptef/Te and Tptef correlated with CL in both groups, but not with CR. Tptif/ti was weakly correlated with CL. No correlation between CL or CL and Ti/Ttot.
Koumbourlis <i>et al.</i> (1997)	Sickle cell disease	20	3-30 m	Tptef/Te, Tptif/Ttot, RR	None	Tptef/Te was lowered compared to literature references on healthy subjects.
Greenough <i>et al.</i> (1998)	Premature infants	120	6-24 m	Tptef/Te	None	Tptef/Te differed between children who, in the neonatal period, had or had not required mechanical ventilation and had or had not had an increased inspired oxygen requirement, and who were or were not symptomatic at follow-up

Filippone <i>et al.</i> (2000)	Normal + stridor + wheezing	15 + 72 + 41	15-48 m	tef50/tif50, Ti/Te, ptef/ptif, Tptef/Te	None	Clinical types of obstructions could be reliably assigned to three characteristic FVL shapes
Frey <i>et al.</i> (2001)	Normal + asymptomatic with wheezing history + CLD	10 + 10 + 10	1 – 18 m (ap-prox.)	Tptef/Te, s, kd	BP	kd was sensitive to maturation and s was sensitive to disease. No BP-induced change in s, kd, or Tptef/Te
Totapally <i>et al.</i> (2002)	Bronchiolitis due to respiratory syncytial virus (RSV)	20	< 12 m	Tptef/Te, Vptef/Ve, tef10, tef25/ptef	Saline and albuterol	Nebulized albuterol does not improve Vptef/Ve and Tptef/Te, but can decrease tef10 and tef25/ptef
Habib <i>et al.</i> (2003)	Premature infants on respiratory support (NCPAP)	16	1 – 14 d	Tptef/Te, s, kd	Comparison between PNT and RIP	No intervention or group comparison, but s and kd found comparable between PNT and RIP
Schmalisch <i>et al.</i> (2003)	Normal + CLD	54 + 35	3 – 162 d	Vb-o, RR, MV, Vt/Ti, ptef/Tptef, ptef/Te, Vptef/Vt, tef25/ptef	None	RR, MV, ptef, Vt/Ti, Tptef, Tptef/Te, Vptef/Ve, ptef/Tptef, tef25/ptef significantly different between normal and CLD, but no difference for Vt, tef25 or Vb-o.
Lødrup Carlsen <i>et al.</i> (2004)	Normal + recurrent bronchial obstruction (rBO)	251 + 265		Tptef/Te	BD	BD-induced change in Tptef/Te larger in rBO than controls. The response was also associated with asthma risk factors. Inhaled corticosteroid (ICS) treatment increased response.

Morris <i>et al.</i> (2004)	Normal + COPD	16 + 15	Mean (SD) 23±5 + 69±8	Tp _{tef} /Te, pt _{ef} , Tr _s , Te, RR	extrathoracic expiratory resistance (EER), post peak shape (convex, linear, concave)	RR, Te, Tp _{tef} similar, but Tp _{tef} /Te, Tr _s different between groups at BL. EER caused change in pt _{ef} , Tr _s , t80 and portion of convex profiles in both groups, but Tp _{tef} /Te changed only in the COPD group.
Schmalisch <i>et al.</i> (2005)	Normal + CLD	48 + 48	36 - 42 w	Ti, RR, (pt _{if} +pt _{ef})/V _t , Te, V _t /Ti, MV, ti _{f50} , pt _{if} , pt _{ef} /Tp _{tef} , pt _{ef} , Tp _{tef} , te _{f75} , te _{f50} , te _{f25} , Vp _{tef} , V _t , Vp _{tef} /V _e , Tp _{tef} /Te, post peak shape (convex, linear, concave)	None	Between group difference was $p < 0.0001$ for Ti, RR, (pt _{if} +pt _{ef})/V _t , Te, V _t /Ti, MV, ti _{f50} , pt _{if} , and $p < 0.05$ pt _{ef} /Tp _{tef} , pt _{ef} , Tp _{tef} , te _{f75} , te _{f50} , te _{f25} , Vp _{tef} . No group difference for V _t , vp _{tef} /ve, Tp _{tef} /Te. Concave expiratory limbs found exclusively in the CLD group. Note: Many TB parameters were scaled with infant weight
Latzin <i>et al.</i> (2009)	Normal + preterm + preterm with BPD	239 + 58 + 127	44 w (post- concep- tion)	Tp _{tef} /Te	None	Tp _{tef} /Te was decreased significantly from normal to preterm to preterm with bronchopulmonary dysplasia (BPD). Within BPD group Tp _{tef} /Te decreased with increasing BPD severity. Group discriminating ability of Tp _{tef} /Te was found better than that of weight-adjusted FRC or lung clearance index (LCI).

Leonhardt <i>et al.</i> (2010)	Normal + obstructed + malacia + stenosis	37 + 91 + 37 + 30	3 – 24 m	Sphericity, triangularity, rectangularity, polynomial fit coefficients, ptef/ve, tef50/ve, tef25/ve, ptif/vi, tef50/tif50, tef50/tif10, tef25/ptef, vptef/ve, Te/Ti, Tptef/Te, Tptif/ti	None	A support vector machine could classify the subjects accurately using the TB parameters into ten clinical categories
Roehr <i>et al.</i> (2011)	Infants with right (R) + double (D) aortic arch anomaly (AAA)	10 + 7	Approx. 40 w (gesta- tional)	Qualitative assessment of TBFVL	None	Significantly more expiratory flow limitation in DAAA group as assessed by TBFVL shape
Schmalisch <i>et al.</i> (2013)	Premature infants that had + had not received mechanical ventilation	247 + 139	approx. 30 w	Tptef/Te	None	Tptef/Te was slightly but significantly higher in the group that had received mechanical ventilation

3.2.5 Longitudinal studies in tidal breathing analysis

Several studies have assessed the TB in a longitudinal setup in the timescale from several hours to 10 years.

In an early work of Martinez *et al.* (1988) the association between T_{ptef}/T_e before the age of 6 months and the incidence of lower respiratory tract illness (LRI) with or without wheezing between the age of 6 months and 1 year was studied in 124 infants. They found lower values of T_{ptef}/T_e to be associated with the wheezing LRI group but not with the non-wheezing LRI group. This trend was more evident in boys than girls. Interestingly, V_{maxFRC} was not associated with the disease outcome.

Clarke *et al.* (1994) studied T_{ptef}/T_e in 22 healthy infants, and 32 infants with mild LRI. T_{ptef}/T_e was found to decrease from the age of 1 to 6 months of age, but not from age 6 to 12 months of age in healthy infants. A similar trend was found in the LRI infants, but it was not statistically significant ($p > 0.05$). In a rather similar study, Yuksel *et al.* (1996) assessed the predictive value of low T_{ptef}/T_e measured during the first week of life for persistent respiratory symptoms at the age of one year. Although the findings were statistically significant, the positive prediction value (PPV) of low T_{ptef}/T_e (< 0.40) was quite modest (PPV 33 % in boys, 47 % in girls) and was considered not to be clinically useful. In a longer 10-year follow-up study having the first measurement shortly after birth Håland *et al.* (2006) found a T_{ptef}/T_e value at or below median value at infancy to predict higher incidence of past or current asthma and severe bronchial hyperresponsiveness. The PPV of low value of T_{ptef}/T_e (here < 0.20) was found to be 31 % for predicting a history of asthma and 14.6 % for current asthma.

Young *et al.* (1994) studied T_{ptef}/T_e in 252 infants at age 1, 6, and 12 months. The group of 19 flow limited children had significantly lower T_{ptef}/T_e than controls at 1 month, and later increased prevalence of atopy and asthma. The value of T_{ptef}/T_e , however, declined in the control group at 6 and 12 months so that there was no significant difference to the flow limitation group.

Lødrup Carlsen *et al.* (1997) found a decrease in T_{ptef}/T_e and V_{ptef}/V_e from the first hour of life to the next day, which was accounted for entirely by an increase in the expiratory time and volume.

In a cohort of 10 healthy infants, 10 infants with a history of wheezing and 10 infants with CLD, Frey *et al.* (2001) found TB parameters to associate with either maturation or disease state depending on the TB parameter at ages 1, 6 and 12 months.

The effect of pharmacological treatment on TB was investigated by Devulapalli *et al.* (2004). They studied the effect of ICS therapy on T_{ptef}/T_e measured at 1 year and 2

years of age. The study included children divided into three groups of controls (n=13) and children with recurrent bronchial obstruction (n=54) with or without ICS treatment. At the age of 1 year there were significant differences ($p < 0.05$) in Tptef/Te between groups, but there were no significant changes in Tptef/Te in any group between the first and second measurement. In the ICS treatment group there was, however, a borderline significant change ($p=0.06$) that correlated with the duration of the treatment ($r=0.48$, $p=0.03$).

Proietti *et al.* (2014) recorded VT, RR, and Tptef/Te shortly after birth in 166 preterm infants. They found all parameters to be associated with wheeze at the age of one year. However, the predictive value in an individual child was found to be weak.

Asai *et al.* (1990, 1991) presented two studies where they recorded inspiratory and expiratory time and their ratio using IP. In the first study they found Te/Ti ratio to increase during asthma attack measured at 3pm in 19 asthmatic and 18 control subjects. In the second, arguably more interesting study, they recorded Te/Ti at 3 pm and overnight in 5-15 year old asthmatics and 11 healthy controls. The subjects had been symptom-free for at least 2 weeks and bronchodilator and antiallergic medication were withdrawn 12 hours before the study. Te/Ti was not found different between the groups at 3 pm, but was significantly different during the night, asthmatics having a higher value of Te/Ti as expected (prolonged expiration). Within the asthmatics there was also a significant difference between the measurement at 3 pm and the night measurement. Such a difference was not seen in the control group. Despite the statistical difference, there was still a rather large overlap between the groups in the Te/Ti values.

Chapter 4

Materials and methods

In the following, a short summary of the materials and methods common to all five studies is presented. Methods specific to each study are presented in their respective Sections 4.1-4.5.

Subjects: Publication I: healthy adult male subjects (n=20); Publication II: healthy adult subjects (n=16, 6 female); Publication III: healthy adult male subjects (n=10); Publication IV: healthy adult subjects (n=17, 4 female); Publication V: children aged 3-7 years with lower respiratory tract symptoms (n=21).

Equipment: In publications I-IV the flow or integrated flow signal was obtained with heated PNT (A. Fleisch No. 3, Lausanne, Switzerland) that was connected to a differential pressure transducer (SS40L, Biopac Systems, Goleta, CA 93117, USA), and the IP and ECG signals were obtained with a bioimpedance measurement device (EBI100C, Biopac Systems). In publication V the flow signal was obtained with an integrated PNT system (Masterscreen PFT, Jaeger, Germany) and the IP and ECG signals with a custom-made portable recorder similar to that presented by Vuorela *et al.* (2010). In publication IV the subjects wore a face mask (7900 Series, Hans Rudolph, Shawnee, KS, USA) connected to resistor element (7100R, Hans Rudolph), but in other studies the PNT was connected to a mouth piece with no added resistance.

CGO attenuation: In Publication I the CGOs were attenuated using a Savitzky-Golay filter (Savitzky & Golay, 1964), but in the later publications the method developed in Publication II was used.

Electrode locations: In Publications I and III various configurations were used. In Publication II a bilateral midaxillary configuration close to the axilla was used and in IV and V the configuration B presented in III was used. All measurements were done using a tetrapolar system.

4.1 Concept of flow measurement with impedance pneumography

A simultaneous recording of impedance and flow with PNT was performed on the subjects. For each subject three lateral and two anteroposterior electrode configurations were tested in standing, dorsal supine and lateral supine postures. The electrodes were textile electrodes sewn into a belt around the thorax. The subjects varied their tidal volume according to a requested respiratory pattern to induce different depths of breaths. Statistically, the agreement of flow signal between PNT and IP was assessed using standard error of measurement (SEM) in order to enable comparison with previous investigators who studied the agreement between RIP and PNT (Carry *et al.*, 1997, Eberhard *et al.*, 2001). SEM is defined as the mean of the squared difference signal IP-PNT divided by the variance of the PNT signal.

Presented as Publication I

4.2 Method for suppressing cardiogenic oscillations

A simultaneous recording of impedance, ECG and flow with PNT was performed on sitting subjects. A signal processing method to attenuate the CGO was developed using the Matlab software suite. The performance of the developed method was benchmarked against a conventional low pass filter and a Savitzky-Golay smoothing filter. The low pass filter was the first obvious candidate for this task because in general the respiratory part of the impedance signal lies at lower frequency than the cardiac part. The Savitzky-Golay filter was included because it was used in our previous study (Publication I).

There are two main requirements for a filter in this purpose. Firstly, it must attenuate the cardiac part maximally and secondly, it must introduce minimal (preferably none at all) distortion to the respiratory part. To assess these properties two types of signal processing tests were devised. In the first test their empirical frequency response with respect to the heart rate frequency was assessed by running them on the recorded impedance signals. In the second test a signal representing the pure respiratory part of the impedance signal was obtained by integrating the PNT flow signal into a volume signal. This signal was then filtered with each of the three methods and T_{ptef}/T_e (see Section 3.2.1), a widely used clinical TB flow parameter, was derived from the signal before and after each filtering. Any change in the value of T_{ptef}/T_e indicated that the filter had distorted the respiratory signal.

Presented as Publication II

4.3 Novel electrode placement strategy

The performance of three earlier used and one new electrode configuration was tested in standing subjects. Alongside impedance measurement, the respired volume signal was obtained simultaneously as integrated PNT flow signal. The test procedure included TB and slow VCMs. The four tested electrode configurations had electrodes A) on the arms between elbow and shoulder, B) on the arms and sides of thorax, C) high and D) low on the side of the thorax. Configuration B had not been presented earlier.

The TB and slow VCMs were analysed separately for linearity between impedance change and lung volume change. The linearity was quantified by fitting a line to the impedance vs volume plot and assessing the coefficient of the determination R^2 . In addition, the shape of each $\Delta Z/\Delta V$ curve was determined as being convex, linear or concave.

Presented as Publication III

4.4 Accuracy during respiratory loading

In this study a simultaneous impedance and PNT recording was performed on supine subjects. The subjects wore a face mask with a two-way valve directing the expired flow to a PNT. The subjects performed three minutes of TB with and without expiratory loading. The loading was realised by placing a a 15 cm_{H₂O}/L flow resistive element after the PNT. In addition, the pressure at mouth was recorded to detect mask leaks and to assess the effect of the expiratory loading.

For each measurement averaged TB expiratory flow-volume curves were derived from PNT and impedance signals under free and loaded conditions. The similarity of the shapes of these curves was assessed as the highest distance between the curves, d_{\max} , after normalising flow and volume to range 0...100 %.

Presented as Publication IV

4.5 Accuracy in wheezy preschool children

This study recruited patients at Helsinki University Central Hospital suspected of having asthma as indicated by recurrent or persistent lower respiratory tract symptoms (wheeze, cough, and/or shortness of breath).

All the children underwent a bronchial challenge test procedure. During the test four one-minute TB recordings were performed simultaneously with IP and a PNT while sitting. Two recordings were performed at BL condition separated by few minutes, one after the highest methacholine dose of the test and one approximately ten minutes after the administration of a bronchodilator. The main rationale for this was to test the potentially degrading effect of a bronchial obstruction on the accuracy of IP.

The agreement between IP and PNT flow signals was analysed in three ways. Firstly, the more or less random difference, which could be considered noise, was assessed as the absolute sample-by-sample difference, D_{SS} , between the flow signals after normalising them with the tidal peak inspiratory flow of each measurement. Secondly, in order to understand whether the signals exhibit a flow rate or respiratory phase dependent disagreement, non-linearity, the signals were plotted against each other and pooled into bins with respect to the flow rate in steps of 25 % of peak inspiratory flow, as illustrated in Figure 5.5A. The absolute mean value of these bins was presented as D_L for each one-minute recording. Finally, the agreement was assessed by deriving previously presented clinically relevant TB indices T_{ptef}/T_e , V_{ptef}/V_e and S from both signals and comparing them.

Presented as Publication V

Chapter 5

Results

5.1 Concept of flow measurement with impedance pneumography

The lateral electrode configurations (C1, C2, and C4 in Figure 5.1) showed better agreement with the PNT in the flow measurement than did the anteroposterior ones (C3 and C5). The mean $\Delta Z/\Delta V$ ratio decreased by up to 80 % from standing position to supine positions. This was accompanied by an even stronger, typically threefold, increase in the CGO amplitude. The CGO was found to be a major source of IP-derived flow signal distortion. The Savitzky-Golay filter was found somewhat inadequate to attenuate the CGO because it introduced distortion (smoothing) in the respiratory waveform.

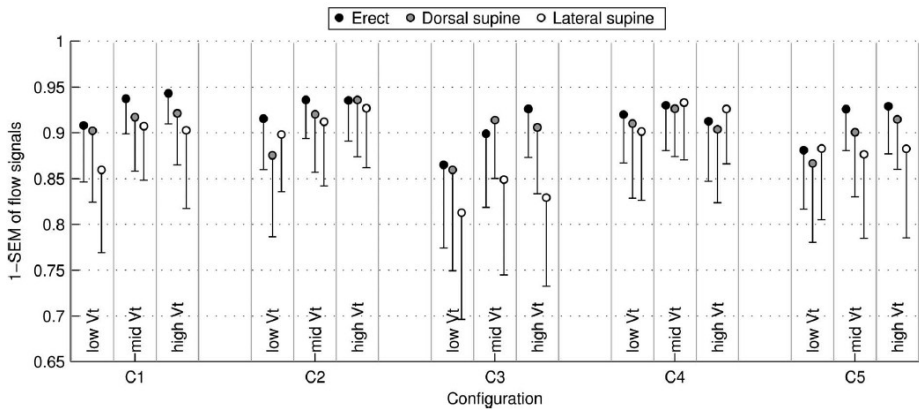


FIGURE 5.1: Flow signal agreement (1-SEM) between IP and PNT signals expressed as mean-SD. Breaths from all subjects were grouped into three categories of low (300–800 mL), middle (800–1800 mL), and high (1800–3500 mL) tidal volumes. Subject and posture-specific $\Delta Z/\Delta V$ ratios were used.

5.2 Method for suppressing cardiogenic oscillations

The developed CGO attenuation method could be considered to be an improved EA technique (Sörnmo & Laguna, 2005) where the averaged waveform (estimate of the CGO) is modulated by the respiration. The algorithm operates through the following steps.

CGO model generation:

1. High pass filter the impedance signal with a cutoff frequency of 0.6 times heart rate to attenuate the respiratory part without affecting the cardiac part.
2. Segment the individual CGOs from the high passed signal using the ECG signal for timing. The segmented CGOs are decimated to a fixed number of knot points (crosses in Figure 5.2) for spline fitting in step 5.
3. Put each decimated CGO into a bin (one of four, for instance) according to the lung volume at which it occurred. The relative lung volume is determined from the impedance signal.
4. Create a mean decimated CGO waveform for each bin and derive a linear equation for each knot point as to how they move according to tidal volume.

CGO cancellation using the model:

5. For each CGO interval in the raw impedance signal, generate a CGO estimate according to the instantaneous lung volume using the generated model. The waveform of matching length is generated by passing the generated knot points from the model to a spline interpolation function.
6. Cancel each CGO by subtracting the generated CGO waveform from the raw IP signal.

The aim of binning the CGOs according to lung volume is to account for the fact that respiration modulates the CGO waveforms (Sections 3.1.7.1, 6.1).

In the attenuation test the median values for signal attenuation at the heart rate frequency were -40 dB for the low pass filter, -10 dB for the Savitzky-Golay filter and -36 dB for the developed method.

In the respiratory signal distortion test the changes (mean \pm standard deviation) in T_{ptef}/T_e were 0.018 ± 0.064 for the low pass filter, 0.046 ± 0.059 for the S-G filter and 0.000 ± 0.018 for the new method.

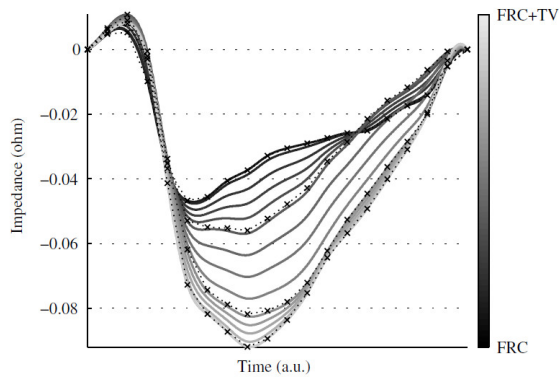


FIGURE 5.2: Typical change in CGO waveform with lung volume change during TB from FRC + tidal volume (TV). The x marks denote the 20 knot points of each of the four averaged volume bins. The waveforms to be subtracted are produced with cubic spline interpolation using the knot points adjusted to different lung volumes. Data from a single subject.

5.3 Novel electrode placement strategy

The new configuration B clearly outperformed the other three in terms of linearity between impedance change and lung volume change. The linearity as assessed by R^2 during TB was (mean \pm standard deviation) 0.92 ± 0.12 for A, 0.99 ± 0.01 for B, 0.97 ± 0.04 for C, and 0.77 ± 0.33 for D, and during the vital capacity manoeuvre 0.92 ± 0.12 for A, 0.99 ± 0.01 for B, 0.91 ± 0.07 for C, and 0.74 ± 0.17 for D. Although the mean value for configuration A and C was relatively close to that of configuration B, they both exhibit multiple individual cases of significant nonlinearity (even below $R^2 < 0.85$), whereas for configuration B the lowest value of all measurements is $R^2 = 0.96$. The characteristic shapes of the $\Delta Z / \Delta V$ curves were slightly convex for A, linear for B, and concave for C and D, as in Figure 5.3.

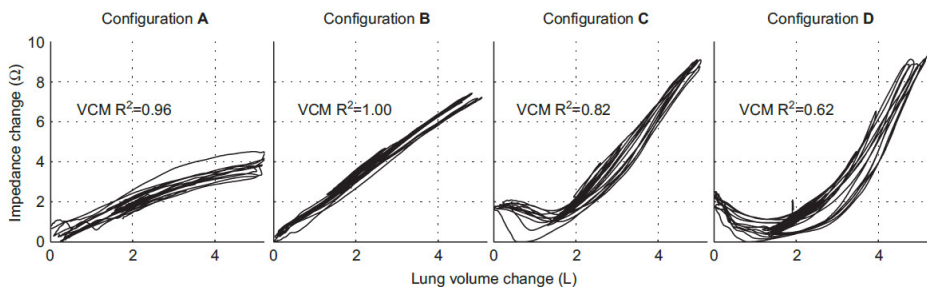


FIGURE 5.3: Typical impedance change-to-volume change curves during TB and VCMs with the four different electrode configurations measured from one subject.

5.4 Accuracy during respiratory loading

The expiratory loading produced changes in the shape of the flow-volume curves and increased the peak expiratory mouth pressure sevenfold, inducing changes in the respiratory mechanics.

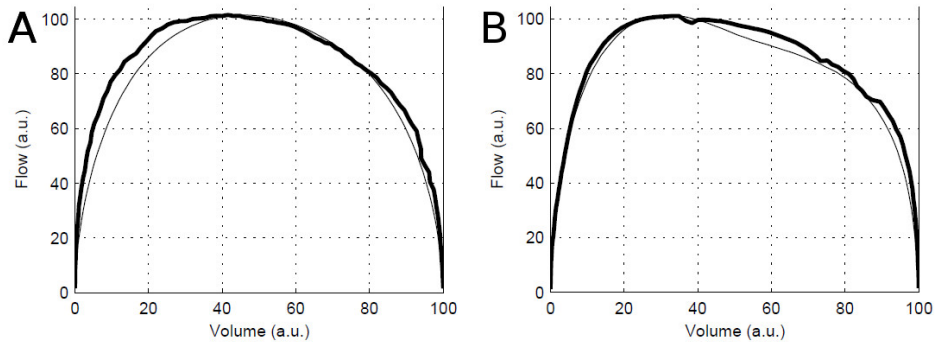


FIGURE 5.4: Expiratory tidal breathing flow-volume curves obtained simultaneously with impedance pneumography (thick line) and pneumotachograph (thin line) during free (upper) and loaded (lower) breathing having largest difference d_{\max} between PNT and IP 5.6 % ja 5.0 %, respectively.

The highest distance between the impedance and PNT derived curves, d_{\max} , was found to be $7.4 \% \pm 3.6 \%$ during free breathing and $6.2 \% \pm 3.0 \%$ under expiratory loading. The difference in d_{\max} between free and loaded condition was statistically non-significant ($p=0.46$).

5.5 Accuracy in wheezy preschool children

The mean absolute sample-by-sample difference, D_{SS} , between IP and PNT was found to be $5.7 \% \pm 1.2 \%$, $6.7 \% \pm 1.9 \%$, $6.9 \% \pm 1.4 \%$, and $7.5 \% \pm 2.0 \%$ at the BL1 and BL2, at MIB and at BD, respectively. The change in D_{SS} from mean of BL1 and BL2 was found significant in MIB ($p=0.003$) but not in BD ($P=0.277$).

The average deviation from linearity, D_L , was $2.4 \% \pm 1.0 \%$, $3.0 \% \pm 1.3 \%$, $2.6 \% \pm 0.9 \%$, and $3.1 \% \pm 1.4 \%$ for BL1, BL2, MIB, and BD, respectively. The change in D_L from mean of BL1 and BL2 was not found significant in MIB ($p=0.330$) nor in BD ($P=0.210$), but change from MIB to BD was found significant ($p=0.018$).

For the three TB parameters the difference (mean and 95 %-confidence interval) between IP and PNT was found to be 0.002 ($-0.097 \dots 0.093$), 0.007 ($-0.102 \dots 0.116$), and 0.083 ($-0.260 \dots 0.094$), respectively for T_{ptef}/T_e , V_{ptef}/V_e and S .

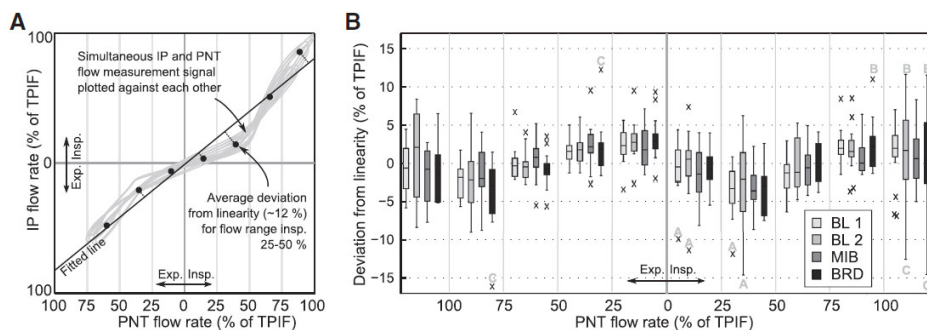


FIGURE 5.5: **A**: method for estimation of linearity between pneumotachograph (PNT) and impedance pneumograph (IP) flow rate signals. For each measurement sample the distance (deviation) from a fitted line is calculated and the median value (black dots) of the deviations is provided in each 25 % flow range. Each measured flow signal was normalized to 100 %, representing median tidal peak inspiratory flow (TPIF). **B**: linearity between PNT and IP in simultaneous flow rate measurement. Each column contains the results from 18-21 patients. The boxes denote the 25th-75th percentiles, the middle lines denote the median, and the whiskers extend to extreme values excluding outliers (crosses). Letters A-C next to extreme results denote the results of specific patients.

The change in T_{ptef}/T_e , V_{ptef}/V_e and S from BL to MIB state exceeded by 1.65 times the standard deviation of BL1 and BL2 of each subject in 6, 6, and 5 subjects respectively as assessed by the PNT, and in 6, 6, and 5 subjects respectively as assessed by the IP.

Chapter 6

Discussion

6.1 Cardiogenic oscillations

The general background on CGO is presented in Section 3.1.7.1, but because respiration-induced variation in the cardiac impedance signal is an essential feature taken into account in the proposed filtering algorithm, some physiological and electrophysiological background on this variation is discussed in the following.

In order to maintain the body homeostasis, the parts of the human cardiopulmonary system act in concert. The central nervous system, the respiratory muscles and the airway smooth muscle, and the heart and the vasculature are neuronally and mechanically interconnected. This enables them to work optimally under varying internal and external conditions. From the thoracic impedance signal standpoint there are two potential sources of respiratory variation in the cardiac signal: firstly, the actual physiological variation in the cardiac function and secondly, changes of and within the sensitivity field. In the following these two sources of variation and their implications for signal processing are discussed.

In healthy subjects, respiration-related cyclic physiological cardiac variation is known to occur within each breath at least in the following haemodynamic properties.

- Heart rate (Respiratory sinus arrhythmia, RSA) (Cloutier, 2007)
- Blood pressure (Dornhorst *et al.*, 1952, Santamore *et al.*, 1984)
- Stroke volume (Guz *et al.*, 1987, Santamore *et al.*, 1984)
- Mismatch between left and right ventricle stroke volume or pressure (Franklin *et al.*, 1962, Santamore *et al.*, 1984, Santamore & Dell'Italia, 1998)

- Variation in pulmonary vascular resistance (PVR). The direction of this change in alveolar capillaries is opposite to that in extra-alveolar vessels (Cloutier, 2007, Howell *et al.*, 1961, Whittenberger *et al.*, 1960)
- Variation in regional pulmonary blood flow distribution (Bouwmeester *et al.*, 2013, Holland *et al.*, 1968, Hughes *et al.*, 1968, Kaneko *et al.*, 1966)
- Lung blood volume (Brower *et al.*, 1985)

These effects may naturally be increased or attenuated in diseased subjects as compared to healthy ones. In addition they may present with other phenomena such as the Pulsus Paradoxus (Hamzaoui *et al.*, 2013). For instance, in asthmatic subjects during an exacerbation the respiratory pleural pressure swings are augmented due to the obstruction which induces abnormal blood pressure swings.

Now considering the recording of thoracic electrical impedance variations, the respiratory modulation of the cardiac activity must be viewed at two levels. Not only as the actual physiological respiratory variation of the various haemodynamic parameters described above, but also as the respiratory variation in how these cardiac oscillations are transformed into recorded impedance variations. Simply put, an increase in the relative blood content in the sensitivity field lowers the measured impedance, and vice versa, but as is the nature of the bioimpedance measurement, it is impossible to focus the measurement sensitivity field onto a certain anatomical structure such as the lungs or the aorta (Section 3.1.2). In practice, the measurement represents a sum signal of all impedance variations within its sensitivity field. Thus, it is difficult to determine in which proportion the recorded cardiac signal will be accounted for by the pulmonary circulation and which by systemic circulation (Section 3.1.7.1). The contents of the sensitivity field will change with breathing because respiration compresses and expands tissues and moves them in and out of the sensitivity field. Moreover, the spatial distribution of the sensitivity field in the thorax is not fixed or static either; instead, it will also likely undergo variations due to respiration.

There are only a few studies that present or discuss the existence of the respiratory variation in the cardiographic impedance signal and even fewer that consider its source. However, considering all the possible ways that respiration can affect the cardiac impedance signal, it would be ignorant not to take it into account when attempting to decompose these two mixed signals from a thoracic impedance signal.

Several important features of the thoracic impedance recordings are illustrated in an experiment in Figure 6.1: 1) CGO is modulated by the instantaneous lung volume, 2) the modulation of the CGO is more complex than simple amplitude modulation

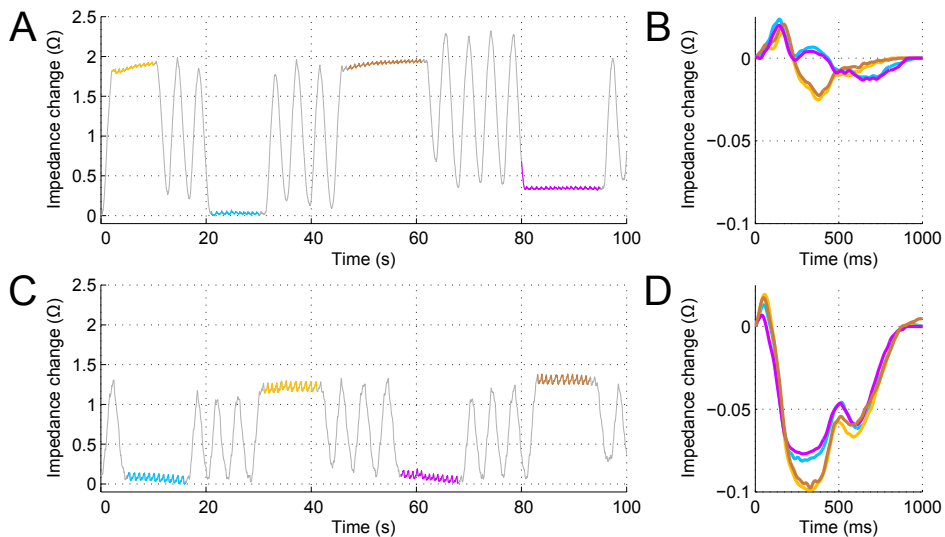


FIGURE 6.1: Illustration of the respiratory and posture originating variation in the CGO. Thoracic impedance measurements from a healthy male subject (age 37 years, height 184 cm, weight 78 kg) while standing (A, B) and supine (C, D) using the electrode configuration presented in the Publication III. The subject maintained apnoea with glottis open at end of inspiration and at end of expiration while breathing to a PNT (V_t approximately 900 mL). Panels B and D: Average CGO waveform established as an EA of each colored apneic section using the ECG R-waves as triggers.

(especially panel B), and 3) supine position increases the relative CGO amplitude and decreases that of respiration.

6.1.1 Considerations on the proposed filtering algorithm

From a signal processing point of view, there are three major features of the recorded thoracic impedance signal that affect the process of decomposing the cardiac and respiratory parts. Firstly, the power spectra of the two summed signals is partially overlapping. Thus, a conventional linear frequency domain filter would have to compromise between removing part of the desired signal and including part of the undesired signal. Secondly, neither one of the periodic signals are stationary, i.e. they vary over time. Thirdly, the signals are mutually dependent (Section 6.1, Figure 6.1). This last feature can be viewed either as a hindering or facilitating property, depending on the chosen signal processing approach. The filtering algorithm proposed in this thesis relies partially on this dependency.

The filtering algorithm presented in Publication II is based on the EA technique. Generally, in EA the aim is to discover the shape of a consistent impulse waveform of interest that occurs at known intervals but is buried in noise. This is achieved by aligning and

averaging a number of signal intervals that contain an impulse. In the averaging process as more and more samples are averaged, any part of the signal that is not aligned in time with the intervals will be attenuated eventually revealing the impulse shape. In this proposed algorithm the impulse is the pulsatile cardiac oscillation, the noise is represented by the respiratory or any other non-cardiac impedance variation and the intervals of the oscillations are determined from the R waves of the ECG signal.

The use of EA in this context was first implemented in an early work of Goldensohn & Zablow (1959) using analog electronics and later in the digital domain by Wilson *et al.* (1982) but they discovered that respiration induces variations in the cardiac oscillations that cannot be captured by a single averaged waveform. The method presented in this thesis aims to adapt the waveform to respiration-induced variations.

In the proposed approach the oscillation samples are divided into a number of bins, typically four, that are then averaged individually. The goal is that the bins would together represent the respiratory modulation of the cardiac oscillatory waveform. A crucial choice here is what attribute to use when selecting the bin for each oscillation. The first choice could be to use the phase of the respiration, for instance, early inspiration, late inspiration, early expiration, late expiration. This choice, even if having a solid physiological rationale, would not be feasible, because EA presumes that the unwanted signal components (respiration) present in the ensemble in a stochastic (random or pseudorandom) way with respect to the oscillatory signal. By binning according to the phase of the respiration, each ensemble would receive a similar kind of respiratory signal, for instance, always a descending convex shape. Thus, the respiratory part would not be removed in the averaging. The next obvious choice is to bin the oscillations according to the instantaneous lung volume. In this way, the respiratory signal part presents in a more stochastic way in the ensembles and can be averaged out as is done in the proposed algorithm.

Considering the various factors that may contribute to the respiratory variation in the haemodynamics and eventually in the recorded cardiac impedance signal (see Section 6.1), one could question whether the instantaneous lung volume is the correct choice as the parameter that modulates the cardiac signal. The actual physiological variation in the cardiac function exhibits rather complex coupling with respiration relating to both lung volume and respiratory phase. The respiratory variations caused in the impedance sensitivity field, however, are likely to have a rather simple lung volume dependency. Now, from a modelling standpoint, one should ask whether the physiological variations or the sensitivity field-related variations dominate the variation that is eventually seen in the impedance measurement. Current knowledge does not comprehensively answer this, but our studies give some evidence supporting the dominance of the sensitivity

field related variation over the physiological one: in Publication IV an intense expiratory loading was applied while having unloaded inspiration. Such loading should give rise to a strong respiratory phase relationship in the cardiac activity (Natarajan *et al.*, 1987), yet the proposed filter that assumes a volume, not phase, relationship performs well. A similar situation is witnessed due to the methacholine challenge as presented in Publication V, but also here, the proposed volume-binning filter performs well.

In general, for the application of IP in TB assessment, whichever approach is taken to remove the cardiac oscillation signal, that approach should not introduce any distortion that is consistent with the respiratory phase. This is because TB is typically analysed by EA of several respiratory cycles (see Section 3.2.3.3) which attenuates any out of phase components (nonrespiratory noise), but will not attenuate distortions that are in phase with respiration.

Within the presented interventions (respiratory loading and MIB) the proposed algorithm works well despite the complex mechanisms of how these interventions may affect the CGO. This suggests that the respiratory CGO modulation is more volume than phase oriented, which further suggests that the modulation stems from variations in the impedance sensitivity field rather than from the physiological haemodynamic changes.

6.2 Linearity between lung volume and impedance

6.2.1 Considerations on achieving maximal linearity

It is essential to understand that how the electrodes of IP are placed defines the spatial distribution of the measurement sensitivity field within the body (Section 3.1.2) which again defines how the physiological activities of interest are transformed into measurable impedance variations. Furthermore, it is important to realise that with a normal single-lead impedance measurement having the electrodes on the skin surface, one cannot achieve a sensitivity field that would include the whole of the lungs, but no other tissues.

When aiming for maximal lung area coverage, one could be tempted, for instance, to measure the impedance between the hip level and shoulder level with wide electrodes. This would, however, involve a considerable amount of other tissue types than lung. Including other tissue types is not a problem if their impedance contribution over time is approximately constant, but if the impedance varies, for instance, due to breathing by tissue movement, expansion, contraction, etc. they are likely to introduce a nonlinearity into the $\Delta Z/\Delta V$ relationship.

On the other hand, when aiming for maximal lung tissue specificity a very localised sensitivity field is desired. This is prone to lead to assessing only a small area of the lungs. Again, a nonlinearity is introduced because the spatial distribution of the lung aeration is known to be heterogeneous (small vs large airways, dependent vs nondependent regions). Thus when aiming for maximal linearity between the impedance and the lung volume one has to compromise between maximal lung area coverage and maximal tissue type (lung tissue) specificity.

6.2.2 Our findings on the linearity of impedance measurement

The linearity between the lung volume and the impedance was not yet a subject of analysis in Publication I, but something can be said about the linearity from the analysis presented in it. From the V_t estimations, one can see that the anteroposterior electrode configurations tend to show a concave $\Delta Z/\Delta V$ curve, whereas the lateral ones seem to be more linear. However, it must be noted that the manoeuvre the subjects performed did not include lung volumes below FRC which, according to our later studies, would have revealed a serious nonlinearity in the lateral configurations as well. Another interesting aspect of Publication I is the prominent decrease in the $\Delta Z/\Delta V$ ratio when lying down. Supine position decreases FRC, and thus one could hypothesise that the decrease is because the $\Delta Z/\Delta V$ curves of the presented configurations were, in fact, strongly concave (Figure 6.2, meas. B) at values below standing FRC level. This suspicion, however, does not seem to be true, as our later (unreported) findings showed that this supine decrease in the $\Delta Z/\Delta V$ ratio occurs in the highly linear electrode configuration of Publication III as well (Figure 6.1). In addition, it is possible that the use of textile electrodes has introduced another type of nonlinearity in the results, because the electrodes were sewn into a band around the thorax, whose tension, and thus electrode surface pressure, was likely to change slightly with the cyclic lung volume changes.

More attention was drawn placed on analysing the linearity of impedance change versus lung volume change after the partially negative results in the first two studies that involved patients instead of healthy volunteers. In the first case, the accuracy of IP to measure T_{ptef}/T_e was studied in 35 patients having airway obstruction of varying cause and severity (Seppä *et al.*, 2011a). Here, we noticed that the impedance signal was heavily distorted in 9 of the 35 patients and on closer examination we found the $\Delta Z/\Delta V$ curve to be concave (Fig. 6.2, Meas B.). These 9 subjects had a significantly increased body mass index (BMI). In the other case where we used impedance to assess the success of jet ventilation (Seppä *et al.*, 2011c), we discovered in many patients that the respiratory impedance signal started to diminish and finally disappeared after the

introduction of intravenous anaesthesia, despite the subjects being constantly ventilated with a mask.

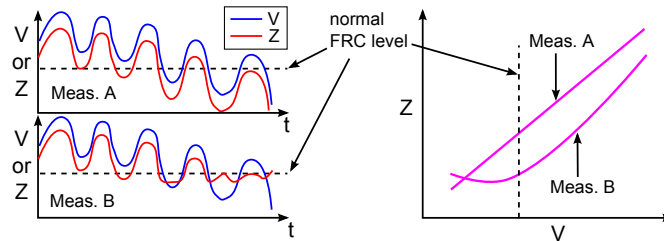


FIGURE 6.2: Illustration of the respiratory manoeuvre that we used to initially discover a nonlinearity in the IP measurement. Measurement A represents a desired impedance signal behaviour, but measurement B exhibits unwanted nonlinearity (concave $\Delta Z/\Delta V$ curve) at low lung volumes. In the manoeuvre TB was performed while gradually decreasing the end-expiratory lung volume. The red curve (Z) represents impedance and the blue curve (V) lung volume.

Soon after these findings we discovered that even in a normal healthy subject the impedance signal can be distorted if lung volume is deliberately lowered below the FRC level. This was revealed to us in an experiment where TB was performed while gradually lowering the tidal volume (Fig. 6.2). At levels above FRC level there were no problems, but when the lung volume was close to or below FRC, the impedance signal ceased to decrease during exhale or even showed a paradoxical increase (Fig. 6.2, Meas B.).

This finding provided a credible explanation for the distorted impedance signals in both previous studies. In the study of the obstructed patients, the problems were encountered in high BMI subjects. High BMI is linked with lowered FRC level (Jones & Nzekwu, 2006), thus these patients were more likely to breathe at low lung volumes, where we had discovered the impedance signal to fail to track volume changes (Fig. 6.2). In the other case of anaesthetised patients the problems arose when anaesthesia was introduced and maintained. General anaesthesia is also known to decrease the FRC level significantly (Barash *et al.*, 2001) and thus result in the same nonlinearity problem.

We discovered that as the location of the electrodes was moved downwards on the the midaxillary line the $\Delta Z/\Delta V$ ratio turned concave earlier during exhale, that is, at higher lung volume (unreported). However, even when the electrodes were placed very high, close to the axilla as in our earlier studies, the discovered nonlinearity was present especially below the normal FRC lung volume level. This led to the idea of placing the other electrode pair (voltage lead) on the arms to further lift the sensitivity field. Indeed, this seemed to provide a very linear $\Delta Z/\Delta V$ curve throughout the complete lung volume as, presented in Publication III. In addition, we included a configuration having the electrodes only on the arms, which was found to produce a convex (lowered impedance change at high volumes) nonlinearity in the $\Delta Z/\Delta V$ curve. The potential reasons for

the thorax-and-arms configuration to succeed are subject to discussion. Ideally, the IP signal should stem from the lung tissue alone (Figure 3.4). The lower configurations may suffer from the diaphragm and other non-lung tissues entering the sensitivity field when expiring deeply. They may also reflect the uneven emptying of the lung during exhalation, the dependent regions (caudal regions when upright) emptying first (Crawford *et al.*, 1989). Similarly, the high (cranial) sensitivity field created by the configuration having electrodes only on the arms tended to have convex shape, potentially reflecting the later emptying of the non-dependent regions. This hypothesis could be verified by repeating the measurements in the supine position. Furthermore, the more closely placed electrode pairs may include tissues closer to the surface of the body or within the region of the elbows. As discussed, any other tissue type than lung tissue that is within the sensitivity field is a potential source of nonlinearity in the $\Delta Z/\Delta V$ curve. One may hypothesise that the newly presented (Publication III) electrode configuration for IP succeeds because it fairly avoids the aforementioned error sources by creating a measurement sensitivity field with an optimal spatial distribution.

In Publication III the linearity was assessed in the volume-domain instead of the flow-domain. However, from a clinical standpoint the respiratory flow signal is more desirable than the volume signal. From the results presented in Publication III one might draw a conclusion that if impedance is linear with lung volume, then time-differentiated impedance should be linear with respiratory flow. However, caution should be exercised here, because differentiating the signals to flow-domain will augment any small, perhaps negligible, non-linearities that may be present in the volume-domain. It may also reveal nonlinearities that can only be seen consistently with respect to flow, not with respect to certain lung volume. This shortcoming was, however, fixed by Młyńczak *et al.* (2015) by flow-domain assessment.

Considering that the physiological source of the respiratory impedance variations has not been entirely agreed upon, one could raise a question as to how linear the impedance measurement is during conditions of altered respiratory mechanics, pressures and flow rates. Evidence on the robustness of IP, at least when using the newly proposed electrode configuration (Publication III), is presented in Publication IV. The expiratory loading increased the peak expiratory pressure at mouth approximately seven-fold, increased expiratory time by 50 % and reduced t_{pef} by 30 %. From the respiratory muscle control standpoint this also rendered normal passive expiration to be an active event involving intense muscle use (Gothe & Cherniack, 1980). This intervention did not degrade the accuracy of IP in deriving flow-volume curves, giving further evidence that the source of the impedance signal is indeed strongly related to the lung air content instead of other factors.

A more clinically relevant proof on the robustness of the linearity was presented in a study in preschool children (Publication V). This measurement protocol involved MIB and BD by salbutamol inhalation. The factors that had the potential to degrade the impedance measurement linearity included thoracoabdominal asynchrony due to obstruction (Allen *et al.*, 1990), and ventilatory heterogeneity and airway closure as induced by the MIB (Downie *et al.*, 2013, Filuk *et al.*, 1987). Despite these factors, the linearity between the impedance-derived and PNT-derived flow signals was very high. There were minor statistically significant changes in the linearity and random noise between the methods between BL, obstruction and BD states, but these were, arguably, below clinical significance.

6.2.3 On comparing two measurement modalities

When assessing the performance of a new measurement instrument against a gold standard reference, one may assess the agreement in different ways, such as the power of the difference signal, as difference in some parameter derived from both signals, or as the linearity between the two signals.

Of these three approaches, analysing the raw signal difference power, a single scalar, provides the least information on the nature of the disagreement between the two measurements. For instance, in the respiratory measurement context, the overall difference signal power could be rather small but there could be a consistent over or underestimation of the measured flow always at the beginning of expiration. This would yield erroneous flow curves, but go undetected if only looking at the difference power.

Deriving parameters that are of importance for the user from both signals could be considered a better option, but also its value is limited because the result is not generalisable to other potential parameters or other uses of the new method. For instance, in the context of TB analysis, deriving the parameter $T_{p\text{tef}}/T_e$ may yield good results even if the measurement is inaccurate in the late expiratory part, because the $T_{p\text{tef}}/T_e$ values are usually defined within the first half of expiration. Also, the parameter derivation itself may often not be straightforward and is thus a potential source of error.

The most generalisable result for the agreement is provided by assessing the linearity between the two measures over the whole value range that can be encountered. However, there are multiple ways of assessing the linearity and no method has been established as the convention for respiratory measurements.

Arguably, the most preferable way for assessing the agreement is to include linearity assessment and complement it with the other two analyses. Moreover, any measure that

allows direct comparison to earlier investigations should be included. Finally, in clinical respiratory measurements the flow signal is more desired over the volume signal, and any assessments should be made in the flow-domain.

6.3 Clinical potential and feasibility

Lung function testing is challenging in patient groups of limited co-operation or abilities such as disabled or elderly people or young children, because they cannot adequately perform the forced exhalations required in conventional spirometry. The current paediatric lung function testing techniques that require less patient co-operation are complicated, time-consuming and require special expertise and rather expensive equipment. Their availability for clinical practice is thus limited.

Continuous TB assessment enabled by the IP measurement employed in an ambulatory wearable measurement device (Vuorela *et al.*, 2010) provides interesting possibilities in the aforementioned patient groups. From a practical standpoint it is suitable for almost any patient group regardless of their physical and cognitive abilities. However, as IP is a rather indirect technique for respiratory flow measurement, the technique needs to be properly validated in the patient groups where one wishes to apply it to ensure its accuracy. In this thesis that particular group of interest was young asthmatic children.

Because of the limitations of suitable lung function tests, asthma diagnosis in preschool children is challenging. Because asthma is characterised by a time-varying spontaneously occurring airway obstruction, the ambulatory IP measurement could be of particular benefit as it enables continuous overnight measurements at home. Furthermore, it avoids the problems of more intrusive conventional TB measurement techniques (Section 3.2.3.1).

The particular findings that support the clinical feasibility of the developed IP method are

- Measures TB accurately in young children with wheezing symptom (Publication V)
- Measures TB accurately also during induced lower airway obstruction, which is a clinically relevant condition and a potential risk for the measurement accuracy (Publication V)
- Robust against severe alterations in respiratory mechanics and breathing style as induced by expiratory loading (Publication IV)

- Measurement device can be made into a wearable format (Vuorela *et al.*, 2010), which enables ambulatory long-term home measurements, for example during sleep.
- It is potentially feasible to measure the IP signal also with fabric electrodes sewn into a shirt (Publication I)

A negative result on the clinical feasibility were the weak BP- and BD-induced changes in the examined TB parameters in preschool children (Publication V). The changes were, however, similar between IP and PNT. Cutrera *et al.* (1991) found in older asthmatic children that the BP caused changes in TB parameter Tptef/Te and spirometric FEV1 that correlated at $r=0.61$ ($p < 0.001$), whereas in our study a correlation of $r=0.45$ ($p < 0.02$) was found between IP-derived Tptef/Te and an oscillometric parameter Rrs5. Morris *et al.* (1995) found no BP-induced change in Tptef/Te in adult asthmatics. However, it is noteworthy that IP avoids several shortcomings of conventional measurement equipment, not least the short assessment period, as discussed in Section 3.2.3.1, and may thus considerably improve the diagnostic accuracy of the TB parameters.

6.4 Limitations of the studies

Some limitations of the presented studies include the following.

- The study on children (Publication V) was performed on sitting subjects, although the planned clinical application of IP involves sleeping, supine subjects.
- The linearity of the proposed novel electrode configuration (Publication III) was assessed in that study only in the upright position. However, in Publication IV the configuration was studied in the supine position, but there only TB was performed, excluding the VCMs. The presented electrode configuration was also studied in other body positions by Młyńczak *et al.* (2015).
- The performance of the developed CGO filtering method was only analysed in upright subjects even though the CGO amplitude is considerably higher in the supine position. The performance of the filter was, however, indirectly assessed also in the supine position in Publication IV.

Chapter 7

Conclusions

From the studies conducted during the presented thesis research the following conclusions can be made.

- The concept of deriving respiratory flow signal from the IP signal was successfully demonstrated for the first time (Publication I)
- A filtering technique that efficiently removes the cardiac component while causing minimal distortion to the respiratory impedance signal was developed (Publication II)
- The impact of the electrode locations on the measured IP signal was studied and a novel electrode positioning that significantly enhances the impedance to lung volume linearity of the IP was presented (Publications I and III)
- With the combination of the filter and the electrode positioning, IP can accurately record tidal respiratory flow profile shapes and numeric TB parameters in a robust manner in adults and young children during different clinically relevant cardiorespiratory interventions (Publications IV and V)

Bibliography

- Abdulhay, E., Gumery, P., Fontecave, J., & Baconnier, P. 2009. Cardiogenic oscillations extraction in inductive plethysmography: Ensemble empirical mode decomposition. *Pages 2240–2243 of: Annual International Conference of the IEEE Engineering in Medicine and Biology Society, 2009. EMBC 2009.*
- Ackerman, M. 1998. The Visible Human Project. *Proceedings of the IEEE*, **86**(3), 504–511.
- Adams, J. A., Zabaleta, I. A., Stroh, D., & Sackner, M. A. 1993. Measurement of breath amplitudes: comparison of three noninvasive respiratory monitors to integrated pneumotachograph. *Pediatric Pulmonology*, **16**(4), 254–258.
- Albisser, A., & Carmichael, A. 1974. Factors in impedance pneumography. *Medical and Biological Engineering and Computing*, **12**(5), 599–605.
- Allen, J. L., Wolfson, M. R., McDowell, K., & Shaffer, T. H. 1990. Thoracoabdominal asynchrony in infants with airflow obstruction. *The American Review of Respiratory Disease*, **141**(2), 337–342.
- Allison, R. D., Holmes, E. L., & Nyboer, J. 1964. Volumetric dynamics of respiration as measured by electrical impedance plethysmography. *Journal of Applied Physiology*, **19**(1), 166–173.
- Ansari, S., Ward, K., & Najarian, K. 2014. Epsilon-Tube Filtering: Reduction of High-Amplitude Motion Artifacts from Impedance Plethysmography Signal. *IEEE Journal of Biomedical and Health Informatics*, **PP**(99).
- Asai, H., Onisawa, S., Furuya, N., Abe, T., & Ichimura, T. 1990. Breathing patterns in asthmatic children during attack. *The Journal of asthma: official journal of the Association for the Care of Asthma*, **27**(4), 229–236.
- Asai, H., Furuya, N., Ando, T., Asai, M., Yoshihara, S., & Ichimura, T. 1991. Breathing patterns during sleep in stable asthmatic children. *The Journal of asthma: official journal of the Association for the Care of Asthma*, **28**(4), 265–272.

- Aston, H., Clarke, J., & Silverman, M. 1994. Are tidal breathing indices useful in infant bronchial challenge tests? *Pediatric Pulmonology*, **17**(4), 225–230.
- Atzler, E., & Lehmann, G. 1932. Über ein neues Verfahren zur Darstellung der Herzstätigkeit (Dielektrographie). *Arbeitsphysiologie*, **5**(6), 636–680.
- Baker, L. E., & Geddes, L. A. 1966. Transthoracic current paths in impedance spirometry. *Pages 181–186 of: Proc. Symp. Biomed. Eng.*, vol. 1. Marquette University, Milwaukee.
- Baker, L. E., & Geddes, L. A. 1967. Transthoracic electrical impedance changes with pneumothorax. *In: 7th International Conference on Medical and Biological Engineering, digest.*
- Baker, L. E., Geddes, L. A., Hoff, H. E., & Chaput, C. J. 1966. Physiological factors underlying transthoracic impedance variations in respiration. *Journal of Applied Physiology*, **21**(5), 1491–1499.
- Banovcin, P., Seidenberg, J., & Der Hardt, H. V. 1995. Assessment of Tidal Breathing Patterns for Monitoring of Bronchial Obstruction in Infants. *Pediatric Research*, **38**(2), 218–220.
- Barash, M. P. G., Cullen, M. B. F., & Stoelting, M. R. K. 2001. *Handbook of Clinical Anesthesia*. Fourth edn. Lippincott Williams & Wilkins.
- Barros, A., Yoshizawa, M., & Yasuda, Y. 1995. Filtering noncorrelated noise in impedance cardiography. *IEEE Transactions on Biomedical Engineering*, **42**(3), 324–327.
- Bates, J. H. 1998. Detecting airways obstruction from the tidal flow profile. *European Respiratory Journal*, **12**, 1008–1009.
- Bates, J., Schmalisch, G., Filbrun, D., & Stocks, J. 2000. Tidal breath analysis for infant pulmonary function testing. ERS/ATS Task Force on Standards for Infant Respiratory Function Testing. European Respiratory Society/American Thoracic Society. *European Respiratory Journal*, **16**(6), 1180–1192.
- Benchetrit, G., Shea, S. A., Dinh, T. P., Bodocco, S., Baconnier, P., & Guz, A. 1989. Individuality of breathing patterns in adults assessed over time. *Respiration Physiology*, **75**(2), 199–209.
- Benoist, M. R., Brouard, J. J., Rufin, P., Delacourt, C., Waernessyckle, S., & Scheinmann, P. 1994. Ability of new lung function tests to assess methacholine-induced airway obstruction in infants. *Pediatric Pulmonology*, **18**(5), 308–316.

- Beydon, N., Davis, S. D., Lombardi, E., Allen, J. L., Arets, H. G. M., Aurora, P., Bisgaard, H., Davis, G. M., Ducharme, F. M., Eigen, H., Gappa, M., Gaultier, C., Gustafsson, P. M., Hall, G. L., Hantos, Z., Healy, M. J. R., Jones, M. H., Klug, B., Lødrup Carlsen, K. C., McKenzie, S. A., Marchal, F., Mayer, O. H., Merkus, P. J. F. M., Morris, M. G., Oostveen, E., Pillow, J. J., Seddon, P. C., Silverman, M., Sly, P. D., Stocks, J., Tepper, R. S., Vilozni, D., Wilson, N. M., & on behalf of the American Thoracic Society/European Respiratory Society Working Group on Infant and Young Children Pulmonary Function Testing. 2007. An Official American Thoracic Society/European Respiratory Society Statement: Pulmonary Function Testing in Preschool Children. *American Journal of Respiratory and Critical Care Medicine*, **175**(12), 1304–1345.
- Black, J., Baxter-Jones, A., Gordon, J., Findlay, A., & Helms, P. 2004. Assessment of airway function in young children with asthma: Comparison of spirometry, interrupter technique, and tidal flow by inductance plethysmography. *Pediatric Pulmonology*, **37**(6), 548–553.
- Bouhuys, A. 1957. The Clinical Use of Pneumotachography. *Acta Medica Scandinavica*, **159**(2), 91–103.
- Bouwmeester, J. C., Belenkie, I., Shrive, N. G., & Tyberg, J. V. 2013. Partitioning pulmonary vascular resistance using the reservoir-wave model. *Journal of Applied Physiology*, **115**(12), 1838–1845.
- Brower, R., Wise, R. A., Hassapoyannes, C., Bromberger-Barnea, B., & Permutt, S. 1985. Effect of lung inflation on lung blood volume and pulmonary venous flow. *Journal of Applied Physiology*, **58**(3), 954–963.
- Brown, B. H., Barber, D. C., Leathard, A. D., Lu, L., Wang, W., Smallwood, R. H., & Wilson, A. J. 1994. High frequency EIT data collection and parametric imaging. *Innovation et technologie en biologie et médecine*, **15**, 1–8.
- Carlsen, K.-H., & Lødrup Carlsen, K. C. 1994. Tidal breathing analysis and response to salbutamol in awake young children with and without asthma. *European Respiratory Journal*, **7**(12), 2154–2159.
- Carry, P.-Y., Baconnier, P., Eberhard, A., Cotte, P., & Benchetrit, G. 1997. Evaluation of Respiratory Inductive Plethysmography: Accuracy for Analysis of Respiratory Waveforms. *Chest*, **111**(4), 910–915.
- Citterio, G., Agostoni, E., Santo, A. D., & Marazzini, L. 1981. Decay of inspiratory muscle activity in chronic airway obstruction. *Journal of Applied Physiology*, **51**(6), 1388–1397.

- Clarke, J. R., Aston, H., & Silverman, M. 1994. Evaluation of a tidal expiratory flow index in healthy and diseased infants. *Pediatric Pulmonology*, **17**(5), 285–290.
- Cloutier, M. M. 2007. *Respiratory Physiology*. 1 edn. Philadelphia: Mosby Elsevier.
- Colasanti, R. L., Morris, M. J., Madgwick, R. G., Sutton, L., & Williams, E. M. 2004. Analysis of Tidal Breathing Profiles in Cystic Fibrosis and COPD. *Chest*, **125**(3), 901–908.
- Cooley, W. L., & Longini, R. L. 1968. A new design for an impedance pneumograph. *Journal of Applied Physiology*, **25**(4), 429–432.
- Crawford, A. B., Cotton, D. J., Paiva, M., & Engel, L. A. 1989. Effect of lung volume on ventilation distribution. *Journal of Applied Physiology*, **66**(6), 2502–2510.
- Cutrera, R., Filtchev, S. I., Merolla, R., Willim, G., Haluszka, J., & Ronchetti, R. 1991. Analysis of expiratory pattern for monitoring bronchial obstruction in school-age children. *Pediatric Pulmonology*, **10**(1), 6–10.
- Dames, K. K., Lopes, A. J., & de Melo, P. L. 2014. Airflow pattern complexity during resting breathing in patients with COPD: Effect of airway obstruction. *Respiratory Physiology & Neurobiology*, **192**, 39–47.
- Devulapalli, C. S., Haaland, G., Pettersen, M., Carlsen, K. H., & Carlsen, K. C. L. 2004. Effect of inhaled steroids on lung function in young children: a cohort study. *European Respiratory Journal*, **23**(6), 869–875.
- Dolfin, T., Duffy, P., Wilkes, D., England, S., & Bryan, H. 1983. Effects of a face mask and pneumotachograph on breathing in sleeping infants. *American Review of Respiratory Disease*, **128**(6), 977–979.
- Donaldson, G. C., Seemungal, T. A. R., Hurst, J. R., & Wedzicha, J. A. 2012. Detrended fluctuation analysis of peak expiratory flow and exacerbation frequency in COPD. *European Respiratory Journal*, **40**(5), 1123–1129.
- Dornhorst, A. C., Howard, P., & Leathart, G. L. 1952. Respiratory Variations in Blood Pressure. *Circulation*, **6**(4), 553–558.
- Downie, S. R., Salome, C. M., Verbanck, S., Thompson, B. R., Berend, N., & King, G. G. 2013. Effect of methacholine on peripheral lung mechanics and ventilation heterogeneity in asthma. *Journal of Applied Physiology*, **114**(6), 770–777.
- Eberhard, A., Calabrese, P., Baconnier, P., & Benchetrit, G. 2001. Comparison between the respiratory inductance plethysmography signal derivative and the airflow signal. *Advances in Experimental Medicine and Biology*, **499**, 489–494.

- Eiken, O., & Segerhammar, P. 1988. Elimination of breathing artefacts from impedance cardiograms at rest and during exercise. *Medical & Biological Engineering & Computing*, **26**(1), 13–16.
- Emralino, F., & Steele, A. M. 1997. Effects of technique and analytic conditions on tidal breathing flow volume loops in term neonates. *Pediatric Pulmonology*, **24**(2), 86–92.
- Fein, A., Grossman, R. F., Jones, J. G., Goodman, P. C., & Murray, J. F. 1979. Evaluation of transthoracic electrical impedance in the diagnosis of pulmonary edema. *Circulation*, **60**(5), 1156–1160.
- Fiamma, M.-N., Straus, C., Thibault, S., Wysocki, M., Baconnier, P., & Similowski, T. 2007a. Effects of hypercapnia and hypocapnia on ventilatory variability and the chaotic dynamics of ventilatory flow in humans. *American Journal of Physiology. Regulatory, Integrative and Comparative Physiology*, **292**(5), R1985–1993.
- Fiamma, M.-N., Samara, Z., Baconnier, P., Similowski, T., & Straus, C. 2007b. Respiratory inductive plethysmography to assess respiratory variability and complexity in humans. *Respiratory Physiology & Neurobiology*, **156**(2), 234–239.
- Filippone, M., Narne, S., Pettenazzo, A., Zacchello, F., & Baraldi, E. 2000. Functional approach to infants and young children with noisy breathing: validation of pneumotachography by blinded comparison with bronchoscopy. *American Journal of Respiratory and Critical Care Medicine*, **162**(5), 1795–1800.
- Filuk, R. B., Berezanski, D. J., & Anthonisen, N. R. 1987. Airway Closure with Methacholine-Induced Bronchoconstriction. *Journal of Applied Physiology*, **63**(6), 2223–2230.
- Fleming, P. J., Levine, M. R., & Goncalves, A. 1982. Changes in Respiratory Pattern Resulting from the Use of a Facemask to Record Respiration in Newborn Infants. *Pediatric Research*, **16**(12), 1031–1034.
- Franco, S. 2002. *Design with operational amplifiers and analog integrated circuits*. New York: McGraw-Hill.
- Franklin, D. L., Van Citters, R. L., & Rushmer, R. F. 1962. Balance between right and left ventricular output. *Circulation Research*, **10**(1), 17–26.
- Frey, U., Stocks, J., Sly, P., & Bates, J. 2000. Specification for signal processing and data handling used for infant pulmonary function testing. ERS/ATS Task Force on Standards for Infant Respiratory Function Testing. European Respiratory Society/American Thoracic Society. *European Respiratory Journal*, **16**(5), 1016–1022.

- Frey, U., Silverman, M., & Suki, B. 2001. Analysis of the harmonic content of the tidal flow waveforms in infants. *Journal of Applied Physiology*, **91**(4), 1687–1693.
- Frey, U., Brodbeck, T., Majumdar, A., Taylor, D. R., Town, G. I., Silverman, M., & Suki, B. 2005. Risk of severe asthma episodes predicted from fluctuation analysis of airway function. *Nature*, **438**(7068), 667–670.
- Geddes, L. A., Hoff, H. E., Hickman, D. M., & Moore, A. G. 1962. The impedance pneumography. *Aerospace Medicine*, **33**(Jan.), 28–33.
- Geddes, L. E., & Baker, L. E. 1972. Thoracic impedance changes following saline injection into right and left ventricles. *Journal of Applied Physiology*, **33**(2), 278–281.
- Geselowitz, D. B. 1971. An Application of Electrocardiographic Lead Theory to Impedance Plethysmography. *IEEE Transactions on Biomedical Engineering*, **18**(1), 38–41.
- Goldensohn, E. S., & Zablow, L. 1959. An electrical impedance spirometer. *Journal of Applied Physiology*, **14**(3), 463–464.
- Gonem, S., Umar, I., Burke, D., Desai, D., Corkill, S., Owers-Bradley, J., Brightling, C. E., & Siddiqui, S. 2012. Airway impedance entropy and exacerbations in severe asthma. *European Respiratory Journal*, **40**(5), 1156–1163.
- Gothe, B., & Cherniack, N. S. 1980. Effects of expiratory loading on respiration in humans. *Journal of Applied Physiology*, **49**(4), 601–608.
- Gracia, J., Seppä, V.-P., Viik, J., & Hyttinen, J. 2012. Multilead Measurement System for the Time-Domain Analysis of Bioimpedance Magnitude. *IEEE Transactions on Biomedical Engineering*, **59**(8), 2273–2280.
- Graham, M. 1965. Guard ring use in physiological measurements. *IEEE Transactions on Biomedical Engineering*, **12**(3), 197–198.
- Greenberg, H., & Cohen, R. I. 2012. Nocturnal asthma. *Current Opinion in Pulmonary Medicine*, **18**(1), 57–62.
- Greenough, A., Zhang, Y.-X., Yüksel, B., & Dimitriou, G. 1998. Assessment of prematurely born children at follow-up using a tidal breathing parameter. *Physiological Measurement*, **19**(1), 111–116.
- Grimnes, S., & Martinsen, O. 2008. *Bioelectricity and bioimpedance basics*. London: Academic.

- Guz, A., Innes, J. A., & Murphy, K. 1987. Respiratory modulation of left ventricular stroke volume in man measured using pulsed Doppler ultrasound. *Journal of Physiology*, **393**(1), 499–512.
- Habib, R. H., Pyon, K. H., Courtney, S. E., & Aghai, Z. H. 2003. Spectral characteristics of airway opening and chest wall tidal flows in spontaneously breathing preterm infants. *Journal of Applied Physiology*, **94**(5), 1933–1940.
- Hamilton, L., & Bruns, W. 1973. Impedance-measuring ventilation monitor for infants. *Annals of Biomedical Engineering*, **1**(3), 324–332.
- Hamilton, L. H., Beard, J. D., & Kory, R. C. 1965. Impedance measurement of tidal volume and ventilation. *Journal of Applied Physiology*, **20**(3), 565–568.
- Hamzaoui, O., Monnet, X., & Teboul, J.-L. 2013. Pulsus paradoxus. *European Respiratory Journal*, **42**(6), 1696–1705.
- Heistad, D. D., Wheeler, R. C., Mark, A. L., Schmid, P. G., & Abboud, F. M. 1972. Effects of adrenergic stimulation on ventilation in man. *Journal of Clinical Investigation*, **51**(6), 1469–1475.
- Hill, R., Jansen, J., & Fling, J. 1967. Electrical impedance plethysmography: a critical analysis. *Journal of Applied Physiology*, **22**(1), 161–168.
- Håland, G., Lødrup-Carlsen, K., Sandvik, L., Devulapalli, C. S., Munthe-Kaas, M. C., Pettersen, M., & Carlsen, K.-H. 2006. Reduced Lung Function at Birth and the Risk of Asthma at 10 Years of Age. *N Engl J Med*, **355**(16), 1682–1689.
- Holland, J., Milic-Emili, J., Macklem, P. T., & Bates, D. V. 1968. Regional distribution of pulmonary ventilation and perfusion in elderly subjects. *Journal of Clinical Investigation*, **47**(1), 81–92.
- Houtveen, J. H., Groot, P. F., & de Geus, E. J. 2006. Validation of the thoracic impedance derived respiratory signal using multilevel analysis. *International Journal of Psychophysiology*, **59**(2), 97–106.
- Howell, J. B. L., Permutt, S., Proctor, D. F., & Riley, R. L. 1961. Effect of inflation of the lung on different parts of pulmonary vascular bed. *Journal of Applied Physiology*, **16**(1), 71–76.
- Hughes, D. M., Lesouëf, P. N., & Landau, L. I. 1987. Effect of Salbutamol on Respiratory Mechanics in Bronchiolitis. *Pediatric Research*, **22**(1), 83–86.
- Hughes, J. M. B., Glazier, J. B., Maloney, J. E., & West, J. B. 1968. Effect of lung volume on the distribution of pulmonary blood flow in man. *Respiration Physiology*, **4**(1), 58–72.

- Hukushima, Y. 1970. Physiological Identification of Variation Sources of Transthoracic Electrical Impedance during Breath Holding. *Japanese Heart Journal*, **11**(1), 74–90.
- Hyvärinen, A., Karhunen, J., & Oja, E. 2001. *Independent Component Analysis*. S.l: Wiley-Interscience.
- Jackson, E., Stocks, J., Pilgrim, L., Dundas, I., & Dezateux, C. 1995. A critical assessment of uncalibrated respiratory inductance plethysmography (Respirace®) for the measurement of tidal breathing parameters in newborns and infants. *Pediatric Pulmonology*, **20**(2), 119–124.
- Jones, R. L., & Nzekwu, M.-M. U. 2006. The Effects of Body Mass Index on Lung Volumes. *Chest*, **130**(3), 827–833.
- Kaneko, K., Milic-Emili, J., Dolovich, M. B., Dawson, A., & Bates, D. V. 1966. Regional distribution of ventilation and perfusion as a function of body position. *Journal of Applied Physiology*, **21**(3), 767–777.
- Kauppinen, P., Hyttinen, J., Heinonen, T., & Malmivuo, J. 1998. Detailed model of the thorax as a volume conductor based on the visible human man data. *Journal of Medical Engineering & Technology*, **22**(3), 126–133.
- Kawakami, K., Watanabe, A., Ikeda, K., Kanno, R., & Kira, S. 1974. An analysis of the relationship between transthoracic impedance variations and thoracic diameter changes. *Medical & Biological Engineering*, **12**(4), 446–453.
- Kekonen, A. 2013. *Bioimpedance measurement device for chronic wound healing monitoring*. Master's thesis, Tampere University of Technology.
- Khambete, N. D., Brown, B. H., & Smallwood, R. H. 2000. Movement artefact rejection in impedance pneumography using six strategically placed electrodes. *Physiological Measurement*, **21**(1), 79–88.
- Kira, S., Hukushima, Y., Kitamura, S., Nakao, K., Kawakami, K., Watanabe, A., & Oshima, M. 1970. Variations of Transthoracic Electrical Impedance in Relation with Hemodynamic Changes of Pulmonary Circulation. *Japanese Heart Journal*, **11**(2), 149–159.
- Koumbourlis, A. C., Hurllet-Jensen, A., & Bye, M. R. 1997. Lung function in infants with sickle cell disease. *Pediatric Pulmonology*, **24**(4), 277–281.
- Krivoshei, A., Kukk, V., & Min, M. 2008. Decomposition method of an electrical bioimpedance signal into cardiac and respiratory components. *Physiological Measurement*, **29**(6), S15–S25.

- Kubicek, W. G., Kinnen, E., & Edin, A. 1964. Calibration of an impedance pneumograph. *Journal of Applied Physiology*, **19**, 557–560.
- Kuryloski, P., Giani, A., Gilani, K., Gravina, R., Seppä, V.-P., Seto, E., Shia, V., Wang, C., Yan, P., Yang, A. Y., Hyttinen, J., Sastry, S., Wicker, S., & Bajcsy, R. 2009. DexterNet: an open platform for heterogeneous body sensor networks and its applications. *Pages 92–97 of: Proceedings of the 6th Workshop on Body Sensor Networks*.
- Kyle, U. G., Bosaeus, I., Lorenzo, A. D. D., Deurenberg, P., Elia, M., Gómez-Meiz, J. M., Heitmann, B. L., Kent-Smith, L., Melchior, J.-C., Pirlich, M., Scharfetter, H., Schols, A. M., & Pichard, C. 2004. Bioelectrical impedance analysis—part II: utilization in clinical practice. *Clinical Nutrition*, **23**(6), 1430–1453.
- Latzin, P., Roth, S., Thamrin, C., Hutten, G. J., Pramana, I., Kuehni, C. E., Casaulta, C., Nelle, M., Riedel, T., & Frey, U. 2009. Lung Volume, Breathing Pattern and Ventilation Inhomogeneity in Preterm and Term Infants. *PLoS ONE*, **4**(2), e4635.
- Lødrup Carlsen, K. C., Mowinckel, P., & Carlsen, K.-H. 1992. Lung function measurements in awake compared to sleeping newborn infants. *Pediatric Pulmonology*, **12**(2), 99–104.
- Lødrup Carlsen, K. C., Stenzler, A., & Carlsen, K.-H. 1997. Determinants of tidal flow volume loop indices in neonates and children with and without asthma. *Pediatric Pulmonology*, **24**(6), 391–396.
- Lødrup Carlsen, K. C., Pettersen, M., & Carlsen, K.-H. 2004. Is bronchodilator response in 2-yr-old children associated with asthma risk factors? *Pediatric Allergy and Immunology*, **15**(4), 323–330.
- Lødrup Carlsen, K., Magnus, P., & Carlsen, K.-H. 1994. Lung function by tidal breathing in awake healthy newborn infants. *European Respiratory Journal*, **7**(9), 1660–1668.
- Lødrup Carlsen, K., Halvorsen, R., Ahlstedt, S., & Carlsen, K.-H. 1995. Eosinophil cationic protein and tidal flow volume loops in children 0-2 years of age. *European Respiratory Journal*, **8**(7), 1148–1154.
- Lehr, J. 1972. A Vector Derivation Useful in Impedance Plethysmographic Field Calculations. *IEEE Transactions on Biomedical Engineering*, **BME-19**(2), 156–157.
- Leonhardt, S., Ahrens, P., & Kecman, V. 2010. Analysis of tidal breathing flow volume loops for automated lung-function diagnosis in infants. *IEEE Transactions on Biomedical Engineering*, **57**(8), 1945–1953.

- Logic, J. L., Maksud, M. G., & Hamilton, L. H. 1967. Factors affecting transthoracic impedance signals used to measure breathing. *Journal of Applied Physiology*, **22**(2), 251–254.
- Lonky, S. A., & Tisi, G. M. 1980. Determining changes in airway caliber in asthma: the role of submaximal expiratory flow rates. *Chest*, **77**(6), 741–748.
- Luo, S., Afonso, V., Webster, J., & Tompkins, W. 1992. The electrode system in impedance-based ventilation measurement. *IEEE Transactions on Biomedical Engineering*, **39**(11), 1130–1141.
- Lynn, P. 1977. Feature filtering: the digital enhancement and suppression of periodic waveforms. *Electronics Letters*, **13**(7), 220–221.
- Macklem, P. T. 2008. Emergent phenomena and the secrets of life. *Journal of Applied Physiology*, **104**(6), 1844–1846.
- Malmivuo, J., & Plonsey, R. 1995. *Bioelectromagnetism: Principles and Applications of Bioelectric and Biomagnetic Fields*. 1 edn. Oxford University Press, USA.
- Manczur, T., Greenough, A., Hooper, R., Allen, K., Latham, S., Price, J., & Rafferty, G. 1999. Tidal breathing parameters in young children: Comparison of measurement by respiratory inductance plethysmography to a facemask pneumotachograph system. *Pediatric Pulmonology*, **28**(6), 436–441.
- Mangin, L., Lesèche, G., Duprey, A., & Clerici, C. 2011. Ventilatory Chaos Is Impaired in Carotid Atherosclerosis. *PLoS ONE*, **6**(1), e16297.
- Martinez, F. D., Morgan, W. J., Wright, A. L., Holberg, C. J., & Taussig, L. M. 1988. Diminished Lung Function as a Predisposing Factor for Wheezing Respiratory Illness in Infants. *New England Journal of Medicine*, **319**(17), 1112–1117.
- Mayer, O. H., Clayton, R. G., Jawad, A. F., McDonough, J. M., & Allen, J. L. 2003. Respiratory Inductance Plethysmography in Healthy 3- to 5-Year-Old Children. *Chest*, **124**(5), 1812–1819.
- Mayer, O. H., Jawad, A. F., McDonough, J., & Allen, J. 2008. Lung function in 3–5-year-old children with cystic fibrosis. *Pediatric Pulmonology*, **43**(12), 1214–1223.
- Min, M., Ojarand, J., Martens, O., Paavle, T., Land, R., Annus, P., Rist, M., Reidla, M., & Parve, T. 2012. Binary signals in impedance spectroscopy. *Pages 134–137 of: 2012 Annual International Conference of the IEEE Engineering in Medicine and Biology Society (EMBC)*.

- Minetti, A. E., Brambilla, I., & Lafortuna, C. L. 1987. Respiratory airflow pattern in patients with chronic airway obstruction. *Clinical physiology (Oxford, England)*, **7**(4), 283–295.
- Mishra, V., Bouayad, H., Schned, A., Hartov, A., Heaney, J., & Halter, R. 2012. A Real-Time Electrical Impedance Sensing Biopsy Needle. *IEEE Transactions on Biomedical Engineering*, **59**(12), 3327–3336.
- Miyamoto, Y., Takahashi, M., Tamura, T., Nakamura, T., Hiura, T., & Mikami, M. 1981. Continuous determination of cardiac output during exercise by the use of impedance plethysmography. *Medical and Biological Engineering and Computing*, **19**(5), 638–644.
- Morris, M. J., & Lane, D. J. 1981. Tidal expiratory flow patterns in airflow obstruction. *Thorax*, **36**(2), 135–142.
- Morris, M. J., Madgwick, R. G., Frew, A. J., & Lane, D. J. 1990. Breathing muscle activity during expiration in patients with chronic airflow obstruction. *European Respiratory Journal*, **3**(8), 901–909.
- Morris, M. J., Madgwick, R. G., & Lane, D. J. 1995. Analysis of tidal expiratory flow pattern in the assessment of histamine-induced bronchoconstriction. *Thorax*, **50**(4), 346–352.
- Morris, M. J., Williams, E. M., Madgwick, R., Banerjee, R., & Phillips, E. 2004. Changes in lung function and tidal airflow patterns after increasing extrathoracic airway resistance. *Respirology*, **9**(4), 474–480.
- Morris, M., Madgwick, R., Collyer, I., Denby, F., & Lane, D. 1998. Analysis of expiratory tidal flow patterns as a diagnostic tool in airflow obstruction. *European Respiratory Journal*, **12**(5), 1113–1117.
- Muskulus, M., Slats, A. M., Sterk, P. J., & Verduyn-Lunel, S. 2010. Fluctuations and determinism of respiratory impedance in asthma and chronic obstructive pulmonary disease. *Journal of Applied Physiology*, **109**(6), 1582–1591.
- Muzi, M., Jeutter, D. C., & Smith, J. J. 1986. Computer-Automated Impedance-Derived Cardiac Indexes. *IEEE Engineering in Medicine and Biology Society*, **33**(1), 42–47.
- Młyńczak, M., Niewiadomski, W., Żyliński, M., & Cybulski, G. 2015. Verification of the Respiratory Parameters Derived from Impedance Pneumography during Normal and Deep Breathing in Three Body Postures. *Pages 881–884 of: 6th European Conference of the International Federation for Medical and Biological Engineering*. Springer.

- Nakesch, H., Pfützner, H., Ruhsam, C., Nopp, P., & Futschik, K. 1994. Five-electrode field plethysmography technique for separation of respiration and cardiac signals. *Medical and Biological Engineering and Computing*, **32**(1), S65–S70.
- Natarajan, T. K., Wise, R. A., Karam, M., Permutt, S., & Wagner, Jr, H. N. 1987. Immediate effect of expiratory loading on left ventricular stroke volume. *Circulation*, **75**(1), 139–145.
- Nopp, P., Rapp, E., Pfützner, H., Nakesch, H., & Rusham, C. 1993. Dielectric properties of lung tissue as a function of air content. *Physics in Medicine and Biology*, **38**(6), 699–716.
- Nopp, P., Harris, N., Zhao, T.-X., & Brown, B. 1997. Model for the dielectric properties of human lung tissue against frequency and air content. *Medical & Biological Engineering & Computing*, **35**(6), 695–702.
- Nyboer, J. 1959. *Electrical Impedance Plethysmography: The Electrical Resistive Measure of the Blood Pulse Volume, Peripheral and Central Blood Flow*. Ch. C. Thomas.
- Olden, C., Symes, E., & Seddon, P. 2010. Measuring tidal breathing parameters using a volumetric vest in neonates with and without lung disease. *Pediatric Pulmonology*, **45**(11), 1070–1075.
- Onnela, N., Savolainen, V., Juuti-Uusitalo, K., Vaaajasaari, H., Skottman, H., & Hyttinen, J. 2012. Electric impedance of human embryonic stem cell-derived retinal pigment epithelium. *Medical & Biological Engineering & Computing*, **50**(2), 107–116.
- Otis, A. B., Fenn, W. O., & Rahn, H. 1950. Mechanics of Breathing in Man. *Journal of Applied Physiology*, **2**(11), 592–607.
- Ouyang, J., Gao, X., & Zhang, Y. 1998. Wavelet-based method for reducing respiratory interference in thoracic electrical bioimpedance. *Pages 1446–1449 vol.3 of: Proceedings of the 20th Annual International Conference of the IEEE Engineering in Medicine and Biology Society, 1998*, vol. 3.
- Pandey, V., Pandey, P., Burkule, N., & Subramanyan, L. R. 2011. Adaptive filtering for suppression of respiratory artifact in impedance cardiography. *Pages 7932–7936 of: 2011 Annual International Conference of the IEEE Engineering in Medicine and Biology Society, EMBC*.
- Patterson, R. 1989. Fundamentals of impedance cardiography. *IEEE Engineering in Medicine and Biology Magazine*, **8**(1), 35–38.

- Patzak, A., Foitzik, B., Mrowka, R., & Schmalisch, G. 2001. Time of measurement influences the variability of tidal breathing parameters in healthy and sick infants. *Respiration Physiology*, **128**(2), 187–194.
- Petro, D. J. 1969. *The origin of the signal in electrical impedance spirometry and application of the technique in clinical medicine*. Master's thesis, Baylor University. College of Medicine. Department of Physiology.
- Petrus, N. C., Thamrin, C., Fuchs, O., & Frey, U. 2014. Accuracy of tidal breathing measurement of floright compared to an ultrasonic flowmeter in infants. *Pediatric Pulmonology*, Pre-print.
- Pfützner, H., Futschik, K., Doblander, A., Schenz, G., & Zwick, H. 1990. A method for the elimination of artefacts in electric field plethysmography of the lung. *Frontiers of medical and biological engineering: the international journal of the Japan Society of Medical Electronics and Biological Engineering*, **2**(1), 53–63.
- Pickerd, N., Williams, E., & Kotecha, S. 2013. Electromagnetic inductance plethysmography to measure tidal breathing in preterm and term infants. *Pediatric Pulmonology*, **48**(2), 160–167.
- Plonsey, R., & Collin, R. 1977. Electrode guarding in electrical impedance measurements of physiological systems—a critique. *Medical and Biological Engineering and Computing*, **15**(5), 519–527.
- Proietti, E., Riedel, T., Fuchs, O., Pramana, I., Singer, F., Schmidt, A., Kuehni, C., Latzin, P., & Frey, U. 2014. Can infant lung function predict respiratory morbidity during the first year of life in preterm infants? *European Respiratory Journal*, **43**(6), 1642–1651.
- Roehr, C. C., Wilitzki, S., Opgen-Rhein, B., Kalache, K., Proquitté, H., Bühner, C., & Schmalisch, G. 2011. Early Lung Function Testing in Infants with Aortic Arch Anomalies Identifies Patients at Risk for Airway Obstruction. *PLoS ONE*, **6**(9), e24903.
- Rosell, J., & Webster, J. 1995. Signal-to-motion artifact ratio versus frequency for impedance pneumography. *IEEE Transactions on Biomedical Engineering*, **42**(3), 321–323.
- Sahakian, A. V., Tompkins, W. J., & Webster, J. G. 1985. Electrode Motion Artifacts in Electrical Impedance Pneumography. *IEEE Transactions on Biomedical Engineering*, **BME-32**(6), 448–451.
- Samara, Z., Raux, M., Fiamma, M.-N., Gharbi, A., Gottfried, S. B., Poon, C.-S., Similowski, T., & Straus, C. 2009. Effects of inspiratory loading on the chaotic dynamics of ventilatory flow in humans. *Respiratory Physiology & Neurobiology*, **165**(1), 82–89.

- Santamore, W. P., Heckman, J. L., & Bove, A. A. 1984. Right and left ventricular pressure-volume response to respiratory maneuvers. *Journal of Applied Physiology*, **57**(5), 1520–1527.
- Santamore, W. P., & Dell'Italia, L. J. 1998. Ventricular interdependence: Significant left ventricular contributions to right ventricular systolic function. *Progress in Cardiovascular Diseases*, **40**(4), 289–308.
- Sato, J., & Robbins, P. A. 2001. Methods for averaging irregular respiratory flow profiles in awake humans. *Journal of Applied Physiology*, **90**(2), 705–712.
- Savitzky, A., & Golay, M. J. E. 1964. Smoothing and Differentiation of Data by Simplified Least Squares Procedures. *Analytical Chemistry*, **36**(8), 1627–39.
- Schmalisch, G., Foitzik, B., Wauer, R., & Stocks, J. 2001a. Effect of apparatus dead space on breathing parameters in newborns: “flow-through” versus conventional techniques. *European Respiratory Journal*, **17**(1), 108–114.
- Schmalisch, G., Schmidt, M., & Foitzik, B. 2001b. Novel technique to average breathing loops for infant respiratory function testing. *Medical & Biological Engineering & Computing*, **39**(6), 688–693.
- Schmalisch, G., Wilitzki, S., & Wauer, R. 2005. Differences in tidal breathing between infants with chronic lung diseases and healthy controls. *BMC Pediatrics*, **5**(1), 36.
- Schmalisch, G., Wauer, R. R., Foitzik, B., & Patzak, A. 2003. Influence of preterm onset of inspiration on tidal breathing parameters in infants with and without CLD. *Respiratory Physiology & Neurobiology*, **135**(1), 39–46.
- Schmalisch, G., Wilitzki, S., Roehr, C. C., Proquitté, H., & Bühner, C. 2013. Differential effects of immaturity and neonatal lung disease on the lung function of very low birth weight infants at 48–52 postconceptional weeks. *Pediatric Pulmonology*, **48**(12), 1214–1223.
- Seddon, P. C., Davis, G. M., & Coates, A. L. 1996. Do tidal expiratory flow patterns reflect lung mechanics in infants? *American Journal of Respiratory and Critical Care Medicine*, **153**(4 Pt 1), 1248–1252.
- Segars, W. P., Sturgeon, G., Mendonca, S., Grimes, J., & Tsui, B. M. W. 2010. 4D XCAT phantom for multimodality imaging research. *Medical physics*, **37**(9), 4902–4915.
- Seppä, V.-P. 2007. *Bioimpedance in a wireless wearable device*. Master’s thesis, Tampere University of Technology.

- Seppä, V.-P., Väisänen, J., Kauppinen, P., Malmivuo, J., & Hyttinen, J. 2007. Measuring respirational parameters with a wearable bioimpedance device. *Pages 663–666 of: Proceedings of the 13th International Conference on Electrical Bioimpedance and the 8th Conference on Electrical Impedance Tomography.*
- Seppä, V.-P., Kööbi, T., Kähönen, M., Hyttinen, J., & Viik, J. 2011a. Impedance pneumography for assessment of a tidal breathing parameter in patients with airway obstruction. *European Respiratory Journal*, **38**(55 Suppl), 219s.
- Seppä, V.-P., Lahtinen, O., Väisänen, J., & Hyttinen, J. 2008. Assessment of breathing parameters during running with a wearable bioimpedance device. *Pages 1088–1091 of: Proceedings of the 4th European Congress for Medical and Biomedical Engineering.*
- Seppä, V.-P., Viik, J., Naveed, A., Väisänen, J., & Hyttinen, J. 2009. Signal waveform agreement between spirometer and impedance pneumography of six chest band electrode configurations. *Pages 689–692 of: Proceedings of the World Congress on Medical Physics and Biomedical Engineering.* Springer.
- Seppä, V.-P., Hyttinen, J., & Viik, J. 2010a. Agreement between impedance pneumography and pneumotachograph in estimation of a tidal breathing parameter. *Chest*, **138**(4 Suppl), 816A.
- Seppä, V.-P., Viik, J., & Hyttinen, J. 2010b. Assessment of pulmonary flow using impedance pneumography. *IEEE Transactions on Biomedical Engineering*, **57**(9), 2277–2285.
- Seppä, V.-P., Hyttinen, J., & Viik, J. 2011b. A method for suppressing cardiogenic oscillations in impedance pneumography. *Physiological Measurement*, **32**(3), 337–345.
- Seppä, V.-P., Wojciech, C., Harrison, L. C. W., Hyttinen, J., & Yli-Hankala, A. 2011c. Using impedance pneumography to estimate ventilatory changes during jet ventilation. *Pages 41–42 of: Proceedings of the 31st Congress of the Scandinavian Society of Anaesthesiology and Intensive Care Medicine.*
- Seppä, V.-P., Hyttinen, J., Uitto, M., Chrapek, W., & Viik, J. 2013a. Novel electrode configuration for highly linear impedance pneumography. *Biomedizinische Technik. Biomedical engineering*, **58**(1), 35–38.
- Seppä, V.-P., Pelkonen, A. S., Kotaniemi-Syrjänen, A., Mäkelä, M. J., Viik, J., & Malmberg, L. P. 2013b. Tidal breathing flow measurement in awake young children by using impedance pneumography. *Journal of Applied Physiology*, **115**(11), 1725–1731.

- Seppä, V.-P., Uitto, M., & Viik, J. 2013c. Tidal breathing flow-volume curves with impedance pneumography during expiratory loading. *Pages 2437–2440 of: Conference proceedings of 35th Annual International Conference of the IEEE Engineering in Medicine and Biology Society.*, vol. 2013.
- Seppänen, T. M., Alho, O.-P., & Seppänen, T. 2013. Reducing the airflow waveform distortions from breathing style and body position with improved calibration of respiratory effort belts. *BioMedical Engineering OnLine*, **12**(1), 97.
- Shee, C. D., Ploy-Song-Sang, Y., & Milic-Emili, J. 1985. Decay of inspiratory muscle pressure during expiration in conscious humans. *Journal of Applied Physiology*, **58**(6), 1859–1865.
- Sörnmo, L., & Laguna, P. 2005. *Bioelectrical Signal Processing in Cardiac and Neurological Applications*. Elsevier Academic Press.
- Stefanescu, S., Schlumberger, C., & Schlumberger, M. 1930. Sur la distribution électrique potentielle autour d'une prise de terre ponctuelle dans un terrain à couches horizontales, homogènes et isotropes. *Journal de Physique et le Radium*, **1**(4), 132–140.
- Stick, S. M., Ellis, E., Lesouëf, P. N., & Sly, P. D. 1992. Validation of respiratory inductance plethysmography ("Respirace") for the measurement of tidal breathing parameters in newborns. *Pediatric Pulmonology*, **14**(3), 187–191.
- Teulier, M., Fiamma, M.-N., Straus, C., & Similowski, T. 2013. Acute bronchodilation increases ventilatory complexity during resting breathing in stable COPD: Toward mathematical biomarkers of ventilatory function? *Respiratory Physiology & Neurobiology*, **185**(2), 477–480.
- Thamrin, C., Stern, G., Strippoli, M.-P. F., Kuehni, C. E., Suki, B., Taylor, D. R., & Frey, U. 2009. Fluctuation analysis of lung function as a predictor of long-term response to beta(2)-agonists. *European Respiratory Journal*, **33**(3), 486–493.
- Thamrin, C., Stern, G., & Frey, U. 2010a. Fractals for physicians. *Paediatric Respiratory Reviews*, **11**(2), 123–131.
- Thamrin, C., Taylor, D. R., Jones, S. L., Suki, B., & Frey, U. 2010b. Variability of lung function predicts loss of asthma control following withdrawal of inhaled corticosteroid treatment. *Thorax*, **65**(5), 403–408.
- Thamrin, C., Nydegger, R., Stern, G., Chanez, P., Wenzel, S. E., Watt, R. A., Fitz-Patrick, S., Taylor, D. R., & Frey, U. 2011. Associations between fluctuations in lung function and asthma control in two populations with differing asthma severity. *Thorax*, **66**(12), 1036–1042.

- Totapally, B. R., Demerci, C., Zureikat, G., & Nolan, B. 2002. Tidal breathing flow-volume loops in bronchiolitis in infancy: the effect of albuterol. *Critical Care*, **6**(2), 160–165.
- Turner, D. J., Morgan, S. E. G., Landau, L. I., & Lesouëf, P. N. 1990. Methodological aspects of flow-volume studies in infants. *Pediatric Pulmonology*, **8**(4), 289–293.
- Ulbrich, M., Mühlsteff, J., Sipilä, A., Kamppi, M., Koskela, A., Myry, M., Wan, T., Leonhardt, S., & Walter, M. 2014. The IMPACT shirt: textile integrated and portable impedance cardiography. *Physiological Measurement*, **35**(6), 1181–1196.
- Valdes, L. B. 1954. Resistivity Measurements on Germanium for Transistors. *Proceedings of the IRE*, **42**(2), 420–427.
- Valentinuzzi, M. E., Geddes, L. A., & Baker, L. E. 1971. The law of impedance pneumography. *Medical and Biological Engineering*, **9**(3), 157–163.
- van der Ent, C. K., Brackel, H. J., Mulder, P., & Bogaard, J. M. 1996a. Improvement of tidal breathing pattern analysis in children with asthma by on-line automatic data processing. *European Respiratory Journal*, **9**(6), 1306–1313.
- van der Ent, C. K., Brackel, H. J., van der Laag, J., & Bogaard, J. M. 1996b. Tidal breathing analysis as a measure of airway obstruction in children three years of age and older. *American Journal of Respiratory and Critical Care Medicine*, **153**(4), 1253–1258.
- van der Ent, C. K., van der Grinten, C. P., Meessen, N. E., Luijendijk, S. C., Mulder, P. G., & Bogaard, J. M. 1998. Time to peak tidal expiratory flow and the neuromuscular control of expiration. *European Respiratory Journal*, **12**(3), 646–652.
- Veiga, J., Lopes, A. J., Jansen, J. M., & Melo, P. L. 2012. Fluctuation analysis of respiratory impedance waveform in asthmatic patients: effect of airway obstruction. *Medical & Biological Engineering & Computing*, **50**(12), 1249–1259.
- Veiga, J., Lopes, A. J., Jansen, J. M., & Melo, P. L. 2011. Airflow pattern complexity and airway obstruction in asthma. *Journal of Applied Physiology*, **111**(2), 412–419.
- Vuorela, T., Seppä, V.-P., Vanhala, J., & Hyttinen, J. 2010. Design and implementation of a portable long-term physiological signal recorder. *IEEE Transactions on Information Technology in Biomedicine*, **14**(3), 718–725.
- Wang, X., Sun, H., & Van de Water, J. 1995. An advanced signal processing technique for impedance cardiography. *IEEE Transactions on Biomedical Engineering*, **42**(2), 224–230.

- Weltman, G., & Ukkestad, D. C. 1969. Impedance pneumograph recording across the arms. *Journal of Applied Physiology*, **27**(6), 907–909.
- Whittenberger, J. L., McGregor, M., Berglund, E., & Borst, H. G. 1960. Influence of state of inflation of the lung on pulmonary vascular resistance. *Journal of Applied Physiology*, **15**(5), 878–882.
- Williams, E. M., Madgwick, R. G., & Morris, M. J. 1998. Tidal expired airflow patterns in adults with airway obstruction. *European Respiratory Journal*, **12**(5), 1118–1123.
- Williams, E. M., Pickerd, N., Eriksen, M., Øyegarden, K., & Kotecha, S. 2011. Estimation of tidal ventilation in preterm and term newborn infants using electromagnetic inductance plethysmography. *Physiological Measurement*, **32**, 1833–1845.
- Wilson, A. J., Franks, C. I., & Freeston, I. L. 1982. Methods of filtering the heart-beat artefact from the breathing waveform of infants obtained by impedance pneumography. *Medical & Biological Engineering & Computing*, **20**(3), 293–298.
- Witsoe, D. A., & Kinnen, E. 1967. Electrical resistivity of lung at 100 kHz. *Medical and Biological Engineering*, **5**(3), 239–248.
- Woltjer, H. H., Bogaard, H. J., & De Vries, P. 1997. The technique of impedance cardiography. *European Heart Journal*, **18**(9), 1396–1403.
- Wysocki, M., Fiamma, M.-N., Straus, C., Poon, C.-S., & Similowski, T. 2006. Chaotic dynamics of resting ventilatory flow in humans assessed through noise titration. *Respiratory Physiology & Neurobiology*, **153**(1), 54–65.
- Yamamoto, Y., Mokushi, K., Tamura, S., Mutoh, Y., Miyashita, M., & Hamamoto, H. 1988. Design and implementation of a digital filter for beat-by-beat impedance cardiography. *IEEE Transactions on Biomedical Engineering*, **35**(12), 1086–1090.
- Young, S., Arnott, J., Le Souef, P. N., & Landau, L. I. 1994. Flow limitation during tidal expiration in symptom-free infants and the subsequent development of asthma. *The Journal of Pediatrics*, **124**(5, Part 1), 681–688.
- Yuksel, B., Greenough, A., Giffin, F., & Nicolaides, K. H. 1996. Tidal breathing parameters in the first week of life and subsequent cough and wheeze. *Thorax*, **51**(8), 815–818.
- Zhang, Y., Qu, M., Webster, J., Tompkins, W. J., Ward, B. A., & Bassett, D. R. 1986. Cardiac Output Monitoring by Impedance Cardiography During Treadmill Exercise. *IEEE Transactions on Biomedical Engineering*, **BME-33**(11), 1037–1042.

Publication I

Seppä, V.-P., Viik, J., & Hyttinen, J. 2010b. Assessment of pulmonary flow using impedance pneumography. *IEEE Transactions Biomedical Engineering*, 57(9), 2277-2285.

In reference to IEEE copyrighted material which is used with permission in this thesis, the IEEE does not endorse any of Tampere University of Technology's products or services. Internal or personal use of this material is permitted. If interested in reprinting/republishing IEEE copyrighted material for advertising or promotional purposes or for creating new collective works for resale or redistribution, please go to http://www.ieee.org/publications_standards/publications/rights/rights_link.html to learn how to obtain a License from RightsLink.

Assessment of Pulmonary Flow Using Impedance Pneumography

Ville-Pekka Seppä, Jari Viik, and Jari Hyttinen

Abstract—There is a lack of noninvasive pulmonary function measurement techniques suitable for continuous long-term measurement of tidal breathing in mobile subjects, although tidal breathing analysis has been shown to contain information that relates to the level airway obstruction. This article is the first to assess the suitability of impedance pneumography (IP) for measurement of continuous pulmonary flow and volume signals instead of only the respiration rate (RR) or tidal volume (V_T). We measured pneumotachograph (PNT) and IP signals simultaneously from 20 healthy male subjects in erect, dorsal supine, and lateral supine positions while voluntarily varying V_T . IP was measured using five different impedance lead configurations with electrodes integrated into a textile chest belt. The IP signals were compared with PNT signals to assess agreement of IP with a more well-established measurement method. The pulmonary flow signal waveform agreement was assessed with Standard Error of Measurement (SEM) between the time-differentiated IP signal and the PNT signal as $\rho=1$ -SEM. Additionally, we assessed the agreement of IP and PNT in V_T estimation, and the magnitude of the cardiogenic oscillation present in the impedance signal. The agreement in the pulmonary flow signal waveform shapes was found excellent at all tidal volumes and postures (mean $\rho > 0.90$). The agreement between the PNT-derived and the IP-derived V_T estimates was very high when IP values were calibrated per subject and posture (mean difference $< 3\%$). The main source of error in visual inspection of the IP signal was the cardiogenic distortion. From the five novel electrode configurations tested, the lateral ones were found clearly better than the anteroposterior ones. IP potentially enables the development of a noninvasive ambulatory measurement device for long-term studies of certain tidal breathing parameters in mobile subjects.

Index Terms—Bioelectric phenomena, impedance measurement, respiratory system.

I. INTRODUCTION

PRESENT clinical studies providing mechanical parameters of the airways involve stationary and bulky equipment as well as active patient co-operation. Due to this, they can only be utilized to reflect the airway patency at a brief moment. These studies involve methods like forced dynamic spirometry, forced oscillations and the interrupter technique [1]. There are less invasive, contact and non-contact methods available for respiration measurement, including impedance pneumography (IP), respiratory inductive plethysmography (RIP), and various magnetic, capacitive and optical methods [2]. They have limitations compared with the more obtrusive ones, but they also have numerous features that support their use. They do

not introduce dead space, increased mechanical respiratory impedance or psychological factors which may cause the subject to alter his respiratory pattern [3], [4], [5], which are important aspects especially in the tidal breathing analysis [6]. In addition, techniques like IP and RIP enable ambulatory measurements unlike, the magnetic, capacitive or optical methods. This enables a longer measurement period, potentially revealing valuable diagnostic information in the same manner as the Holter ECG in cardiologic studies. Respiratory volume and flow signal waveforms during tidal breathing contain pathological signs of, for instance, asthma [7], chronic obstructive pulmonary disease (COPD), cystic fibrosis, and airway obstruction in general [8], [9], [10]. Currently a tidal breathing study consists of a few minutes recording of free breathing conducted at a clinic using a face mask or a mouthpiece, but the use of the noninvasive recording equipment could extend these studies to longer periods in a more naturalistic setting, like at patient's home or work.

Several studies have tried to validate RIP and IP for respiration rate (RR) and tidal volume (V_T) estimation under various conditions [2]. Typically the noninvasive methods are found very accurate for RR estimation, but the V_T accuracy is degraded with subject posture or breathing mechanics (abdominal/rib cage) change due to a volume calibration factor change [11]. This compromises their suitability for long-term measurements requiring absolute volume information. While RR and V_T accuracy have been studied extensively, the ability of the methods to derive continuous flow or volume waveform shape has been ignored almost completely. Waveform shape is sufficient to estimate the two most referenced tidal breathing parameters, ratio of the volume at the tidal peak expiration flow to the expired volume (V_{PEF}/V_E) and the ratio of time at the tidal peak expiration flow to the expiration time (t_{PEF}/t_E), since they do not depend on absolute volume information [12]. Four published articles deal directly with the noninvasive breathing volume signal waveform by comparing it with a more established and direct measurement method like a pneumotachograph (PNT) or body plethysmograph. In one of these studies the IP technique [13] was utilized and its output compared with a pneumotachograph (PNT) integrated volume signal, and the rest [14], [15], [16] used the RIP technique in direct comparison with PNT flow signal.

The objective of this study was to evaluate the ability of the IP method in pulmonary air flow measurement. We compared IP-derived flow signal to the PNT signal of healthy male subjects using five novel electrode lead configurations in erect, dorsal supine, and lateral supine positions. In addition, the tidal volume estimation accuracy and the magnitude of the IP signal

Authors are with the Department of Biomedical Engineering, Tampere University of Technology, Tampere, FIN-33720 Finland. e-mail: ville-pekka.seppa@tut.fi

This work was funded by a grant from the Finnish Cultural Foundation. Manuscript received March XX, 2010; revised XX, 2010.

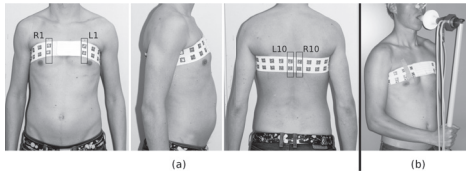


Fig. 1. (a) Subject with the wearable electrode array from anterior, lateral, and posterior views with four annotated electrode pairs and (b) subject with the complete measurement equipment setup. The electrodes were integrated into an elastic belt to enable easy and fast measurement of multiple impedance pneumography lead configurations. Photos shown with permission of the subject.

cardiogenic oscillations were assessed.

II. MATERIALS AND METHODS

A. Test Subjects and Measured Signals

The volunteers for the study were invited with an open call at the university. The measurement procedure and setup was described in detail with text and photos in the call. The subjects were not rewarded nor given any benefits. Written consents were obtained from all volunteers. Approval from the institutional review board was not required as the subjects were healthy students of the university, noninvasive instrumentation was used, physical challenge was minimal, and the subjects did not have chronic diseases or implanted devices. The study also gave the students valuable hands-on experience on physiological measurements for their studies.

The test population consisted of 20 healthy male subjects aged [24, 44] (mean 29.3) years. The body mass indexes were [20.8, 32.9] (mean 25.3), with five subjects over 28.0 and four subjects below 22.0. The thoracic circumferences on the level of the electrode belt were [85 cm, 116 cm] (mean 99 cm). None were smokers.

We recorded the IP signal using textile electrodes integrated into a chest belt (Fig. 1a), and pulmonary flow from mouth with a PNT (Fig. 1b).

B. Equipment

Bioimpedance was measured with a Biopac EBI100C electroimpedance amplifier. The bioimpedance device was used in tetrapolar configuration with excitation current of 400 μ A at 100 kHz frequency.

To connect the bioimpedance device with the subject, we used a custom-made flexible textile chest belt with 40 electrodes embroidered of silver yarn with snap buttons to connect the leads (Fig. 1a). Beneath each electrode there was a 2-mm-thick foam pad to improve the electrical conductivity of the skin-electrode interface. The electrode matrix consisted of two 20 electrode rows of square electrodes with an area of 225 mm² per electrode. The electrode center-to-center separation was 30 mm in vertical and horizontal direction. There was a 10-cm-long electrodeless area at both ends of the belt covered with a Velcro fastener to enable easy and fast placement.

All connection paths from the subject to the mains power network were through Biopac equipment satisfying the

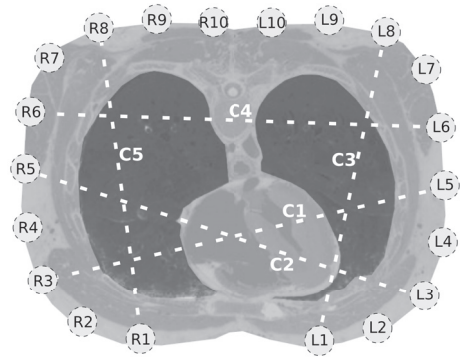


Fig. 2. An approximate sketch of the anatomical electrode locations. Each location L1-L10 or R1-R10 denotes a pair of vertically residing electrodes with a separation of 30 mm. Each configuration C1-C5 consists of two pairs (voltage and current), that is, four electrodes. The dashed lines showing the lead configurations do not represent the actual lead fields in the volume conductor. The figure is modified from a transversal slide photo at the axilla level from Visible Human Project® Man.

IEC60601-1 Medical Safety Test Standard and the Class I type BF medical equipment classification.

Pulmonary flow was measured with a heated PNT (A. Fleisch No. 3, Lausanne, Switzerland) with a mouth piece, a bacterial filter, and a light rigid plastic tube to support the device in front of the mouth. The pressure difference/flow value pairs reported by the manufacturer for the unit were 1/0.866, 5/4.331, 10/8.249 mmH₂O/l_s⁻¹. Thus, the unit operates in a region of high linearity in the range of flows that are encountered in normal human respiration.

The PNT was connected to a SS40L differential pressure transducer (Biopac Systems Inc., Goleta, CA 93117, USA). According to the specifications of the manufacturer, the operational pressure range of the transducer was ± 25 mmH₂O and the combined linearity and hysteresis error $\pm 0.05\%$. Thus, for the utilized PNT unit, with a flow of 1 l/s the flow error accounted for by the pressure transducer was ± 0.6 ml/s.

The pressure difference signal was amplified, conditioned with a 65 Hz low pass anti-aliasing filter and A/D converted with a Biopac MP35 unit at a 200 Hz sampling frequency. The MP35 unit was connected to a laptop computer that recorded and displayed the signal. A volume signal V_{PNT} was produced from the recorded flow signal \dot{V}_{PNT} by simple summing as $V_{PNT}(n) = \sum_{i=1}^n \dot{V}_{PNT}(i)T$, where n is the sample number and T is the sampling interval.

The fully-heated PNT and pressure transducer system was calibrated using a 3.00 liter calibration cylinder. The obtained PNT flow signal was integrated by the software and the volume value was observed for error. If error above $\pm 1\%$ was encountered, the system was re-calibrated. The room temperature or humidity were not monitored, but they were assumed to be quite static as the room was air conditioned.

C. Lead Configurations

In the tetrapolar impedance measurement, four electrodes are used: one pair (I+, I-) for injecting the excitation current

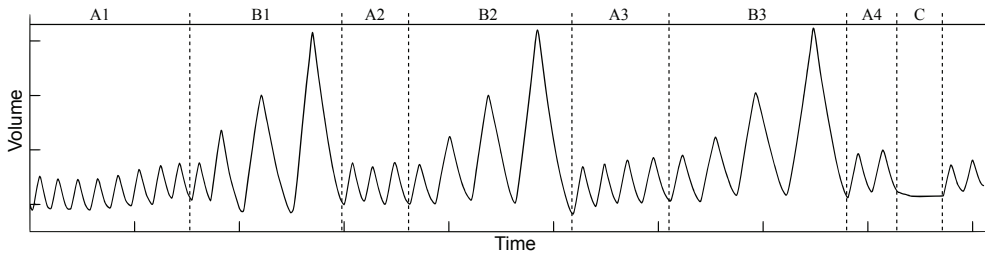


Fig. 3. An illustrative lung volume trace of the sequence of breathing maneuvers that the test subjects were asked to perform during the measurement. Phase A1-4: breathing with free rate and tidal volume. Phase B1-3: four breaths of increasing depth. Phase C: breath holding. The axes are left without units as the absolute volumes or times of respiration were not controlled.

and the other one ($V+$, $V-$) for measuring the voltage caused by the current. Changes in the measured voltage reflect the conductivity changes of the measured tissue region. Tetrapolar measurement configuration is usually favored over the bipolar one due to its capability of focusing the measurement sensitivity field into the area of interest and ignoring the electrode-skin impedance. The sensitivity field strength in the tissue is formed as the dot product of the lead fields of current electrodes \mathbf{J}_{LE} and voltage electrodes \mathbf{J}_{LI} . Thus the measured impedance value Z is obtained as

$$Z = \int_v \frac{1}{\rho} \mathbf{J}_{LE} \cdot \mathbf{J}_{LI} dv \quad (1)$$

where ρ is the conductivity distribution within the volume conductor v , the tissue region under examination [17].

$V+$ and $I+$ wires are connected to a vertical pair of electrodes, V wire in the upper electrode (Fig. 1a). The same applies for $V-$ and $I-$ wires. This should intuitively result in a sensitivity field distribution ($\mathbf{J}_{LE} \cdot \mathbf{J}_{LI}$) that is zero in the electrodes and weak in the subcutaneous fat, bone, and muscle tissues, but still has a large strong sensitivity area in the lung region. The resulting impedance signal is proportional to the changes in the lung air content.

The electrode array enables hundreds of different lead configurations, but we selected five of them for this study (Fig. 2). These five were chosen according to a preliminary single subject study using 38 different configurations considering high correlation with PNT signal and their mutual geometric independence. At the level of axilla the array is located approximately at the vertical middle line of the lungs which should intuitively focus the measurement sensitivity in the lung region. The five chosen configurations are referred to as lateral ($C1$, $C2$, $C4$) and anteroposterior ($C3$, $C5$) ones.

D. Measurement Procedure

The subjects were asked to control their breathing according to a sequence shown in Figure 3 consisting of different phases A, B, and C. The order of phases (ABABABAC) was the same for all subjects. The same measurement procedure was carried out while the subject was standing, lying on his back (dorsal supine) and lying on his right side (lateral supine) on a bed. These three measurements in different postures were repeated

for each of the five lead configurations (Fig. 2). Thus, the measurement procedure was conducted 15 times in total per subject. The configurations were always tested in the order of their numbering, but the number of the first configuration was always incremented by one between subjects. For example, if the order was $C1$, $C2$, $C3$, $C4$, $C5$ for first subject, then for the next one it was $C2$, $C3$, $C4$, $C5$, $C1$. This was to avoid systematic error due to the nervousness of the subject during the first measurements.

Phases A1-A4 consisted typically of 7, 4, 4, and 2 cycles of breathing at free pace and depth, but some variation in the cycle amount was allowed. For phases B1-B3, the subjects were asked to gradually increase their tidal volume during four consecutive breathing cycles so that the last one would be very deep. This induced variation in both volume and flow parameters. The respiration rate was completely free throughout the measurement except during phase C when the subjects were asked to hold their breath for approximately 10 seconds. This was to enable recording the pure cardiogenic oscillations of the impedance signal that can be considered noise in IP. They are caused by the pulsatile flow of blood in the thorax and their amplitude of the oscillations depends on the sensitivity field strength of a particular electrode configuration in areas of blood entering or leaving tissues.

To ensure good electrical conductivity at the electrode-skin interface, all four electrodes involved in the configuration to be tested were moistened with tap water right before each measurement using a syringe. To keep the belt in place while the subject was changing between positions, we added four strips of tape, two on the anterior and two on the posterior side. Subject was holding the PNT with one or both hands and wearing a nose clip (Fig. 1b). The electrodeless area of the belt was placed in the middle of the anterior side of the subject, where good electrode contact would have been hard to achieve due to the convex shape of the thorax. The electrode pairs were named L1-L10 and R1-R10 on the left and right side of the thorax, respectively, with the numbering ascending from the anterior to the posterior side (Fig. 2).

E. Signal Processing

The conditioning steps of the impedance signals is presented in Figure 4. Both the PNT volume signal and the impedance signal were first treated with linear filters (steps 1 and 2 in

Fig. 4). A low-pass filter ($f_p = 10 \text{ Hz}$, $f_s = 16 \text{ Hz}$, $A_s = 40 \text{ dB}$, $r_p = 0.1 \text{ dB}$, 10 Hz recommended by Bates et al. [18]) was applied to remove instrumentation noise. Then a high-pass filter was applied to remove baseline fluctuations and drift ($f_s = 0.01 \text{ Hz}$, $f_p = 0.1 \text{ Hz}$, $A_s = 40 \text{ dB}$, $r_p = 0.01 \text{ dB}$). The cardiogenic oscillations (CGO) in the impedance signal could not be removed with linear filtering due to their overlapping frequency spectrum with the breathing signal; instead, we applied a Savitzky-Golay (S-G) smoothing filter [19] (frame size 1000 ms, 2nd order fitting). The effect of the S-G filter is illustrated in Figure 5. It has the advantage of preserving the high frequency content of the signal occurring especially at the peaks of the cycles, but still effectively attenuating the CGO. The conditioned volume-related impedance signal V_{IP} was then turned into a flow-related one by differentiating it over time with an S-G filter (frame size 250 ms, 2nd order fitting). Finally, the \dot{V}_{IP} signal was obtained after further attenuating the CGO with a smoothing S-G filter (frame size 2000 ms, 2nd order fitting). The smoothing S-G filter frame size is an important consideration. The frame needs to be short to preserve the high frequency content and shape, but still long enough so, that it steps over the CGOs. The optimal frame sizes were found experimentally by comparing the filtered IP signal with the PNT signal. None of the processing steps introduced time delay in the signals.

To analyze individual breaths, the signals were segmented using the PNT flow signal as trigger. The applied algorithm is similar to the thresholding method described by Bates et al. [18] To illustrate the V_T and flow signal waveform estimation in breaths of different tidal volumes, each segmented breath was categorized by its V_T into regions of 300-800 ml, 800-1800 ml, and 1800-3500 ml.

The impedance-volume ratio was found for each breathing cycle, and the median value of these ratios was then used as a volume calibration factor throughout the recording to turn ohms into milliliters. This calibration was performed for each subject and posture. Increase in the calibration factor causes underestimation of volume and vice versa.

Cardiogenic oscillation magnitude measured during procedure phase C (Fig. 3) were defined as the ratios of peak-to-peak impedance change caused by cardiogenic oscillations (Ω) to impedance-volume sensitivity (Ω/ml) of that measurement. This results in magnitudes of oscillations in milliliters, which are then easy to relate to breathing volume signal magnitude.

F. Statistical Analysis

The flow signal agreement ρ between \dot{V}_{IP} and \dot{V}_{PNT} for each segmented breathing cycle consisting of n samples was assessed using the standard error of measurement (SEM) value as

$$\rho = 1 - SEM = 1 - \frac{\frac{1}{n} \sum_{i=1}^n [\dot{V}_{PNT}(i) - \dot{V}_{IP}(i)]^2}{Var(\dot{V}_{PNT})}, \quad (2)$$

to use the same measure as previous investigators [15], [16]. The value of ρ reflects the similarity of the \dot{V}_{IP} and \dot{V}_{PNT} signals calculated sample-by-sample. Value $\rho=1$ means that the signals

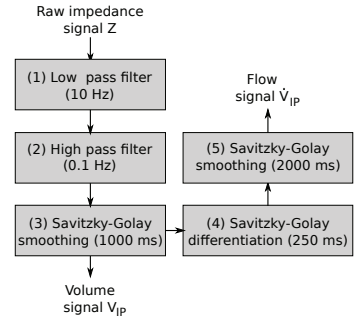


Fig. 4. Signal processing scheme from raw impedance signal to impedance-derived pulmonary volume and flow signals. The values in parentheses denote filter cutoff frequencies or Savitzky-Golay filter frame sizes.

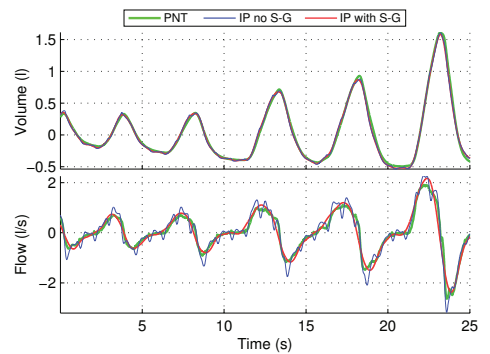


Fig. 5. Recorded pneumotachograph (PNT) and impedance pneumograph (IP) signals from subject 3 in erect posture using electrode configuration C4. IP signals are presented with and without the Savitzky-Golay (S-G) smoothing (phases 3 and 5 in Fig. 4) that attenuates the cardiogenic oscillations in IP signal. The non-filtered signal is not used in this study, it is merely presented to illustrate the effect of the filter.

are identical, a value below 1 means that they differ at some degree.

Few complete measurements were discarded due to the inability to obtain any sensible IP signal from the subject. The rejection was verified by a Pearson correlation value below 0.50 between V_{PNT} and V_{IP} . Some individual breathing cycles were also removed from otherwise acceptable measurement due to external errors of short duration. These cycles were verified to have ρ value below 0.50.

III. RESULTS

A. Flow Signal Waveform Agreement

\dot{V}_{IP} and \dot{V}_{PNT} signal waveform agreement using subject and posture specific impedance-volume calibrations are summarized in Figure 6. Additionally, results for each single measurement from the best configuration, C4, are presented in Table II. In most configurations, the signal agreement is highest (ρ close to 1.0) in the erect position and smallest in the lateral dorsal. In all configurations, the agreement improves with higher V_T . The signal agreement is generally higher in the lateral configurations (C1, C2, C4) than in the anteroposterior

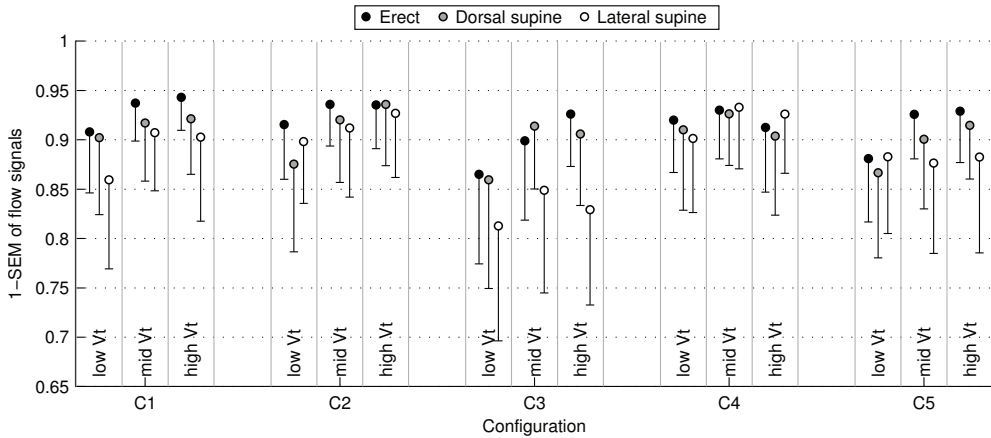


Fig. 6. Flow signal agreement (1-SEM) between the IP and the PNT signals expressed as mean-SD. Values include all non-discarded (Table I) individual breaths from all subjects grouped into three categories of low (300-800 ml), middle (800-1800 ml), and high (1800-3500 ml) tidal volumes. Subject and posture specific impedance-volume ratios were used.

ones (C3, C5). C4 was found best with mean ρ values between 0.90-0.95 in all postures and tidal volumes. A segment of flow signals from subject 3 using C4 are presented in Figure 5 having ρ values between 0.92-0.95.

B. Tidal Volume Agreement

The tidal volume estimation difference between IP and PNT using subject and posture specific impedance-volume calibrations are presented in Figure 7. In configurations C1 and C2, the difference means are under 3% in all postures and V_T regions except for the underestimation in C1 in dorsal and lateral supine posture with higher V_T . The anteroposterior configurations (C3, C5) exhibit a trend of moving from volume underestimation to overestimation in the IP-derived values as the V_T increases. C4 shows an opposite trend. The standard deviations (SD) of the differences are 8-16%.

Relative changes in the impedance-volume ratio (volume calibration factor) when changing from erect to dorsal and lateral supine postures are shown in Figure 8. In most cases, the ratio decreases. In C3 and C5 the mean change from erect to dorsal supine is only -6% and -3%, but the inter-subject variability in the change is still quite high, having SD 31% and 18%, respectively. Also, the change in the baseline thoracic impedance value had no correlation with the change in the calibration factor.

C. Cardiogenic Oscillations

Figure 9 presents the magnitudes of cardiogenic oscillations recorded during the measurement procedure phase C, breath holding (Fig. 3). For all configurations, the mean magnitudes of cardiogenic oscillations are at the lowest in the erect position, corresponding to a breathing volume signal of 70-100 ml. The lateral configurations (C1, C2, C4) exhibit mutually similar values with 70-85 ml median oscillation magnitude in the erect position and 180-210 ml in both supine postures. The

anteroposterior configurations (C3, C5) differ from the lateral ones mainly in the lower oscillation magnitude in the dorsal supine posture. If considering a normal tidal volume to be 500 ml, these oscillations have 15-45% magnitude compared to the tidal breathing signal.

D. Discarded Measurement Data

In total there were 300 measurement attempts, 100 per posture, of which 28 were unsuccessful. The distribution of the unsuccessful rejected measurements is presented in Table I. The measurements were almost completely successful in erect and dorsal supine positions, only 3 and 5 rejects, respectively. However, in lateral supine position 20 measurements were rejected. Configuration C2 was found to be most reliable with only 1 reject of the total of 60 measurement attempts. Generally, the lateral configurations (C1, C2, C4) were more reliable than the anteroposterior ones (C3, C5).

In the amount of discarded individual respiratory cycles (lower values in Table I) the lateral configurations have rejection rate at or below 4.0% in all postures, whereas the anteroposterior ones mostly have rates above 4.0%. Even a rate of 16.8% was found in lateral supine posture with configuration C3.

IV. DISCUSSION

We tested IP for the novel application of producing pulmonary flow signal. The agreement between IP-derived and PNT flow signal was found excellent ($\rho > 0.90$). In long-term ambulatory measurements, only semi-quantitative volume and flow values can be reliably produced, as the volume calibration factor changes with posture. However, this is not a problem for most tidal breathing parameters, like t_{PEEP}/t_E .

A. Flow Signal Waveform Estimation

This is the first article to report results on using the IP technique for establishing pulmonary flow signal. Similar

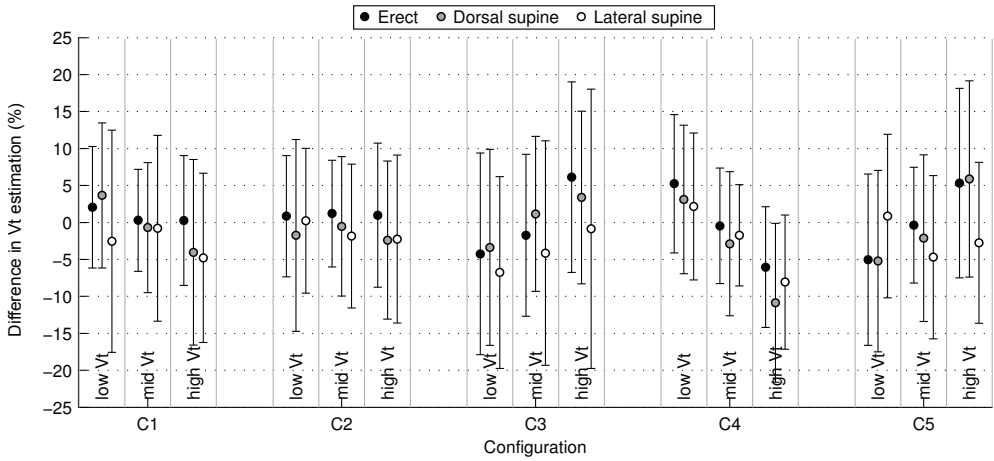


Fig. 7. Tidal volume assessment expressed as relative difference ($V_{T,IP} - V_{T,PNT}$) between the IP and PNT results as mean \pm SD. Values include all non-discarded (Table I) individual breaths from all subjects grouped into three categories of low (300-800 ml), middle (800-1800 ml), and high (1800-3500 ml) tidal volumes. Subject and posture specific impedance-volume ratios were used.

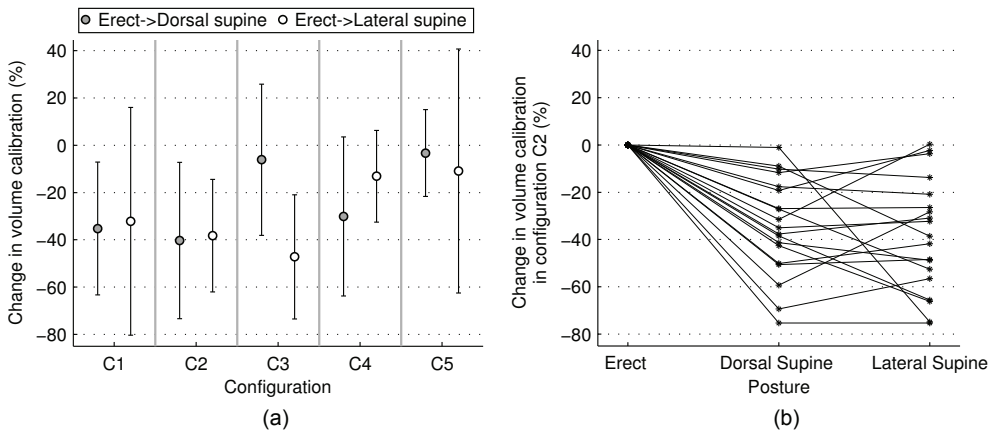


Fig. 8. (a) Relative changes in the impedance-volume sensitivity (calibration) expressed as mean \pm SD when changing from erect to dorsal or lateral supine positions. (b) Relative changes in the impedance-volume sensitivity (calibration) of each individual measured subject using lead configuration C2.

studies have been conducted by Carry et al. [15] and Eberhard et al. [16], but they used the RIP technique. Our findings are comparable to theirs (Fig. 6). The general trend in all configurations is that the signal waveform agreement between \hat{V}_{IP} and \hat{V}_{PNT} is better in breaths of higher V_T than lower V_T . Moreover, the agreement is higher in erect posture than in supine postures. The lower agreement in supine postures and in low V_T breaths is most likely explained by the higher relative magnitude of the cardiogenic oscillations in the IP signal. The fact that in configuration C4 the agreements are quite high (mean ρ above 0.90) in breaths of both low V_T and high V_T suggests that the IP method accuracy is not degraded by changes in the respiration mechanics (abdominal/rib cage), but this would need further examination. The lateral configurations (C1, C2, C4) were found to be clearly better than the anteroposterior ones (C3, C5). The performance of the lateral

configurations is quite similar, which suggests that the choice between the lateral lead configurations is not very critical.

It should be noted, that even though we used subject and posture specific impedance-volume calibration values, they are merely scalar coefficients and do not change the shape of the flow signal waveform. Thus, for deriving flow or volume related parameters that do not depend on absolute quantities, like most tidal breathing parameters, the accuracy of an uncalibrated IP measurement is essentially the same as that presented here.

B. Tidal Volume Agreement

In tidal volume estimation (Fig. 7), the IP method performance is at the same level with that found by earlier investigators for IP [20], [11]. The accuracy is generally

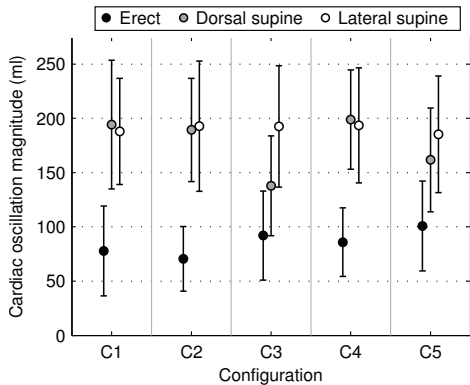


Fig. 9. Magnitudes of cardiogenic oscillations in unfiltered impedance signal for each configuration C1-C5 and posture expressed as mean \pm SD. The values are defined as ratios of peak-to-peak impedance change caused by cardiogenic oscillations (Ω) to impedance-volume sensitivity (Ω/ml) of that measurement resulting in magnitudes of oscillations in milliliters.

quite high when subject and posture specific calibration is applied. In all tested configurations, the calibration factor changes with the posture, and the change has a relatively large inter-subject SD (Fig. 8). At least in the case of the configurations C1 and C2, the change in the calibration factor is most likely caused by the change in the anatomic geometry of the thorax and movement of the internal organs, not by the change in breathing mechanics that also takes place in posture change [21]. This claim is supported by the fact that the change from small V_T (<800 ml) to larger V_T (>1800 ml) changes the breathing mechanics, yet this does not significantly affect the V_T estimation agreement of C1 and C2 between the two methods (Fig. 7). If the change in the calibration factor had a small SD, the calibration could be done in a single posture, and a simple automatic adaptive calibration using an accelerometer to detect posture could be considered. This approach could still be feasible if the intra-subject variability in the calibration factor during the posture change is small and the calibration would be done in multiple postures.

C. Cardiogenic Oscillations

The typically 3-fold increase in CGO magnitude from the erect to supine postures could be explained by the change in the direction of the force that the gravitational field exerts on the internal organs and fluids. When changing from erect to supine posture, the heart and the aorta move toward the superior direction, thus residing more at the level of the electrodes. In a visual inspection of the signals, it is clear that the CGO is the main reason for degraded accuracy in the measured waveform.

The amplitude of the cardiac oscillations can be almost half of the breathing signal amplitude. There are at least two approaches in removing or attenuating the cardiogenic distortions. First, such electrode configurations should be found that have smaller sensitivity for areas of pulsatile blood flow than the ones presented here. This might prove hard to achieve

since Brown et al. [22] suggested that the pulmonary tree itself is a source of pulsatile impedance change, not only the larger vessels and the heart. In addition, in our study we found only small differences in the oscillation magnitudes between different lead configurations. Second, signal processing could be applied to attenuate the oscillations [23]. As the frequency band of the oscillations and the flow signal overlap, linear filtering strategies cannot be used if the complete breathing signal waveform needs to be preserved. Here we utilized the nonlinear S-G filtering. Another approach would be to exploit the electrocardiogram (ECG) signal that can be obtained from the same electrodes [24].

D. Long-term Noninvasive Respiration Measurement

An accurate semi-quantitative ambulatory pulmonary volume and flow measurement system could introduce new diagnostic tools in diseases involving degrees of airway obstruction or otherwise distorted respiration patterns. For instance, as shown by Carlsen et al. [7], certain parameters of tidal breathing flow-volume loop reflect level of obstruction. An ambulatory system could thus be used to monitor diurnal or other variation in the symptoms of asthma over day and night. In epidemiologic studies, light ambulatory IP would be ideal to monitor people who are exposed to environmental air pollution. In studies with subjects of insufficient co-operation for traditional lung function measurements, like children or infants, long-term IP could give supportive information for clinical decision. In addition, home recordings are significantly more cost-efficient than controlled laboratory measurements that require attendance of trained personnel.

Considering a Holter-type 24-hour or longer noninvasive breathing measurement with portable equipment while the posture of the subject is constantly changing, absolute volume information is somewhat challenging to establish with both IP and RIP techniques as shown in this and other studies. The question becomes then, how accurately can the noninvasive methods measure the parameters that depend only on the signal waveform shape without information on the absolute volumes.

Strömberg et al. [14] investigated the concept of continuous pulmonary waveform assessment by comparing the RIP plethysmographic signal waveform to that of the integrated PNT signal of adult subjects in sitting and supine positions, while varying the abdominal and rib cage contributions to breathing. However, their results are related to RIP volume calibration techniques, not to signal waveform accuracy as such. Carry et al. [15] and Eberhard et al. [16] instead assessed directly the waveform accuracy using time-differentiated RIP belts sum signal as the pulmonary flow signal estimate. They measured free-paced tidal breathing in adults with simulated increased airway resistance simultaneously with RIP and PNT. Carry had subjects in the sitting position, but Eberhard varied the posture between erect, lateral supine, and dorsal supine. The researchers compared the RIP-derived flow signal with the PNT signal.

Even though our results in PNT and IP flow waveform agreement are comparable to those obtained with RIP in earlier studies in terms of standard error of measurement (SEM), this

TABLE I

MEASUREMENTS LEFT OUT FROM THE STATISTICAL RESULTS ANALYSIS DUE TO EXTERNAL ERRORS. THE UPPER NUMBER DENOTES THE NUMBER OF COMPLETE MEASUREMENTS (OF 20) THAT WERE UNSUCCESSFUL AND THE LOWER PERCENTAGE SHOWS THE AMOUNT OF INDIVIDUAL RESPIRATION CYCLES LEFT OUT FROM THE OTHERWISE ACCEPTED MEASUREMENTS AS ERRONEOUS.

	C1	C2	C3	C4	C5
Erect	0	0	1	0	2
	2.1%	0.8%	5.4%	3.0%	4.4%
Dorsal supine	0	0	2	1	2
	2.9%	2.8%	6.2%	4.0%	2.7%
Lateral supine	6	1	4	3	6
	3.9%	2.3%	16.8%	3.9%	5.7%

type of error analysis does not describe how the difference in the two signals is distributed in each breathing cycle. If the error is systematically at the same phase of the cycle (deterministic) it is difficult to overcome, but if the error is more randomly distributed (stochastic) over each cycle, averaging techniques [25] could efficiently cancel it. This lack of information in the SEM analysis regarding the nature of the error signal allows for the following discussion. The plethysmographic volume signal output of RIP is a sum of the rib cage and abdomen inductive belts that essentially measure the independent motion of the two thoracic compartments [26]. A change in the dynamics of the contribution of rib cage and abdominal signals to the sum signal may compromise the volume signal accuracy, even when considering only the signal shape without absolute quantities. Indeed, Jackson et al. [27] and Manczur et al. [28] found the accuracy of RIP in measuring the ratio of the expiratory time at the tidal peak flow to the total expiratory time ($t_{p,TEF}/t_E$) somewhat inadequate and Jackson hypothesized that the inaccuracy might be due to changes in rib cage and abdominal motion contributions. These results combined with the knowledge that rib cage and abdomen motion dynamics change with subject posture [21], [29] suggest that RIP might not be suitable for measurements of tidal breathing parameters in free living conditions where subject posture cannot be controlled. Where RIP is based on the quite indirect measures of the motion of chest compartments, IP, on the other hand, is at some level directly related to the lung air content [22], [30].

A recent publication by Vuorela et al. presented a prototype device implementing the long-term IP measurement [31]. Their article is focused on the technical implementation of the system and presents only one short example segment of comparative IP and PNT signals.

E. Limitations of the Method

One limitation of the method is the inability to maintain the volume calibration when changing postures. However, this is not a problem when only parameters that do not need absolute values are derived from the signal, as the shape of the volume and flow signals remains accurate despite posture change.

Another issue is the susceptibility to motion artefact. This was not assessed in our study, but it is a widely recognized problem related with the IP technique [32], [31]. The motion

TABLE II

FLOW WAVEFORM AGREEMENT ρ BETWEEN FLOW SIGNALS \dot{V}_{IP} AND \dot{V}_{PNT} WITH IP ELECTRODE CONFIGURATION C4. "S" DENOTES THE SUBJECT NUMBER. THE LABELS "LOW", "MID", AND "HIGH" DENOTE THE AGREEMENT ρ AT DIFFERENT TIDAL VOLUMES V_T OF RESPIRATION, 300-800 ML, 800-1800 ML, AND 1800-3500 ML, RESPECTIVELY. LABEL "O" DENOTES THAT THE SUBJECT DID NOT HAVE ANY RESPIRATION CYCLES IN THAT V_T REGION. LABEL "- -" DENOTES A COMPLETELY UNSUCCESSFUL RECORDING.

S	Erect			Supine dorsal			Supine lateral		
	low	mid	high	low	mid	high	low	mid	high
1	0.90	0.95	0.96	0.92	0.94	0.95	0.92	0.94	0.96
2	0.94	0.95	0.94	0.94	0.94	0.97	0.94	0.95	0.96
3	0.92	0.94	0.95	0.93	0.94	0.95	0.89	0.95	0.92
4	0.96	0.94	0.95	0.85	0.90	0.93	0.90	0.94	0.95
5	0.92	0.95	0.96	0.58	0.93	0.95	0.81	0.89	0.91
6	0.73	0.92	0.96	o	0.92	0.67	0.54	0.97	0.98
7	0.90	0.92	0.89	0.95	0.96	0.95	0.95	0.96	0.77
8	0.83	0.95	0.98	0.97	0.96	0.98	0.96	0.98	0.97
9	0.95	0.96	0.94	0.95	0.95	0.89	0.91	0.94	0.88
10	0.93	0.96	0.96	0.95	0.96	0.94	0.98	0.98	0.97
11	o	0.96	0.95	0.53	0.94	0.95	0.89	0.97	0.97
12	0.95	0.96	0.96	0.98	0.97	0.94	0.93	0.96	0.93
13	0.90	0.87	0.91	0.84	0.88	0.88	0.79	0.86	0.93
14	0.95	0.96	0.93	0.95	0.94	0.94	0.94	0.93	0.96
15	o	0.95	0.95	o	0.95	0.96	o	0.94	0.94
16	o	0.91	0.82	0.93	0.93	0.84	-	-	-
17	0.85	0.90	0.90	0.93	0.94	o	0.91	0.93	o
18	o	o	0.83	o	0.90	0.89	o	0.92	0.93
19	o	0.95	0.94	-	-	-	-	-	-
20	0.93	0.94	o	0.93	0.95	0.98	-	-	-

artefact could be attenuated using ensemble averaging techniques over multiple breathing cycles.

Some of the tests were unsuccessful and they have been summarized in Table I. The amounts of completely unsuccessful measurements (upper values in Table I) are clearly higher in the lateral supine posture. This is probably due to the difficulty of fitting the electrode belt properly when the subject is lying on his/her side. Also, if the electrical electrode contact is weak due to, for example, strong hair, even a slight motion or change in the surface pressure of the electrodes with respiration can heavily distort the signal. This electrode motion and pressure change is naturally augmented when the electrode is pressed between the skin and the bed in the supine postures or if the belt becomes locally loose because of the thorax geometry change. The small amount of rejected measurements in C2 can thus be explained by these practical reasons of geometry. The large difference in the amounts of rejected measurements of the similar configurations C1 and C2 in the lateral supine posture is because the subject was always lying on his/her right side.

In individual cycle removal, the reasons include unintentional short-time subject activity like body position adjustment, coughing or talking. However, their rate also follows the same trend as that of the completely unsuccessful measurements.

The reliability of the IP measurement could be improved by using larger electrodes so that the skin-contact is more likely to be preserved even when the belt moves or bends. Possibly even

electrodes spanning the complete side of the thorax could be used as it seems that all the lateral lead configurations perform quite equally.

V. CONCLUSION

We have presented the concept of deriving pulmonary flow from IP and compared the signal with a more well-established measurement technique. The agreement between the IP-derived and the PNT flow signal waveform shapes was found excellent in all postures and with all V_T ranges. The agreement between the PNT-derived and the IP-derived V_T estimates was very high when IP values were calibrated per subject and posture. The main source of error in the IP signal was the cardiogenic distortion, and a more advanced technique should be developed to attenuate it. From the five novel electrode configurations tested, the lateral ones were found clearly better than the anteroposterior ones.

Natural progress of the IP research will be to expand these method validation studies to diseased populations and to children, and to use IP to derive clinical parameters from flow-volume loops.

IP potentially enables the development of a noninvasive ambulatory measurement device for long-term studies of tidal breathing.

REFERENCES

- [1] U. Frey, B. Suki, R. Kraemer, and A. C. Jackson, "Human respiratory input impedance between 32 and 800 hz, measured by interrupter technique and forced oscillations," *J Appl Physiol*, vol. 82, no. 3, pp. 1018–1023, Mar. 1997.
- [2] M. Folke, L. Cernerud, M. Ekström, and B. Hök, "Critical review of non-invasive respiratory monitoring in medical care," *Med. Biol. Eng. Comput.*, vol. 41, no. 4, pp. 377–383, Jul. 2003.
- [3] F. Emralino and A. M. Steele, "Effects of technique and analytic conditions on tidal breathing flow volume loops in term neonates," *Pediatr. Pulm.*, vol. 24, no. 2, pp. 86–92, 1997.
- [4] P. J. Fleming, M. R. Levine, and A. Goncalves, "Changes in respiratory pattern resulting from the use of a facemask to record respiration in newborn infants," *Pediatr. Res.*, vol. 16, no. 12, 1982.
- [5] J. Askanazi, P. A. Silverberg, R. J. Foster, A. I. Hyman, J. Milic-Emili, and J. M. Kinney, "Effects of respiratory apparatus on breathing pattern," *J. Appl. Physiol.*, vol. 48, no. 4, pp. 577–580, Apr. 1980.
- [6] K. C. Lødrup Carlsen, "Tidal breathing at all ages," *Monaldi Archives for Chest Disease*, vol. 55, no. 5, pp. 427–434, Oct. 2000.
- [7] K. Carlsen and K. C. Lødrup Carlsen, "Tidal breathing analysis and response to salbutamol in awake young children with and without asthma," *Eur. Respir. J.*, vol. 7, no. 12, pp. 2154–2159, Dec. 1994.
- [8] C. van der Ent, H. Brackel, J. van der Laag, and J. Bogaard, "Tidal breathing analysis as a measure of airway obstruction in children three years of age and older," *Am. J. Respir. Crit. Care Med.*, vol. 153, no. 4, pp. 1253–1258, Apr. 1996.
- [9] R. L. Colasanti, M. J. Morris, R. G. Madgwick, L. Sutton, and E. M. Williams, "Analysis of tidal breathing profiles in cystic fibrosis and COPD," *Chest*, vol. 125, no. 3, pp. 901–908, 2004.
- [10] E. Williams, R. Madgwick, and M. Morris, "Tidal expired airflow patterns in adults with airway obstruction," *Eur. Respir. J.*, vol. 12, no. 5, pp. 1118–1123, Nov. 1998.
- [11] J. H. Houtveen, P. F. Groot, and E. J. de Geus, "Validation of the thoracic impedance derived respiratory signal using multilevel analysis," *Int. J. Psychophysiol.*, vol. 59, no. 2, pp. 97–106, Feb. 2006.
- [12] N. Beydon, S. D. Davis, E. Lombardi, J. L. Allen, H. G. M. Arets, P. Aurora, H. Bisgaard, G. M. Davis, F. M. Ducharme, H. Eigen, M. Gappa, C. Gaultier, P. M. Gustafsson, G. L. Hall, Z. Hantos, M. J. R. Healy, M. H. Jones, B. Klug, K. C. Lødrup Carlsen, S. A. McKenzie, F. Marchal, O. H. Mayer, P. J. F. M. Merkus, M. G. Morris, E. Oostveen, J. J. Pillow, P. C. Seddon, M. Silverman, P. D. Sly, J. Stocks, R. S. Tepper, D. Vilozni, N. M. Wilson, on behalf of the American Thoracic Society/European Respiratory Society Working Group on Infant, and Y. C. P. F. Testing, "An official american thoracic Society/European respiratory society statement: Pulmonary function testing in preschool children," *Am. J. Respir. Crit. Care Med.*, vol. 175, no. 12, pp. 1304–1345, Jun. 2007.
- [13] V. Seppä, J. Viik, A. Naveed, J. Väisänen, and J. Hyttinen, "Signal waveform agreement between spirometer and impedance pneumography of six chest band electrode configurations," in *IFMBE Proceedings*, ser. VII, vol. 25. Springer, 2009, pp. 689–692.
- [14] N. O. Strömberg, G. O. Dahlbäck, and P. M. Gustafsson, "Evaluation of various models for respiratory inductance plethysmography calibration," *J. Appl. Physiol.*, vol. 74, no. 3, pp. 1206–1211, Mar. 1993.
- [15] P. Carry, P. Baconnier, A. Eberhard, P. Cotte, and G. Benchetrit, "Evaluation of respiratory inductive plethysmography: Accuracy for analysis of respiratory waveforms," *Chest*, vol. 111, no. 4, pp. 910–915, Apr. 1997.
- [16] A. Eberhard, P. Calabrese, P. Baconnier, and G. Benchetrit, "Comparison between the respiratory inductance plethysmography signal derivative and the airflow signal," *Adv. Exp. Med. Biol.*, vol. 499, pp. 489–494, 2001.
- [17] J. Malmivuo and R. Plonsey, "Impedance plethysmography," in *Bioelectromagnetism*. New York: Oxford University Press, 1995, pp. 405–419.
- [18] J. Bates, G. Schmalisch, D. Filbrun, and J. Stocks, "Tidal breath analysis for infant pulmonary function testing. ERS/ATS task force on standards for infant respiratory function testing. european respiratory Society/American thoracic society," *Eur. Respir. J.*, vol. 16, no. 6, pp. 1180–1192, Dec. 2000.
- [19] A. Savitzky and M. J. E. Golay, "Smoothing and differentiation of data by simplified least squares procedures," *Anal. Chem.*, vol. 36, no. 8, pp. 1627–1639, Jul. 1964.
- [20] K. Cohen, W. Ladd, D. Beams, W. Sheers, R. Radwin, W. Tompkins, and J. Webster, "Comparison of impedance and inductance ventilation sensors on adults during breathing, motion, and simulated airway obstruction," *IEEE T. Bio-med. Eng.*, vol. 44, no. 7, pp. 555–566, 1997.
- [21] J. Verschakelen and M. Demedts, "Normal thoracoabdominal motions. influence of sex, age, posture, and breath size," *Am. J. Respir. Crit. Care Med.*, vol. 151, no. 2, pp. 399–405, Feb. 1995.
- [22] B. Brown, D. Barber, A. Morice, and A. Leathard, "Cardiac and respiratory related electrical impedance changes in the human thorax," *IEEE T. Bio-med. Eng.*, vol. 41, no. 8, pp. 729–734, 1994.
- [23] A. Krivosei, "Model based method for adaptive decomposition of the thoracic bioimpedance variations into cardiac and respiratory components." PhD Thesis, Tallinn University of Technology, 2009.
- [24] T. F. Schuessler, S. B. Gottfried, P. Goldberg, R. E. Kearney, and J. H. T. Bates, "An adaptive filter to reduce cardiogenic oscillations on esophageal pressure signals," *Ann. Biomed. Eng.*, vol. 26, no. 2, pp. 260–267, Mar. 1998.
- [25] G. Schmalisch, M. Schmidt, and B. Foitzik, "Novel technique to average breathing loops for infant respiratory function testing," *Med. Biol. Eng. Comput.*, vol. 39, no. 6, pp. 688–693, Nov. 2001.
- [26] K. Konno and J. Mead, "Measurement of the separate volume changes of rib cage and abdomen during breathing," *J Appl Physiol*, vol. 22, no. 3, pp. 407–422, 1967.
- [27] E. Jackson, J. Stocks, L. Pilgrim, I. Dundas, and C. Dezateux, "A critical assessment of uncalibrated respiratory inductance plethysmography (Respirace®) for the measurement of tidal breathing parameters in newborns and infants," *Pediatr. Pulm.*, vol. 20, no. 2, pp. 119–124, 1995.
- [28] T. Manczur, A. Greenough, R. Hooper, K. Allen, S. Latham, J. Price, and G. Rafferty, "Tidal breathing parameters in young children: Comparison of measurement by respiratory inductance plethysmography to a facemask pneumotachograph system," *Pediatr. Pulm.*, vol. 28, no. 6, pp. 436–441, 1999.
- [29] O. H. Mayer, R. G. Clayton, A. F. Jawad, J. M. McDonough, and J. L. Allen, "Respiratory inductance plethysmography in healthy 3- to 5-Year-Old children," *Chest*, vol. 124, no. 5, pp. 1812–1819, Nov. 2003.
- [30] P. Nopp, N. Harris, T. Zhao, and B. Brown, "Model for the dielectric properties of human lung tissue against frequency and air content," *Med. Biol. Eng. Comput.*, vol. 35, no. 6, pp. 695–702, Nov. 1997.
- [31] T. Vuorela, V. Seppä, J. Vanhala, and J. Hyttinen, "Design and implementation of a portable longterm physiological signal recorder," *IEEE T. Inf. Technol. B.*, 2010, accepted for publication.
- [32] N. D. Khambete, B. H. Brown, and R. H. Smallwood, "Movement artefact rejection in impedance pneumography using six strategically placed electrodes," *Physiol. Meas.*, vol. 21, no. 1, pp. 79–88, 2000.

Publication II

Seppä, V.-P., Hyttinen, J., & Viik, J. 2011b. A method for suppressing cardiogenic oscillations in impedance pneumography. *Physiological Measurement*, 32(3), 337-345.

A method for suppressing cardiogenic oscillations in impedance pneumography

V-P Seppä, J Hyttinen and J Viik

Department of Biomedical Engineering, Tampere University of Technology, Biokatu 6,
FIN-33520 Tampere, Finland

E-mail: ville-pekka.seppa@tut.fi

Received 22 June 2010, accepted for publication 12 October 2010

Published 14 February 2011

Online at stacks.iop.org/PM/32/337

Abstract

The transthoracic electrical impedance signal originates from the cardiac and respiratory functions. In impedance pneumography (IP) the lung function is assessed and the cardiac impedance signal, cardiogenic oscillations (CGOs), is considered an additive noise in the measured signal. In order to accurately determine pulmonary flow parameters from the signal, the CGO needs to be attenuated without distorting the respiratory part of the signal. We assessed the suitability of a filtering technique, originally described by Schuessler *et al* (1998 *Ann. Biomed. Eng.* **26** 260–7) for an esophageal pressure signal, for CGO attenuation in the IP signal. The technique is based on ensemble averaging the CGO events using the electrocardiogram (ECG) R-wave as the trigger signal. Lung volume is known to affect the CGO waveforms. Therefore we modified the filtering method to produce a lung volume-dependent parametric model of the CGO waveform. A simultaneous recording of ECG, IP and pneumotachograph (PNT) was conducted on 41 healthy, sitting adults. The performance of the proposed method was compared to a low-pass filter and a Savitzky–Golay filter in terms of CGO attenuation and respiratory signal distortion. The method was found to be excellent, exhibiting CGO attenuation of 35.0 ± 12.5 dB (mean \pm SD) and minimal distortion of the respiratory part of the impedance signal.

Keywords: pulmonary flow, bioimpedance, ensemble averaging, signal decomposition

1. Introduction

The transthoracic electrical impedance varies over time due to the cardiac function and respiration. The cardiogenic impedance signal Z_c originates from the movement of blood volumes in the thorax, and the respiratory impedance signal Z_r is directly proportional to the lung volume (Brown *et al* 1994). These measurable signals can be exploited to analyse the

cardiac function, as in impedance cardiography (ICG), or the lung function, as in impedance pneumography (IP). Depending on the application, either one of the signals is considered an additive noise signal that should be suppressed to enable accurate and reliable analysis of the cardiac or pulmonary variables of interest.

The frequency spectra of Z_c and Z_r have their corresponding main power components at the frequencies of heart rate (HR) and respiration rate (RR), respectively. Thus, the main cardiac component is typically at a frequency at least two times higher than that of the respiration. However, the harmonic frequencies of Z_r contain power that reach the HR frequency causing the power spectrum of the two signals overlap. Thus, removing the cardiogenic oscillations (CGOs) with a normal linear low-pass filter, with cut-off frequency slightly below the HR, will also remove some information of the Z_r signal. This problem is naturally pronounced in subjects with high RR to HR ratio. Preserving the harmonic components of the respiration signal is important in the emerging IP applications, such as ambulatory long-term lung function assessment, where variables more complex than RR or tidal volume are extracted from the signal (Vuorela *et al* 2010, Seppä *et al* 2010). The presence of the CGO considerably hinders the accurate segmentation of the impedance signal into respiratory cycles and finding the points of interest, such as the time of peak expiratory flow.

We analyse the performance of a signal processing method that aims at removing the CGO in the IP signal while preserving the power accounted for by the respiratory activity completely, and compare the results with two other filtering techniques. The method is based on the research of Schuessler *et al* (1998) on CGO removal in esophageal balloon catheter pressure measurements. A similar approach was applied by Wilson *et al* (1982) on the IP signal, but they found it to be unsuccessful due to the change in the CGO waveform with respiratory cycle phase. We extended this technique to adapt to CGO waveform changes with lung volume changes, which is, indeed, a recognized interaction between the cardiogenic and respiratory impedance signals (Nagel *et al* 1989).

2. Materials and methods

2.1. Test population

The test subjects were students at the university of the authors and were recruited from a biomedical engineering laboratory course. They were not given financial nor any other benefit for volunteering. The study and the written consent forms obtained from all subjects were approved by the ethical committee of the regional hospital district.

The test subject population consisted of 41 subjects of which 16 (6 female) exhibited clear CGO in their IP signal and were chosen for analysis. The criterion for selection was Z_c amplitude above 5% of the Z_r amplitude. These 16 subjects were aged 22.6 ± 1.1 years and had body mass index of 23.5 ± 3.5 kg m⁻².

For the pre- versus post-filtering t_{PTEF}/t_E (ratio of time of peak tidal expiratory flow to expiratory time) comparison described in section 2.4, the 26 subjects for whom a mouth piece was used for the pneumotachograph (PNT) measurement were chosen. The use of the mouth piece instead of the mask with a two-way valve enabled the recording of the inspiratory flow signal as well, which was necessary to conduct the presented analysis.

2.2. Measurement procedure

A simultaneous recording of IP, ECG and PNT was conducted on sitting subjects for the duration of 50 respiration cycles at a sampling frequency of 200 Hz. The IP signal was recorded with a tetrapolar electroimpedance amplifier (EBI100C, Biopac Systems Inc.,

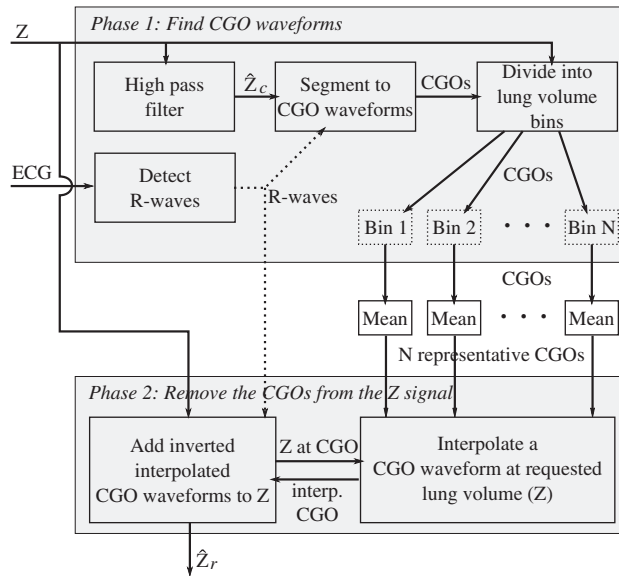


Figure 1. The signal processing scheme of the modified Schuessler–Bates method.

Goleta, CA 93117, USA) with 100 kHz excitation current. ECG was measured with a Biopac main unit (MP35, Biopac Systems Inc.). For both measurements, disposable Ambu Blue Sensor P Ag–AgCl electrodes (Ambu A/S, Ballerup, Denmark) having circular gel areas of 154 mm² were used. Pulmonary flow was measured with a heated PNT flow head (A Fleisch No. 3, Lausanne, Switzerland) connected to a differential pressure transducer (SS40 L, Biopac Systems Inc.). The PNT was calibrated with 3.00 litre calibration syringe (PCS-3000, Piston Medical, Budapest, Hungary) before each measurement. The PNT was connected to the subject's airways using a face mask with a two-way non-rebreathing valve (Hans Rudolph Inc., Shawnee, KS, USA), if a proper fit was established, or with a mouth piece using a nose clip. The two modes of measurement may have different effect on the respiration mechanics and control, but in the type of analysis presented in this paper, it is irrelevant. The measurement equipment was described in more detail by Seppä *et al* (2010).

The IP measurement configuration had one electrode approximately 5 cm posterior of the left mid axillary line on the level of the third intercostal space, another electrode 3 cm below the previous one, and another two electrodes on corresponding locations on the right side forming the configuration C4 presented by Seppä *et al* (2010). The current and voltage leads of the impedance measurement were connected to the upper and lower electrodes, respectively. For ECG measurement, lead II of the standard 12-lead system was used in order to obtain a strong R-wave for easy detection.

2.3. Signal processing

The IP signal was processed using a modified version of the Schuessler–Bates method (mSBM) (1998). Briefly (figure 1): an estimate of the Z_c component of the impedance signal is obtained by high-pass filtering the original impedance signal Z with a high-pass filter with a cut-off frequency of 0.6 times HR. The resulting signal consists mostly of cardiogenic components, but also contains some traces of the respiratory signal as the frequency spectra of the two signals

overlap. The signal is ensemble averaged using the ECG R-wave as an event trigger and normalizing the sample amount in each extracted R–R interval. After ensembling all extracted segments, they are averaged to obtain a representative CGO waveform. The averaging by mean function suppresses the traces of the respiratory signal left after the high-pass filtering because they are stochastic with respect to the CGO events. The obtained representative CGO waveform is inverted and added to the impedance signal at the time of each ECG signal R-wave to cancel the CGOs.

As the Z_c signal is known to be modulated by the lung air content variation, we modified the algorithm to distribute the CGO ensembles into four bins according to the instantaneous lung volume at the time of their occurrence. The limits of the bins were equally distributed along the lung volume range between functional residual capacity (FRC) and FRC + tidal volume (TV) of each subject. After finding the four CGO ensemble averages corresponding to the mean lung volume of each bin, the averages were decimated to 20 samples. Each of the samples was given a piece-wise continuous first-order function consisting of three pieces (for four bins) with the lung volume as an argument. Thus, a 20-sample estimate of the CGO waveform could be recalled for any arbitrary lung volume between the FRC and FRC+TV. To produce a correct length waveform for each R–R interval, the 20 samples were used as knot points for a cubic spline interpolation function.

We did not implement the recursive adaptive features of the method described in the original paper, as we considered our measurement period to be short and the setting static so that the physiological changes during the measurement would be minimal. This also allowed us to use the complete measurement period first for finding the ensemble average (phase 1 in figure 1) and then for filtering (phase 2 in figure 1), without need for an adaptation period.

In order to provide a benchmark for the proposed method, two other filters, a linear equiripple low-pass filter and a Savitzky–Golay (S-G) smoothing filter (Savitzky and Golay 1964), were implemented. The low-pass filter is an obvious first candidate for the presented task, and the S-G filter is known to be able to preserve high-frequency content although having some behaviour of a low-pass filter, and it has been used previously for this purpose (Seppä *et al* 2010). The low-pass filter was adjusted to have a cut-off frequency 0.9 times the individual mean HR and a stop band attenuation of 40 dB ($f_p = 0.9 * HR - 0.4$ Hz, $f_s = 0.9 * HR$, $A_s = 40$ dB, $r_p = 1$ dB). The S-G filter was adjusted to a fixed fitting frame size of 2000 ms as in the paper of Seppä *et al* (2010).

2.4. Assessment of the filtered signals

A filter for CGO attenuation in the IP signal has two main requirements: (1) it has to attenuate the power accounted for by the heart activity in the impedance signal Z_c , and (2) it must minimally, preferably not at all, alter the respiration-induced impedance signal Z_r . The ability of the three filters to meet these requirements was analysed by their effect on the power frequency spectrum of the IP signal, especially at the frequency of the HR, and by assessment of their distortive effect on an integrated PNT signal that has minimal CGO and is morphologically very close to Z_r .

To assess the attenuation features of the filters, they were applied on the measured IP signals. The power spectrum of the signals was estimated with the fast Fourier transformation (FFT) with 8192 points. The power spectrum of each subject was normalized in abscissa to have frequency 1 at the individual mean HR frequency and the gain for each subject was assessed by comparing the spectrum of the filtered signals to that of the unfiltered signal.

In order to assess the distortive effect of the filters, the PNT flow signal was integrated by the trapezoid method (Bates 2009, pp 31–2) to produce a lung volume signal. The signal was

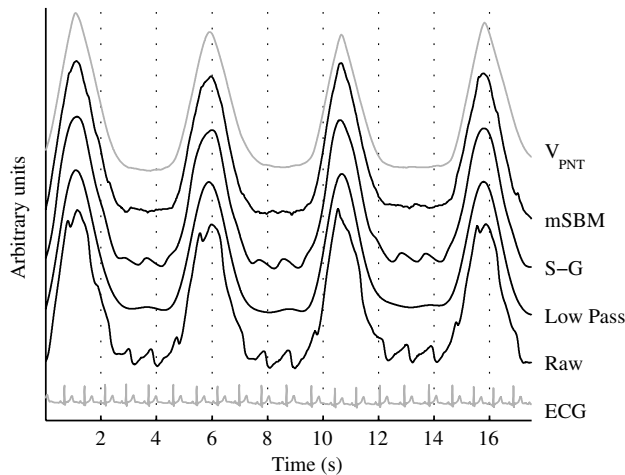


Figure 2. Example signals illustrating the effect of filtering. V_{PNT} is the lung volume signal obtained by integrating the pneumotachograph (PNT) signal. The raw signal exhibits CGOs after each R-wave of the electrocardiogram (ECG) signal. S-G and mSBM stand for the Savitzky–Golay and modified Schuessler–Bates methods, respectively.

treated with the three filters, and the unfiltered and the three filtered signals were derivated back to flow signals using an S-G differentiating filter with frame size 100 ms. The effect of the consecutive integration and derivation on the unfiltered signal was negligible, as intended. The four signals were segmented individually into expiratory cycles using flow thresholding, and a well-established tidal breathing parameter, $t_{\text{PTEF}}/t_{\text{E}}$, was derived from the last 20 respiratory cycles of each measurement using the cycle selection algorithm described by van der Ent *et al* (1996). This complete procedure enabled us to assess the distortive effect of the filters on a signal that very closely resembles pure Z_r , by comparing the signal shape-dependent $t_{\text{PTEF}}/t_{\text{E}}$ values extracted from the unfiltered signal to those extracted from the filtered signals.

3. Results

The effect of the filters on the IP signal is illustrated in figure 2.

3.1. Distortive effects

In the unfiltered versus filtered PNT volume signal $t_{\text{PTEF}}/t_{\text{E}}$ estimation test, the mSBM performs clearly best (figure 3). The difference between $t_{\text{PTEF}}/t_{\text{E}}$ values derived from the signal before and after filtering with the low-pass filter, the S-G filter and the new method shows the differences of $0.018 (\pm 0.064)$, $0.046 (\pm 0.059)$ and $0.000 (\pm 0.018)$, respectively.

3.2. CGO attenuation

The CGO waveform shows typically an increase in amplitude with increasing lung volume, but the waveform change is not necessarily only a simple amplitude modulation (figure 4).

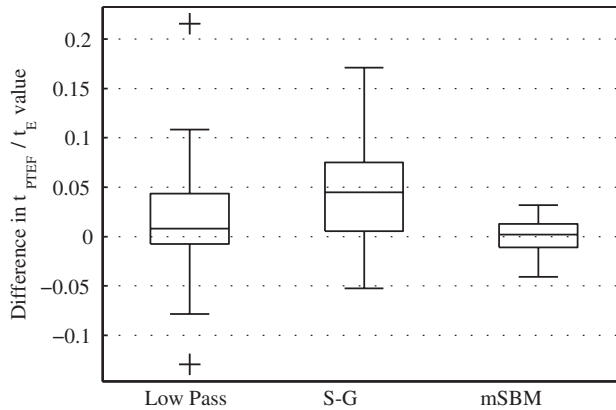


Figure 3. Difference between the estimated ratio of time of peak tidal expiratory flow to expiratory time (t_{PTEF}/t_E) values before and after filtering an integrated pneumotachograph (PNT) signal. The integrated PNT signal should be very close to the respiratory part of the impedance signal (Z_r); thus, the difference reflects the unwanted distortive effect of the filters on Z_r . S-G and mSBM stand for the Savitzky–Golay and modified Schuessler–Bates methods, respectively. The middle line denotes the median value, the box denotes the 25–75% range, the whiskers extend to the measurement values closest to ± 2.7 times standard deviation (SD) and the + marks are outliers. Data from 26 subjects.

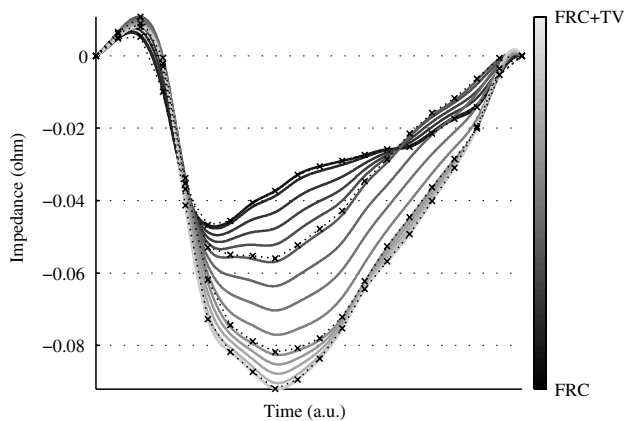


Figure 4. Typical change in CGO waveform with lung volume change during tidal breathing from functional residual volume (FRC) to FRC + tidal volume (TV). The x marks denote the 20 knot points of each of the four volume bins. The waveforms are produced with cubic spline interpolation using the knot points adjusted to different lung volumes. Data from a single subject.

There are clear differences in the ability of the filters to attenuate the CGO main frequency component (figure 5). The attenuations compared to an unfiltered signal for the low-pass filter, S-G filter and the mSBM were -44.9 ± 15.4 dB, -12.6 ± 10.3 dB, -35.0 ± 12.5 dB, respectively.

In the frequency spectrum analysis (figure 6), the new method shows the most consistent behaviour of the three filters having below -1 dB gain until frequency 0.77 (times HR) which

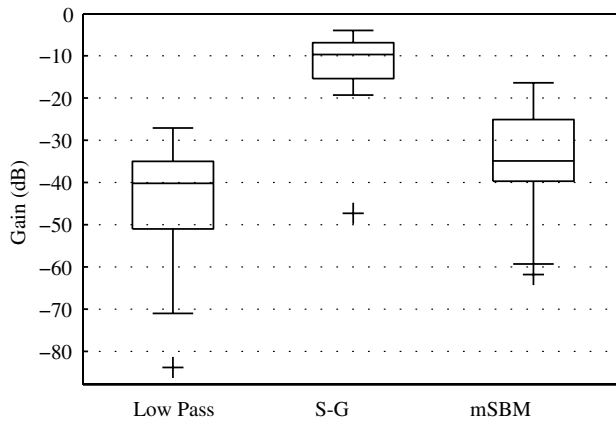


Figure 5. The attenuation of the different filtering methods at the frequency of the HR. S-G and mSBM stand for the Savitzky–Golay and modified Schuessler–Bates methods, respectively. The middle line denotes median value, the box denotes the 25–75% range, the whiskers extend to the measurement values closest to ± 2.7 times standard deviation (SD) and the + marks are outliers. Data from 16 subjects.

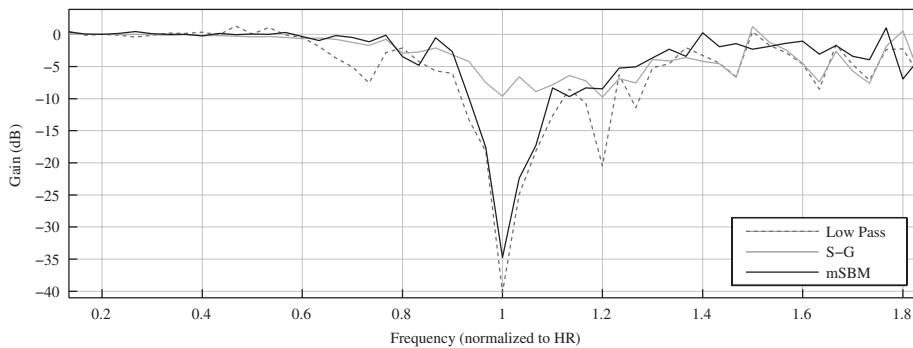


Figure 6. Gain–frequency plot normalized with HR showing median gain values of the three filter methods for all subjects. The harmonic frequencies (integral values on the abscissa) were generally low on power and are not included in the figure. S-G and mSBM stand for the Savitzky–Golay and modified Schuessler–Bates methods, respectively. Data from 16 subjects.

is followed by a strong gain drop peaking at frequency 1.0 and a gradual return to gain near close to 0 dB as the frequency increases. The spectrum shows no unexpected gain drops except for a -5 dB drop at 0.82.

The low-pass filter shows a strong drop at frequency 1.0 as well, but it also exhibits drops outside the HR frequency at $0.6 \dots 0.8$ (-7.5 dB), and at 1.2 (-20 dB). In the frequency region above 1.4, the gain level is generally lower than that of the mSBM.

The S-G filter shows gain close to 0 dB gain until frequency 0.8 where it gradually drops to $-7 \dots -10$ dB, not showing a clear drop at 1.0. After returning to gain above -5 dB at 1.3 the gain curve starts to follow closely that of the low-pass filter towards the higher frequencies.

4. Discussion

4.1. Performance of the methods

In the presented analysis, the proposed filtering technique performs excellently, presenting minimal respiration signal distortion and strong CGO attenuation. At HR frequency the gain is less than -18 dB on all subjects, whereas for the S-G filter it can be as high as -5 dB, which is an insufficient attenuation (figure 5). The low-pass filter can be adjusted to virtually any sensible attenuation level, but due to its linear nature, it will attenuate everything, including the important Z_r signal harmonics, above its cut-off frequency. This is reflected in the poor performance in the pre- and post-filtering t_{PTEF}/t_E estimation test (figure 3). The S-G filter also performs poorly in the t_{PTEF}/t_E test, whereas the mSBM introduces minimal change to the values. However, one should not draw overly direct conclusions on the distortion performance from a situation where CGO is absent, as the presence of CGO might alter the performance of a complex nonlinear filtering method such as the mSBM.

The magnitude of the CGO can be multifold in supine position (Seppä *et al* 2010), but, considering the way the proposed method functions, this should not affect its performance.

4.2. Properties of the modified Schuessler–Bates method

Schuessler *et al* (1998) have presented a signal processing technique for attenuation of the CGO in esophageal pressure signals. We modified the algorithm to take lung volume induced changes in the CGO waveform into account, and assessed its performance on IP signals instead of pressure signals.

The CGO waveform is modulated by the lung volume (figure 4), which is most likely due to a combination of physiological changes in the heart pumping function and in the impedance measurement sensitivity field. Regardless of the origin of the phenomenon, as long as it is consistent and significant, it is beneficial to take it into account when filtering the CGO. In this proposed extension of the method of Schuessler *et al*, the ensembled CGO waveforms are divided into bins according to the momentary lung volume. The number of bins is an important factor. Smaller number of bins will increase the amount of ensembles in each bin resulting presumably in a more accurate estimate of the CGO waveform, but at the same time it will decrease the ability to track lung volume induced changes in the CGO waveform. We considered four bins to be a reasonable compromise between these two issues. Two or three bins could have been insufficient amount as illustrated by the highly nonlinear waveform change with volume change in figure 4 around the 14th knot point.

When IP is used for longer measurement periods, for instance, in an ambulatory 24 h recording (Vuorela *et al* 2010), it is clear that the CGO waveform will change due to postural and physiological changes. Although the algorithm version in this evaluation did not incorporate recursive waveform adaptation over time, there are no constraints for implementing the adaptive features presented in the original paper of Schuessler *et al*. It should be noted though that the adaptation will be slower in the presented modified version of the algorithm, because multiple CGO ensemble averages, one per each lung volume bin, need to be recursively adapted, instead of only a single average. Thus, in situations where fast adaptation to CGO waveform changes is needed, the original Schuessler–Bates method could be more successful.

Both required control signals, the ECG and the lung volume, are readily available in the IP measurement; the ECG signal can be measured from the same leads as IP and the lung volume information is intrinsically available in the IP signal. This increases the attractiveness of the method.

4.3. Conclusion

The modified Schuessler–Bates method for attenuating CGOs in IP performs excellently in terms of the CGO signal attenuation and preservation of the respiratory part of the impedance signal. Its use is highly recommended, especially when more demanding pulmonary volume or flow parameters such as t_{PTEF}/t_E are to be derived from the IP signal.

Acknowledgment

This work was supported by a grant from the Finnish Cultural Foundation.

References

- Bates J H T 2009 *Lung Mechanics: An Inverse Modeling Approach* 1st edn (Cambridge: Cambridge University Press)
- Brown B, Barber D, Morice A and Leathard A 1994 Cardiac and respiratory related electrical impedance changes in the human thorax *IEEE Trans. Biomed. Eng.* **41** 729–34
- Nagel J, Shyu L, Reddy S, Hurwitz B, McCabe P and Schneiderman N 1989 New signal processing techniques for improved precision of noninvasive impedance cardiography *Ann. Biomed. Eng.* **17** 517–34
- Savitzky A and Golay M J E 1964 Smoothing and differentiation of data by simplified least squares procedures *Anal. Chem.* **36** 1627–39
- Schuessler T F, Gottfried S B, Goldberg P, Kearney R E and Bates J H T 1998 An adaptive filter to reduce cardiogenic oscillations on esophageal pressure signals *Ann. Biomed. Eng.* **26** 260–7
- Seppä V-P, Viik J and Hyttinen J 2010 Assessment of pulmonary flow using impedance pneumography *IEEE Trans. Biomed. Eng.* **57** 2277–85
- van der Ent C, Brackel H, Mulder P and Bogaard J 1996 Improvement of tidal breathing pattern analysis in children with asthma by on-line automatic data processing *Eur. Respir. J.* **9** 1306–13
- Vuorela T, Seppä V-P, Vanhala J and Hyttinen J 2010 Design and implementation of a portable long-term physiological signal recorder *IEEE Trans. Inform. Technol. Biomed.* **14** 718–25
- Wilson A J, Franks C I and Freeston I L 1982 Methods of filtering the heart-beat artefact from the breathing waveform of infants obtained by impedance pneumography *Med. Biol. Eng. Comput.* **20** 293–8

Publication III

Seppä, V.-P., Hyttinen, J., Uitto, M., Chrapek, W., & Viik, J. 2013a. Novel electrode configuration for highly linear impedance pneumography. *Biomedizinische Technik. Biomedical engineering*, 58(1), 35-38.

Short communication

Ville-Pekka Seppä*, Jari Hyttinen, Marko Uitto, Wojciech Chrapek and Jari Viik

Novel electrode configuration for highly linear impedance pneumography

Abstract: Impedance pneumography (IP) is a non-invasive respiration measurement technique. Emerging applications of IP in respiratory medicine use the measured signal to monitor pulmonary flow and volume parameters related to airway obstruction during tidal breathing (TB). This requires a high impedance change (ΔZ)-to-lung volume change (ΔV) linearity. Four potential electrode configurations were tested on 10 healthy subjects. Only the novel configuration where the electrodes were placed in both the thorax and the arms yielded a highly linear $\Delta Z/\Delta V$ in all subjects. The presented electrode configuration may expand the clinical use of IP from the conventional tidal volume estimation to flow measurement.

Keywords: functional residual capacity; lung function testing; lung volume; thoracic electrical impedance; tidal breathing.

*Corresponding author: Ville-Pekka Seppä, Department of Electronics and Communications Engineering, Tampere University of Technology, Biokatu 6, FIN-33520 Tampere, Finland, Phone: +358 445062797, E-mail: ville-pekka.seppa@tut.fi

Jari Hyttinen, Marko Uitto and Jari Viik: Department of Electronics and Communications Engineering, Tampere University of Technology, Tampere, Finland

Wojciech Chrapek: Department of Anesthesia and Intensive Care, Tampere University Hospital, Tampere, Finland

Impedance pneumography (IP) provides a minimally intrusive mode of measurement for lung volume changes. In the IP recording, a small high-frequency current is passed through a pair of skin electrodes and another pair of electrodes is used to record the generated voltage that is related to the impedance (Z), which in turn is related to the lung volume (V). Although several studies have shown a linear relation between the thoracic impedance change and the lung volume change ($\Delta Z/\Delta V$), which enables an even pulmonary flow rate signal derivation [16], the clinical applications of IP are still limited mainly to respiration rate and apnea detection in hospitalized patients. The novel approach of long-term assessment of respiratory flow-volume diagrams during tidal breathing (TB)

[13, 15, 16] using ambulatory IP recording equipment [18] may have important clinical implications, especially in the evaluation of obstructive respiratory diseases in non-cooperative patients such as infants and preschool children [4, 11, 17]. Flow signal derivation will, however, introduce strict requirements for the linearity of the $\Delta Z/\Delta V$ ratio at all lung volumes.

Previous investigations have demonstrated a fairly linear $\Delta Z/\Delta V$ ratio on different lung volumes and body postures [2, 8, 12, 16], although the comparison is hindered by different measures used in the reports. Baker et al. [2] and Logic et al. [12] made a relevant finding that a higher midaxillary electrode placement (below axilla) exhibits a more linear $\Delta Z/\Delta V$ ratio than lower placements. Goldensohn and Zablou [7] even placed the electrodes in the arms and claimed that it yielded a high $\Delta Z/\Delta V$ linearity. However, the respiratory maneuvers of the previous studies only involved deep inspirations, excluding deep expirations that would have reduced the lung volume below the level of normal functional residual capacity (FRC). Baker and Geddes [1] did publish an example IP recording of full vital capacity maneuver (VCM), but a close examination of the presented recording reveals a detail neglected in the article: at low lung volumes, the IP signal is highly non-linear with the lung volume. Non-linearity as such is not always harmful, but if the mathematical relation of ΔZ and ΔV is unknown or varies from subject to subject, as is the case here, having a linear relationship is clearly more preferred.

The understanding of the $\Delta Z/\Delta V$ linearity throughout the full lung volume is important even when the measurements are conducted during TB because TB may occur at a different FRC level, even in the same subject at different times. FRC can change considerably due to many commonly encountered factors, such as supine posture, anatomical differences, mild obesity, and pathological conditions such as chronic obstructive pulmonary disease, and asthma. Thus, for the emerging IP applications that derive pulmonary flow parameters, knowledge on the IP signal behavior on the complete range of lung volume is important. In a previous clinical experiment, we found severe $\Delta Z/\Delta V$ non-linearity in eight of 35 patients measured with a high midaxillary electrode configuration

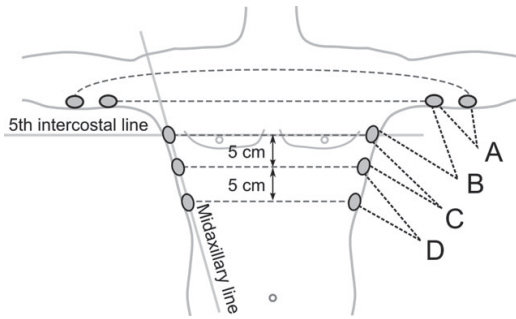


Figure 1 The four different electrode configurations used for IP recording.

The electrodes of configuration A were placed on the arms between biceps and triceps brachii muscles at the level of the electrodes of configuration C and attention was paid to prevent skin contact between the arms and the sides. The electrode pair used for voltage measurement in the IP measurement was the one closer to the axilla in configuration A, and the lower one in configurations B-D.

even during TB. A common feature of these subjects was overweight, which strongly lowers the FRC [10], which as a consequence of the lowered lung volume, may render IP highly nonlinear as shown in this communication. This non-linearity may have prevented earlier clinical use of IP in flow measurement or in other more demanding uses than respiratory rate monitoring.

The electrode configurations tested in this study are illustrated in Figure 1. Example $\Delta Z/\Delta V$ relations from one subject are plotted in Figure 2. They illustrate a typical finding of configuration A having a convex $\Delta Z/\Delta V$ curve and C and D being concave, but this was not always the case as summarized in Table 1.

Configuration B was clearly superior to the other ones in terms of the $\Delta Z/\Delta V$ linearity (Figure 3). Its R^2 values for TB and the VCM were 0.99 ± 0.01 (mean \pm standard

deviation, lowest 0.98) and 0.99 ± 0.01 (lowest 0.96), respectively. The corresponding values for configuration A were 0.92 ± 0.12 (lowest 0.67) and 0.90 ± 0.12 (lowest 0.65), for configuration C 0.97 ± 0.04 (lowest 0.88) and 0.91 ± 0.07 (lowest 0.77), and for configuration D 0.77 ± 0.33 (lowest 0.07) and 0.74 ± 0.17 (lowest 0.53). Although some of the mean R^2 values of the other configurations are close to those of configuration B, it is important to note that they all exhibit multiple exceptionally low R^2 values on individual subjects, whereas configuration B is consistently very linear. The inter-subject variation in the $\Delta Z/\Delta V$ curves was high for all configurations. Also for configuration B as high as approximately 100% inter-subject variation in the $\Delta Z/\Delta V$ slope was found.

We observed a severe $\Delta Z/\Delta V$ non-linearity in the IP recordings, especially during a slow VCM, when the measurement electrodes were placed only on the arms (configuration A) or only on the sides of the chest (configurations C and D). However, this non-linearity was not encountered when the electrodes were placed in both chest and arms (B). Abdominal vs. thoracic breathing was not directly controlled in our study, but generally, TB is considered to happen predominantly abdominally, whereas the VCM will also involve the use of the secondary respiratory muscles and thoracic expansion. Thus, we consider that this is at least indirectly taken into account. The potential causes for the findings are discussed in the following.

For the lower electrode placements (configurations C and D), there are at least two potential reasons for the non-linearity: first, the motion and shape change of the thorax and thoracic organs, particularly the diaphragm and liver; second, the inhomogeneous ventilation distribution and small airway closing. Regarding the effect of the thorax shape change, Logic et al. [12] found an improvement in the linearity of the low-placed electrode configurations

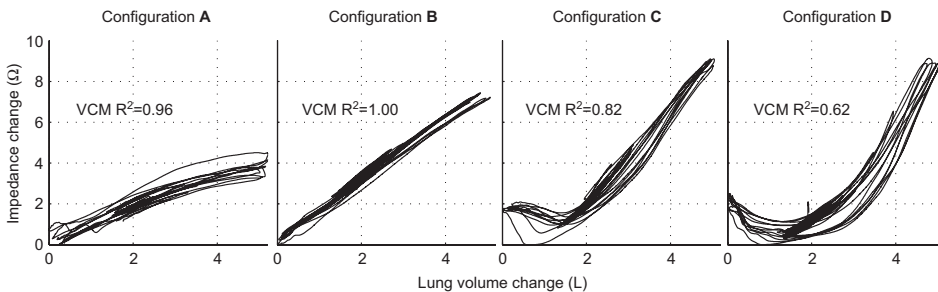


Figure 2 Typical impedance change-to-volume change curves during TB and VCMs with four different electrode configurations (Figure 1) measured from one subject.

The IP signal was recorded with Biopac EBI100C (Biopac Systems Inc., Goleta, CA, USA) using a 100-kHz, 400- μ A excitation current. The cardiogenic oscillations were removed by a filtering technique developed for this purpose [13]. The respiratory sequence consisted of free TB for three to four cycles followed by two slow VCMs, with the whole sequence repeated three times.

Table 1 Visual description of the shapes of the impedance change to volume change ($\Delta Z/\Delta V$) linearity curves.

Configuration	Convex	Concave	Mixed	Inverted	Total
A	3	1	0	0	4
B	0	0	0	0	0
C	0	8	0	0	8
D	0	5	2	1	8

The values represent the number of patients (out of 10) for whom the curve was clearly non-linear ($R^2 < 0.95$). Here convex means a curve such as that of configuration A, and concave, such as those of configurations C and D in Figure 2. In the two mixed cases, the curve was otherwise concave, except that there was a sharp downward deflection of impedance in the very low lung volume. In the inverted case, impedance decreased with increasing volume.

when the subjects wore a cast that prevented thoracic deformation during respiration. Also, the movement of the diaphragm and liver potentially causes non-linearity [3], as they have significantly different electrical conductivity from the lung tissue [5]. After a deep exhalation and generally in lowered FRC, the diaphragm and liver reside more cephalad (headward) and thus are closer to the sensitivity field of the recording electrodes. Regarding the second contributor, inhomogeneous ventilation and small airway closure occur even in healthy young subjects when the lung volume is lowered below FRC level. As the lung volume decreases, the smaller intraparenchymal airways decrease in caliber until they close at low lung volume.

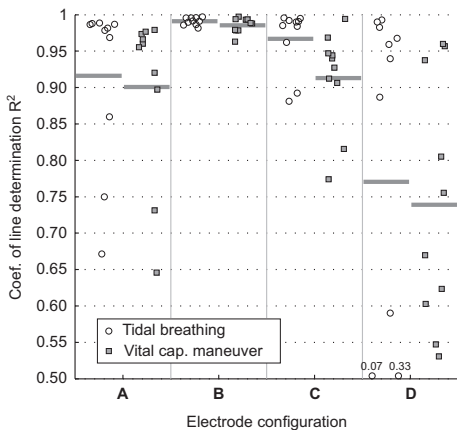


Figure 3 The impedance change-to-volume change ($\Delta Z/\Delta V$) linearity of each measurement was calculated as a least-squares line-fit coefficient of the determination R^2 of the impedance-to-volume curves, separately for TB and the VCMs. Simultaneous IP and pneumotachograph (A. Fleisch No. 3, Lausanne, Switzerland, with Biopac SS40L pressure transducer) recording was conducted on 10 lung-healthy male volunteers (age 24–46 years, height 168–197 cm, weight 63–113 kg, body mass index 21.1–34.1) in standing position.

During exhalation in an upright posture, this deflation and closure occurs predominantly and earlier in the lower part of the lung. As airway closure is known to affect the electrical impedance of the lung [9], this could partially explain why the low configurations exhibit the presented $\Delta Z/\Delta V$ non-linearity usually in the manner illustrated in Figure 2. Both the reasons mentioned above could be attributed to the finding that the $\Delta Z/\Delta V$ non-linearity especially occurs during deep exhalation in the lower electrode locations (configurations C and D).

For the highest electrode placement (configuration A), the non-linearity cannot be explained by the same contributors as in configurations C and D. However, IP measurement is sensitive to impedance changes in those tissue regions where the current and voltage lead fields both exist and are parallel [6]. Thus, in configuration A, the weak performance might stem from the ill-focused IP measurement sensitivity field that involves the arms and shoulders. It thus measures impedance changes, for example, due to motion and slight geometry changes, in areas that do not linearly contribute to lung volume changes. Moreover, it may not span the whole of the lung as well as configuration B.

Configuration B avoids the above-mentioned weaknesses of the other configurations and thus performs consistently very well.

We conclude that correct electrode placement is very important for the linearity of the measurement when IP is used to assess lung volume changes and, consecutively, respiratory flow rate. The three electrode configurations where electrodes were placed only on the arms or only on the sides of the chest were found to be clearly non-linear (multiple $R^2 < 0.85$) when assessed in the complete lung volume range. This is important even in TB measurements because TB may occur at various lung volume levels. The newly presented configuration, with one electrode pair on the sides of the thorax and the other one in the arms, was the only one that was linear in all subjects ($R^2 > 0.95$ for all). This new configuration combined with appropriate cardiogenic filtering enables the clinical use of IP in tidal flow measurement.

Acknowledgments: The authors have received funding from the Finnish Cultural Foundation, the Jalmari and Rauha Ahokas Foundation, and the Tampere Tuberculosis Foundation for this work.

Conflict of interest statement

None.

Ethical standards: This study was approved by the Institutional Review Board of the Pirkanmaa Hospital District, Finland.

Received August 13, 2012; accepted January 2, 2013; online first January 24, 2013

References

- [1] Baker LE, Geddes LA. The measurement of respiratory volumes in animals and man with use of electrical impedance. *Ann NY Acad Sci* 1970; 170: 667–688.
- [2] Baker L, Geddes L, Hoff H. A comparison of linear and non-linear characterizations of impedance spirometry data. *Med Biol Eng Comput* 1966; 4: 371–379.
- [3] Baker LE, Geddes LA, Hoff HE, Chaput CJ. Physiological factors underlying transthoracic impedance variations in respiration. *J Appl Physiol* 1966; 21: 1491–1499.
- [4] Beydon N, Davis SD, Lombardi E, et al. An official American Thoracic Society/European Respiratory Society statement: pulmonary function testing in preschool children. *Am J Respir Crit Care Med* 2007; 175: 1304–1345.
- [5] Gabriel S, Lau RW, Gabriel C. The dielectric properties of biological tissues: II. Measurements in the frequency range 10 Hz to 20 GHz. *Phys Med Biol* 1996; 41: 2251–2269.
- [6] Geselowitz DB. An application of electrocardiographic lead theory to impedance plethysmography. *IEEE Trans Biomed Eng* 1971; 18: 38–41.
- [7] Goldensohn ES, Zablou L. An electrical impedance spirometer. *J Appl Physiol* 1959; 14: 463–464.
- [8] Grenvik A, Ballou S, McGinley E, Millen JE, Cooley WL, Safar P. Impedance pneumography. Comparison between chest impedance changes and respiratory volumes in 11 healthy volunteers. *Chest* 1972; 62: 439–443.
- [9] Hinz J, Moerer O, Neumann P, Dudykevych T, Hellige G, Quintel M. Effect of positive end-expiratory-pressure on regional ventilation in patients with acute lung injury evaluated by electrical impedance tomography. *Eur J Anaesthesiol* 2005; 22: 817–825.
- [10] Jones RL, Nzekwu M-MU. The effects of body mass index on lung volumes. *Chest* 2006; 130: 827–833.
- [11] Lødrup Carlsen KC. Tidal breathing at all ages. *Monaldi Arch Chest Dis* 2000; 55: 427–434.
- [12] Logic JL, Maksud MG, Hamilton LH. Factors affecting transthoracic impedance signals used to measure breathing. *J Appl Physiol* 1967; 22: 251–254.
- [13] Seppä V-P, Hyttinen J, Viik J. A method for suppressing cardiogenic oscillations in impedance pneumography. *Physiol Meas* 2011; 32: 337–345.
- [14] Seppä V-P, Hyttinen J, Viik J. Agreement between impedance pneumography and pneumotachograph in estimation of a tidal breathing parameter. *Chest* 2010; 138: 816A.
- [15] Seppä V-P, Kööbi T, Kähönen M, Hyttinen J, Viik J. Impedance pneumography for assessment of a tidal breathing parameter in patients with airway obstruction. *Eur Respir J* 2011; 38: 219s.
- [16] Seppä V-P, Viik J, Hyttinen J. Assessment of pulmonary flow using impedance pneumography. *IEEE Trans Biomed Eng* 2010; 57: 2277–2285.
- [17] Thamrin C, Nydegger R, Stern G, et al. Associations between fluctuations in lung function and asthma control in two populations with differing asthma severity. *Thorax* 2011; 66: 1036–1042.
- [18] Vuorela T, Seppä V-P, Vanhala J, Hyttinen J. Design and implementation of a portable long-term physiological signal recorder. *IEEE Trans Inf Technol Biomed* 2010; 14: 718–725.

Publication IV

Seppä, V.-P., Uitto, M., & Viik, J. 2013c. Tidal breathing flow-volume curves with impedance pneumography during expiratory loading. Conference proceedings: Annual International Conference of the IEEE Engineering in Medicine and Biology Society. IEEE Engineering in Medicine and Biology Society. Conference, 2013, 2437-2440.

In reference to IEEE copyrighted material which is used with permission in this thesis, the IEEE does not endorse any of Tampere University of Technology's products or services. Internal or personal use of this material is permitted. If interested in reprinting/republishing material for advertising or promotional purposes or for creating new collective works for resale or redistribution, please go to http://www.ieee.org/publications_standards/publications/rights/rights_link.html to learn how to obtain a License from RightsLink.

Tidal Breathing Flow-Volume Curves with Impedance Pneumography During Expiratory Loading

Ville-Pekka Seppä, Marko Uitto, and Jari Viik

Abstract—Diagnosis of asthma in the preschool children is difficult due to lack of objective lung function tests suitable for this age group. Impedance pneumography (IP) is a mode of measurement that may potentially enable ambulatory 24h recording of tidal breathing indices and respiratory dynamics that are known to relate to small airway obstruction. The aim of this research was to induce changes in breathing control and mechanics and study the ability of IP to reproduce TBFVC and track its changes under potentially difficult conditions. This was achieved by a comparison of direct mouth pneumotachograph (PNT) and IP tidal breathing flow-volume curves (TBFVC) during free breathing and expiratory loading obtained from 17 young lung-healthy subjects. The expiratory loading produced strong and significant changes in the respiratory pattern and mouth pressure. The agreement of PNT and IP normalized TBFVCs was found excellent having the highest distance between the normalized TBFVCs of (mean \pm SD) 7.4 % \pm 3.6 % and 6.2 % \pm 3.0 % during free and loaded breathing, respectively. The agreement was not affected by the presence of the expiratory load despite it poses multiple potential hazards for the IP measurements. We conclude that by using correct electrode placement and cardiac filtering, IP was able to accurately reproduce and track changes in normalized TBFVCs under normal and abnormal respiratory conditions in healthy adult subjects.

I. INTRODUCTION

Diagnosis of asthma in preschool children is difficult because of unsuitability of the conventional lung function testing [1]. However, measurements during spontaneous tidal breathing (TB) require minimal co-operation, thus being suitable for small children and infants. There is a large body of research suggesting that parameters derived from TB flow curves or flow-volume curves (TBFVC) change in a deterministic way with obstructive respiratory diseases in young patients. The studies have shown for instance that TB parameters relate to forced expiratory volume in 1 second (FEV1) [2], airway resistance [3], bronchodilator response [4], [5], and methacholine challenge [6], [7] and that they can be used to discriminate between pathological respiratory conditions [8]. The current methods for assessing the TB pattern are hindered by the need of a direct access with the airways. Sedation can sometimes be used to overcome the psychological aspects of the measurement, but the physical face contact [9] and the increased dead space [10] still distort the respiratory pattern. Recently, we have presented highly accurate TB measurements in healthy adults and in

adult patients with airway obstruction using a noninvasive mode of measurement, namely the impedance pneumography (IP) [11]–[13]. IP overcomes the presented shortcomings of the conventional measurements. In addition, through 24h TB pattern recording with ambulatory instrumentation [14], IP potentially enables assessing the temporal manifestations of asthma that are receiving increasing research interest [15]–[17].

It is a common misconception that the lung volume signal produced by the IP technique would stem solely, or at least mostly, from chest wall motion as in other noninvasive modes of respiration measurement. This would imply that abnormal respiratory mechanics could distort the IP measurement, and that IP would not be accurate enough to track subtle changes in the respiratory flow pattern. However, IP signal originates largely from the lung tissue [18], not only from the chest wall motion enabling making it potentially resistant to changes in breathing style.

The presented study serves two purposes: Firstly, to show that abnormal respiratory physics, mechanics and control, as induced by intense expiratory loading, do not degrade the IP measurement accuracy, and secondly, to show that IP can be used to accurately reproduce the TBFVC and track its changes in individual subjects.

II. MATERIALS AND METHODS

1) *Subjects and Procedures:* The subjects were 17 healthy young subjects (age 22-28, body mass index 19.2-26.9, 4 females) with no self-reported chronic respiratory diseases. The study was approved by the institutional review board and a written consent was obtained from all participants. Three-minute recordings of tidal breathing were acquired simultaneously with a pneumotachograph attached to the expiratory limb of the system and with an IP system (Figure 1). The measurements were conducted in supine position and the recording was repeated after attaching a flow resistor element on the expiratory limb. The current feeding IP electrodes were placed on the fifth intercostal space on the midaxillary line and the voltage measurement electrodes on the same level on the proximal side of the arm between the biceps and triceps brachii muscles. This electrode configuration has been previously reported to produce a highly linear impedance change to lung volume change ratio [19]. In addition, single channel ECG was measured to enable the use of a signal filtering algorithm that removes the cardiogenic part of the impedance signal (23).

2) *Equipment:* The subjects wore a face mask (7900 Series, Hans Rudolph, Shawnee, KS 66227, USA) of the

*This work was supported by research grants from the Finnish Cultural Foundation, the Jalmari and Rauha Ahokas Foundation, and the Tampere Tuberculosis Foundation

All authors are with the Department of Electronics and Communications Engineering, Tampere University of Technology, Biokatu 6, 33520, Tampere, Finland ville-pekka.seppa at tut.fi

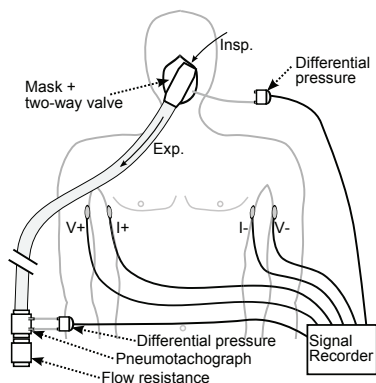


Fig. 1. The measurement setup used for simultaneous pneumotachograph and impedance pneumography tidal breathing recording. The current feeding electrodes of the impedance measurement (I+, I-) were placed on the fifth intercostal space on the midaxillary line and the voltage electrodes (V+, V-) on the arms in a matching position in the proximal side. The flow resistance was attached when indicated. An additional differential pressure sensor was attached to the mask to monitor mouth pressure for post-measurement detection of possible mask leaking.

best fitting size (XS, S, M, L). The mask was connected to a two-way valve system (Series 2700 Large, Hans Rudolph) where the inspiratory limb was free and the expiratory limb was connected to the PNT and the 15 cm_{H₂O}/l resistor element (7100R, Hans Rudolph) with a three meter tube. For a post-measurement detection of mask leaks, the mouth pressure was continuously recorded inside the mask with a pressure sensor (SS42L, Biopac Systems). The heated PNT (A. Fleisch No. 3, Lausanne, Switzerland) was connected to a differential pressure transducer (SS40L, Biopac Systems, Goleta, CA 93117, USA) with a declared combined linearity and hysteresis error of $\pm 0.05\%$. The flow measurement system was calibrated before each subject using a three-litre calibration syringe (PCS-3000, Piston Medical, Budapest, Hungary). IP signal was recorded with a bioimpedance measurement device (EB1100C, Biopac Systems) using a 100 kHz, 400 μ A excitation current. All the transducers were connected to a Biopac MP35 unit that digitized and stored the signals at 500 Hz sampling frequency.

3) *Signal Processing and Statistical Analysis*: In addition to the respiratory component, the thoracic impedance signal also contains a cardiogenic component that originates from the pulsatile blood movement in the thorax. This distortive part of the signal was attenuated using a slightly modified version of the filtering algorithm presented by Seppä et al (23). For producing a representative TBFVC a number of breaths were averaged as instructed by the official guidelines on tidal breathing analysis [20]. The most similar respiratory cycles were discovered from the IP signal by an algorithm based on comparing the correlations of the flow signals of the cycles. If less than four similar cycles were found due to slow and irregular breathing, the measurement was excluded

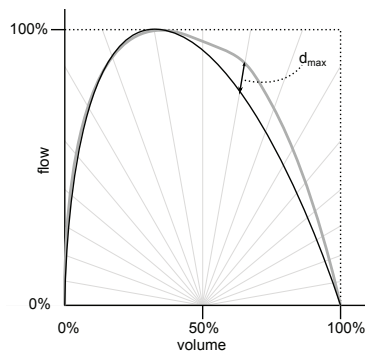


Fig. 2. The difference between the normalized expiratory tidal breathing flow volume curves obtained with pneumotachograph and impedance pneumograph was calculated along each of the radial grey lines in steps of 10 degrees. The largest found difference, d_{max} , was reported.

from the analysis. Each TBFVC was normalized in volume and flow for range 0...100 % and the chosen individual TBFVCs were averaged in 100 angle segments in a manner resembling the one illustrated in Figure 2 to produce a single representative TBFVC. Then the corresponding cycles in the PNT recording were normalized and averaged in the same way. The difference between IP and PNT for each pair of averaged TBFVCs was assessed by calculating their difference along radial lines with 10 degree separation and choosing the highest of those values to represent the difference d_{max} as illustrated in Figure 2. The statistical difference between measurements during the free and loaded breathing was assessed by the paired Wilcoxon signed rank test.

III. RESULTS

Two successful recordings of TBFVC were obtained from all but one subjects simultaneously with PNT and IP yielding a total of 33 measurements. For one subject the loaded respiration was too irregular to produce four similar TBFVCs as required for the analysis. The amount of similar breaths included in the averaging of the TBFVC ranged from 6 to 57 (mean 28.1).

The expiratory loading produced strong changes in the TBFVCs (Fig. 3) along with significant ($p < 0.05$) changes in peak expiratory mouth pressure (PEP_m), tidal peak expiratory flow (TPEF), expiratory time (t_e), ratio of inspiratory to expiratory time ($t_i:t_e$), and respiratory rate (RR) as measured by the PNT (Table I).

The difference between the IP and PNT TBFVCs as assessed by the d_{max} value was found to be (mean \pm SD) 7.4 \pm 3.6 % and 6.2 \pm 3.0 % during free and loaded breathing, respectively (Fig. 4). Most measurements (28 of 33) were found to have d_{max} below 10 %. The difference in d_{max} values between free and loaded breathing was not statistically significant ($p = 0.46$).

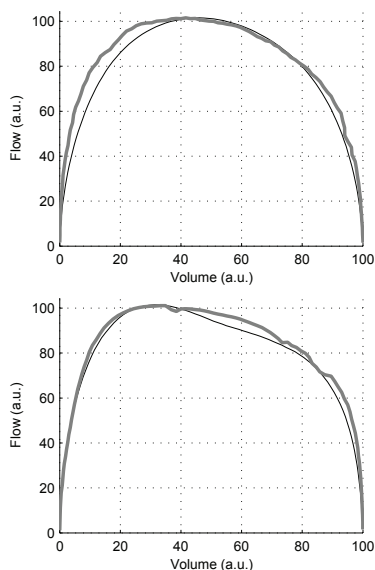


Fig. 3. Expiratory tidal breathing flow-volume curves obtained simultaneously with impedance pneumography (black) and pneumotachograph (gray) during free (upper) and loaded (lower) breathing having largest difference d_{\max} between PNT and IP 5.6 % ja 5.0 %, respectively.

IV. DISCUSSION

The intense expiratory loading used in this study produced clear effects on the control and mechanics of the breathing (Table I). This poses multiple potential hazards for the accuracy of IP measurements for example through substantial changes in the cyclic pattern of the respiratory muscle activation and motion of the chest wall [21], and changes in cardiorespiratory coupling and cardiac mechanics [22]. Indeed, one of the major difficulties in accurate respiratory flow measurement with IP has been posed by the cardiogenic oscillations (CGO). Recently a filter algorithm based on CGO ensemble averages modulated by instantaneous lung volume was proposed to solve the problem [23]. This study

TABLE I

PEAK EXPIRATORY MOUTH PRESSURE (PEPM), TIDAL PEAK EXPIRATORY FLOW (TPEF), EXPIRATORY TIME (T_E), RATIO OF INSPIRATORY TO EXPIRATORY TIME ($T_I:T_E$), RESPIRATORY RATE (RR), AND TIDAL VOLUME (VT) GIVEN AS MEAN \pm SD OBTAINED WITH A PNEUMOTACHOGRAPH ILLUSTRATE THE EFFECT OF THE EXPIRATORY LOADING ON RESPIRATION. *: P-VALUE < 0.05

Parameter	Free	Loaded
PEP _m (cmH ₂ O/s/l) *	0.61 \pm 0.03	4.38 \pm 0.28
TPEF (ml/s) *	327 \pm 17	228 \pm 14
t_E (s) *	2.65 \pm 1.24	3.95 \pm 1.88
$t_I:t_E$ (1) *	0.80 \pm 0.03	0.53 \pm 0.02
RR (min ⁻¹) *	14.8 \pm 4.3	12.6 \pm 4.8
VT (ml)	533 \pm 195	576 \pm 271

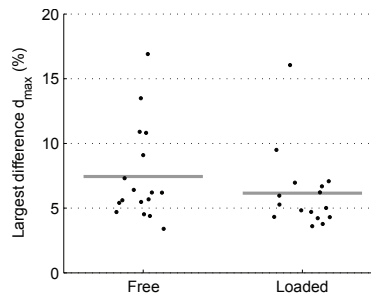


Fig. 4. Largest difference (d_{\max}) between the normalized tidal breathing flow volume curves obtained with pneumotachograph and impedance pneumograph as illustrated in Figure 2. Each dot represents one measurement and the lines denote the mean value.

brings further evidence of its efficacy under conditions that are rather complex from a cardiopulmonary standpoint. Namely, the pleural pressure changes modulate the heart rate and stroke volume [22], which contribute to the shape and frequency of the measured CGOs.

Furthermore, the electrode placement is most important in determining the dynamic ratio between the lung volume changes and the measured impedance. The electrode configuration used in this study had been previously presented only for prone subjects [19], but was now used in the supine position and found to work appropriately.

We conclude that the agreement between normalized TBFVCs produced with PNT and IP was found excellent. This was enabled by correct electrode positioning and appropriate filtering of the cardiac impedance signal. The agreement was not affected by change in respiratory flow pattern or the changes in the respiratory mechanics as induced by the respiratory loading.

REFERENCES

- [1] "NHLBI expert panel report 3 (EPR-3): guidelines for the diagnosis and management of asthma-summary report 2007." *J. Allergy. Clin. Immunol.*, vol. 120, no. 5 Suppl, pp. S94–138, 2007.
- [2] R. Cutrera, S. I. Filchev, R. Merolla, G. Willim, J. Haluszka, and R. Ronchetti, "Analysis of expiratory pattern for monitoring bronchial obstruction in school-age children," *Pediatr. Pulmonol.*, vol. 10, no. 1, pp. 6–10, 1991.
- [3] M. Morris, R. Madgwick, I. Collyer, F. Denby, and D. Lane, "Analysis of expiratory tidal flow patterns as a diagnostic tool in airflow obstruction," *Eur. Respir. J.*, vol. 12, no. 5, pp. 1113–1117, 1998.
- [4] C. van der Ent, H. Brackel, J. van der Laag, and J. Bogaard, "Tidal breathing analysis as a measure of airway obstruction in children three years of age and older," *Am. J. Respir. Crit. Care Med.*, vol. 153, no. 4, pp. 1253–1258, 1996.
- [5] K. C. Lødrup Carlsen, M. Pettersen, and K.-H. Carlsen, "Is bronchodilator response in 2-yr-old children associated with asthma risk factors?" *Pediatr. Allergy. Immunol.*, vol. 15, no. 4, pp. 323–330, 2004.
- [6] M. R. Benoist, J. J. Brouard, P. Rufin, C. Delacourt, S. Waernessyckle, and P. Scheinmann, "Ability of new lung function tests to assess methacholine-induced airway obstruction in infants," *Pediatr. Pulmonol.*, vol. 18, no. 5, pp. 308–316, 1994.
- [7] C. van der Ent, H. Brackel, P. Mulder, and J. Bogaard, "Improvement of tidal breathing pattern analysis in children with asthma by on-line automatic data processing," *Eur. Respir. J.*, vol. 9, no. 6, pp. 1306–13, 1996.

- [8] S. Leonhardt, P. Ahrens, and V. Kecman, "Analysis of tidal breathing flow volume loops for automated lung-function diagnosis in infants," *IEEE Trans. Biomed. Eng.*, vol. 57, no. 8, pp. 1945–1953, 2010.
- [9] T. Dolfin, P. Duffty, D. Wilkes, S. England, and H. Bryan, "Effects of a face mask and pneumotachograph on breathing in sleeping infants," *Am. Rev. Respir. Dis.*, vol. 128, no. 6, pp. 977–979, 1983.
- [10] M. J. Marsh, D. Ingram, and A. D. Milner, "The effect of instrumental dead space on measurement of breathing pattern and pulmonary mechanics in the newborn," *Pediatr. Pulmonol.*, vol. 16, no. 5, pp. 316–322, 1993.
- [11] V.-P. Seppä, J. Viik, and J. Hyttinen, "Assessment of pulmonary flow using impedance pneumography," *IEEE Trans. Biomed. Eng.*, vol. 57, no. 9, pp. 2277–2285, 2010.
- [12] V.-P. Seppä, J. Hyttinen, and J. Viik, "Agreement between impedance pneumography and pneumotachograph in estimation of a tidal breathing parameter," *Chest*, vol. 138, no. 4 Suppl, p. 816A, 2010.
- [13] V.-P. Seppä, T. Kööbi, M. Kähönen, J. Hyttinen, and J. Viik, "Impedance pneumography for assessment of a tidal breathing parameter in patients with airway obstruction," *Eur. Respir. J.*, vol. 38, no. 55 Suppl, p. 219s, 2011.
- [14] T. Vuorela, V.-P. Seppä, J. Vanhala, and J. Hyttinen, "Design and implementation of a portable long-term physiological signal recorder," *IEEE Trans. Inf. Technol. Biomed.*, vol. 14, no. 3, pp. 718–725, 2010.
- [15] U. Frey, T. Brodbeck, A. Majumdar, D. R. Taylor, G. I. Town, M. Silverman, and B. Suki, "Risk of severe asthma episodes predicted from fluctuation analysis of airway function," *Nature*, vol. 438, no. 7068, pp. 667–670, 2005.
- [16] U. Frey and B. Suki, "Complexity of chronic asthma and chronic obstructive pulmonary disease: implications for risk assessment, and disease progression and control," *Lancet*, vol. 372, no. 9643, pp. 1088–1099, 2008.
- [17] J. Veiga, A. J. Lopes, J. M. Jansen, and P. L. Melo, "Airflow pattern complexity and airway obstruction in asthma," *J. Appl. Physiol.*, vol. 111, no. 2, pp. 412–419, 2011.
- [18] P. Nopp, N. Harris, T.-X. Zhao, and B. Brown, "Model for the dielectric properties of human lung tissue against frequency and air content," *Med. Biol. Eng. Comput.*, vol. 35, no. 6, pp. 695–702, Nov. 1997.
- [19] V.-P. Seppä, J. Hyttinen, M. Uitto, W. Chrapek, and J. Viik, "Novel electrode configuration for highly linear impedance pneumography," *Biomed. Eng.*, vol. 58, no. 1, pp. 35–38, Jan. 2013.
- [20] N. Beydon, S.D. Davis, E. Lombardi, J.L. Allen JL, H.G.M. Arets, P. Aurora, et al., "An Official American Thoracic Society/European Respiratory Society Statement: Pulmonary Function Testing in Preschool Children," *Am. J. Respir. Crit. Care Med.* vol. 172, no. 12, pp. 1304–1345, 2007.
- [21] B. Gothe and N. S. Cherniack, "Effects of expiratory loading on respiration in humans," *J. Appl. Physiol.*, vol. 49, no. 4, pp. 601–608, 1980.
- [22] A. Guz, J. A. Innes, and K. Murphy, "Respiratory modulation of left ventricular stroke volume in man measured using pulsed doppler ultrasound," *J. Physiol.*, vol. 393, no. 1, pp. 499–512, 1987.
- [23] V.-P. Seppä, J. Hyttinen, and J. Viik, "A method for suppressing cardiogenic oscillations in impedance pneumography," *Physiol. Meas.*, vol. 32, no. 3, pp. 337–345, 2011.

Publication V

Seppä, V.-P., Pelkonen, A. S., Kotaniemi-Syrjänen, A., Mäkelä, M. J., Viik, J., & Malmberg, L. P. 2013b. Tidal breathing flow measurement in awake young children by using impedance pneumography. *Journal of Applied Physiology*, 115(11), 1725-1731.

Tidal breathing flow measurement in awake young children by using impedance pneumography

Ville-Pekka Seppä,¹ Anna S. Pelkonen,² Anne Kotaniemi-Syrjänen,² Mika J. Mäkelä,² Jari Viik,¹ and L. Pekka Malmberg²

¹Department of Electronics and Communications Engineering, Tampere University of Technology, Tampere, Finland; and ²Department of Allergy, University Central Hospital, Helsinki, Finland

Submitted 6 June 2013; accepted in final form 30 September 2013

Seppä V-P, Pelkonen AS, Kotaniemi-Syrjänen A, Mäkelä J, Viik J, Malmberg LP. Tidal breathing flow measurement in awake young children by using impedance pneumography. *J Appl Physiol* 115: 1725–1731, 2013. First published October 3, 2013; doi:10.1152/jappphysiol.00657.2013.— Characteristics of tidal breathing (TB) relate to lung function and may be assessed even in young children. Thus far, the accuracy of impedance pneumography (IP) in recording TB flows in young children with or without bronchial obstruction has not been evaluated. The aim of this study was to evaluate the agreement between IP and direct flow measurement with pneumotachograph (PNT) in assessing TB flow and flow-derived indices relating to airway obstruction in young children. Tidal flow was recorded for 1 min simultaneously with IP and PNT during different phases of a bronchial challenge test with methacholine in 21 wheezy children aged 3 to 7 years. The agreement of IP with PNT was found to be excellent in direct flow signal comparison, the mean deviation from linearity ranging from 2.4 to 3.1% of tidal peak inspiratory flow. Methacholine-induced bronchoconstriction or consecutive bronchodilation induced only minor changes in the agreement. Between IP and PNT, the obstruction-related tidal flow indices were equally repeatable, and agreement was found to be high, with intraclass correlation coefficients for T_{V_{TEF}/V_E} , V_{V_{TEF}/V_E} , and parameter S being 0.94, 0.91, and 0.68, respectively. Methacholine-induced changes in tidal flow indices showed significant associations with changes in mechanical impedance of the respiratory system assessed by the oscillometric technique, with the highest correlation found in V_{V_{TEF}/V_E} ($r = -0.54$; $P < 0.005$ and $r = -0.55$; $P < 0.005$ by using IP or PNT, respectively). The results indicate that IP can be considered as a valid method for recording tidal airflow profiles in young children with wheezing disorders.

lung function; tidal breathing; wheezing; children; impedance pneumography

LUNG FUNCTION ASSESSMENT OF preschool children is hindered by their limited cooperation in conventional tests such as peak expiratory flow (PEF) or spirometry, and the methods available for younger children are laborious and time-consuming. However, indices derived from spontaneous tidal respiratory air flow and the shape of tidal expiratory flow-volume and flow-time curves relate to lung function such as forced expiratory volume in 1 s (FEV1) (3) or airway resistance (18), and they are easier to record even in young children. As a more advanced approach, the time dynamics and complexity properties of the tidal air flow signal have been analyzed and found to relate to various respiratory conditions (7, 9, 22, 30, 34). These analyses require accurate recording of tidal air flow profiles, which thus far has been possible primarily in a laboratory

setting directly from the mouth with a pneumotachograph for limited time periods (2).

Recently, a novel option for assessing tidal flow has emerged as a result of development in signal processing of impedance pneumography (IP) (26), which records continuous lung volume changes through skin electrodes. This method has shown excellent pulmonary flow signal waveform agreement in healthy adults in a laboratory setting (25, 27), and has additional potential advantages by avoiding interference with breathing pattern by a pneumotachograph and enabling tidal flow measurement in an ambulatory long-term setting; for instance, overnight at home. There are, however, no previous data on the accuracy of IP in tidal flow measurement of young children with or without airflow obstruction. Age-dependent changes in regional ventilation (4), ventilation-perfusion mismatch during obstructive episodes of asthma (21), and irregular breathing patterns of awake, noncooperative young children may potentially compromise the linear behavior of airflow signal recorded with IP. This study presents for the first time a thorough analysis on the accuracy of IP in tidal flow assessment in young children in an experimental design, including induced bronchoconstriction.

The primary objective of this work was to study the agreement between IP and a direct mouth pneumotachograph (PNT) in tidal flow measurement in preschool children. The agreement was assessed at baseline conditions and during methacholine-induced bronchoconstriction (MIB). As the secondary aim, the changes in tidal flow characteristics during MIB were compared with mechanical impedance measurements of the respiratory system by using an oscillometric technique.

MATERIALS AND METHODS

Patients and clinical procedure. The study subjects included 21 children aged 3–7 years who were referred to the Pediatric Unit of the Department of Allergy, Helsinki University Central Hospital because of recurrent or persistent lower respiratory tract symptoms (wheeze, cough, and/or shortness of breath). The baseline characteristics of the children are presented in Table 1. Most (90%) children were born full term. Two prematurely born children had a history of very low birth weight (<1,500 g). At the time of testing, none of the children had experienced a respiratory tract infection in the preceding 2 wk. One child used oral montelukast and one child used inhaled budesonid at the time of testing, and the other children were without regular medication. Short-acting β_2 -agonists were withheld for at least 12 h preceding the test. The study was approved by the institutional pediatric ethics committee of Helsinki University Central Hospital.

The design of the study included simultaneous recordings of tidal breathing (TB) by using a PNT and IP lasting at least 60 s in a sitting position. The recordings were repeated at baseline before and after the

Address for reprint requests and other correspondence: V.-P. Seppä, Biokatu 6/Finmedi 1 4-206, 33520 Tampere, Finland (e-mail: ville-pekk.a.seppa@tut.fi).

Table 1. Characteristics of the study children

Study children, <i>n</i>	21
Boys, <i>n</i> (%)	16 (76)
Gestational age, median (range), wk	40 (27–42)
Birthweight, median (range), g	3,500 (980–4,770)
Age, median (range), years	6.0 (3.6–7.9)
Height, median (range), cm	118 (99–125)
Weight, median (range), kg	21.5 (15.5–31.8)
Skin prick test positive, <i>n</i> (%)	12 (57)
Allergic rhinitis, <i>n</i> (%)	3 (14)
Atopic eczema, <i>n</i> (%)	12 (57)
Wheeze, <i>n</i> (%)	21 (100)
Parental smoking, <i>n</i> (%)	7 (33)
Parental asthma, <i>n</i> (%)	11 (52)
Baseline <i>Rrs</i> 5, median (range), kPa ⁻¹ ·s ⁻¹	0.77 (0.54–1.84)
Baseline <i>Xrs</i> 5, median (range), kPa ⁻¹ ·s ⁻¹	–0.20 (–0.10–0.50)
Baseline <i>Rrs</i> 5, median (range), z-score	–0.46 (–2.47–5.48)
Baseline <i>Xrs</i> 5, median (range), z-score	0.68 (–4.27–2.41)

*Rrs*5, respiratory resistance at 5 Hz; *Xrs*5, respiratory reactance at 5 Hz.

lung function measurements with oscillometry, during MIB, and 10 min after inhalation of a bronchodilator (BRD).

Lung function measurements. For tidal flow recordings, the flow was measured at the airway opening via a mouthpiece by using a calibrated, heated, Lilly-type PNT (Masterscreen PFT; Jaeger, Germany) with a dead space of 90 ml. A nose clip was used, and the child was in a sitting position. After body temperature pressure saturated correction, data were digitized with a sampling frequency of 100 Hz and later oversampled to 256 Hz to match the IP recording. Real-time visualization of the PNT signal was used to ensure stable and regular respiratory breathing pattern before the start of recording (2).

The methodology of lung function measurements by using the oscillometric technique has been previously described in detail (16). The output pressure and flow signals were analyzed for their amplitude and phase difference to determine the resistance (*Rrs*) and reactance (*Xrs*) of the respiratory system, both components of the respiratory impedance (*Zrs*). During the measurement, the child was in a sitting position, breathing quietly through a mouthpiece. A nose clip was used and the cheeks were supported by the hands of the investigator. Measurements were repeated to obtain three acceptable data sets at baseline, and two acceptable data sets at each challenge phase, which were used to calculate the mean values for the oscillometric parameters at each time point. The parameters of interest in this study were respiratory resistance and respiratory reactance at 5 Hz (*Rrs*5 and *Xrs*5, respectively), and the total respiratory impedance at 5 Hz (*Zrs*5).

A dosimetric bronchial provocation test adjusted for preschool children was applied (14). After baseline measurements of *Rrs*5, increasing doses of methacholine chloride were administered by using an inhalation-synchronized dosimeter (Spira Electro 2; Spira Respiratory Care Centre, Hämeenlinna, Finland) connected to a calibrated nebulizer (Salter Labs 8900; Arvin, CA), and after every dose, *Rrs*5 was remeasured. The procedure included five dose steps (15, 60, 210, 660, and 2,010 µg), and was continued until a 40% increase in *Rrs*5 was observed or the maximum dose of methacholine was administered. After the final measurement of *Rrs*5, TB measurements were recorded. The provocative dose of methacholine causing a 40% fall in *Rrs*5 (*PD*₄₀ *Rrs*5) was determined from the dose-response curves. Following the challenge test, the children received inhaled salbutamol (0.3 mg, 0.1 mg/dose; Ventoline Evohaler; GlaxoSmithKline, Middlesex, UK) via Babyhaler (GlaxoSmithKline, Brentford, UK), and the measurement of *Rrs*5 was repeated 15 min after salbutamol inhalation.

Impedance pneumography. In IP, the electrical impedance of the thorax is measured by feeding a small, high-frequency current, *I*, through one electrode pair and measuring the resulting voltage signal, *U*, by another electrode pair. The electrical impedance, *Z* = *U*/*I*,

increases as air enters the lungs during inspiration and decreases with expiration. The resulting volume-oriented signal can be differentiated to obtain a flow rate signal (28). IP does not enable measuring absolute values of flow rate as milliliters per second (ml/s) because the intersubject and interposture variation in the ratio of impedance change, ΔZ , to volume change, ΔV , is rather large (28). However, using correct electrode placement, the $\Delta Z/\Delta V$ ratio is highly linear, which is the satisfactory property for almost all types of tidal air flow analysis. Here the current feeding electrodes were placed on both sides of the thorax on the midaxillary line at the height of the fifth intercostal space and the voltage measurement electrodes on the arms opposing the other electrode pair. This configuration has been shown to establish a highly linear $\Delta Z/\Delta V$ ratio in healthy adults (24). The distortive impedance oscillations resulting from cardiac activity were removed by a filtering technique developed for this purpose (26). IP and electrocardiogram (ECG) signals were recorded and stored at a 256-Hz sampling rate by a small device of our own construct, similar to the one presented by Vuorela et al. (31) using normal Ag-AgCl ECG electrodes (Blue Sensor P; Ambu, Ballerup, Denmark). Because the conventional four-electrode IP is susceptible to motion artifact, the recorded signals were visually inspected for motion distortions and those segments were discarded.

Tidal breathing indices used for assessment of airflow obstruction. Tidal respiratory flow was quantified by parameters T_{PTEF}/T_E , V_{PTEF}/V_E , and the parameter *S* introduced by Williams et al. (32), as defined in the European Respiratory Society and American Thoracic Society statement (2) and illustrated in Fig. 1. From each 1-min recording, the parameters were determined by manually extracting a segment of regular breathing containing at least four consecutive breaths. If no such segment could be found, the recording was excluded from the

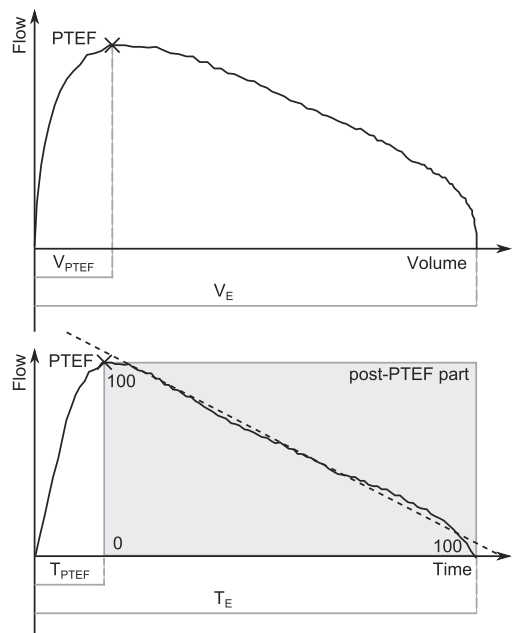


Fig. 1. Illustration of the three tidal breathing parameters T_{PTEF}/T_E , V_{PTEF}/V_E , and *S*. PTEF denotes peak tidal expiratory flow. T_{PTEF}/T_E is defined as the ratio of time to reach PTEF to total duration of expiration. V_{PTEF}/V_E is defined as the ratio of volume expired at time of PTEF to total expired volume. *S* is defined in the post-PTEF part of the flow-time curve (light gray background) by normalizing the flow and time range to 0 . . . 100 and fitting a line as $flow(t) = St + b$, where *t* is time.

analysis. The TB parameters were derived from each breath and averaged for each recording with trimmed mean that rejected the highest and lowest 5% of values. Putatively, T_{PTEF}/T_E , V_{PTEF}/V_E , and the parameter S should decrease as a result of bronchial obstruction (MIB phase), and increase after bronchodilation (BRD phase).

Statistical analysis. The agreement between IP flow signal, \dot{V}_{IP} , and PNT flow signal, \dot{V}_{PNT} , for each measurement was analyzed in two ways. First by forming the sample-by-sample absolute difference signal as $d(n) = |\dot{V}_{PNT}(n) - \dot{V}_{IP}(n)|$, $n = 1 \dots m$, where n is sample number and m is signal length, and presenting the median of d for each measurement as D_{SS} . This gives a measure of the average difference between the two signals, but does not contain information on whether the difference is distributed randomly in time or does it relate to the phase of respiration. Considering the analysis of the shapes of the expiratory flow curves for instance, a measurement error distributed randomly can be less deceiving and easier to remove than one that is consistently occurring in the same phase. This motivates the second analysis that reveals the distribution of the differences by plotting the value pairs $\dot{V}_{IP}(n)$ and $\dot{V}_{PNT}(n)$ for each sample, fitting a line to the distribution, and assessing the distance from the line for each sample, as illustrated in Fig. 2A. Then the distances are divided into k bins according their respective values of $\dot{V}_{PNT}(n)$ and the deviation from linearity of each bin m is represented by the median of the distances in it as $D_{bin,m}$ (Fig. 2A). The average deviation from linearity, D_L , is then defined as the mean of all $D_{bin,m}$. For each measurement the \dot{V}_{IP} and \dot{V}_{PNT} signals were normalized such that 100% flow means the median tidal peak inspiratory flow (TPIF) encountered during that measurement. Bins containing less than 2% of the samples of a measurement were discarded from the analysis.

The repeatability of TB indices was determined by using the paired recordings at the baseline. Within-subject standard deviation, SD_{ws} , was calculated for each patient for each of the baseline variables as $SD_{ws} = |X_{BL1} - X_{BL2}|/\sqrt{2}$ where X is the measured value obtained during first and second baseline measurement, BL1 and BL2, respectively. MIB and BRD induced changes in $Rrs5$, $Xrs5$, and $Zrs5$ were assessed and compared with those of the indices of TB flow, assessed either by PNT or IP recordings. Changes in assumed direction that exceeded 1.65 times SD_{ws} during MIB or BRD, were considered significant.

A two-tailed paired t -test was used to compare the oscillometric parameters between the test phases and the TB parameters between test phases. Where a t -test was used, the variables were first tested to have normal distribution using the Kolmogorov-Smirnov test. A

paired Wilcoxon signed rank test was used for comparing changes in D_{SS} and D_L between the test phases and for comparing SD_{ws} between IP and PNT for each TB parameter. Pearson linear correlation was calculated between oscillometric and TB parameters for changes induced by MIB and BRD. Intraclass correlation coefficient, ICC, was used for assessing the TB parameter agreement between IP and PNT. To relate the difference between IP and PNT to the range of the encountered TB parameter values, the difference was also assessed as intersubject z-scores [i.e., by normalizing (dividing) the difference with intersubject standard deviation of the PNT TB parameter].

Statistical analyses were performed using Matlab (version R2012b) and SPSS (version 21) software. Criteria for statistical significance was $P < 0.05$.

RESULTS

Lung function of study subjects. The baseline lung function assessed by impulse oscillometry was abnormal ($Rrs5$ z-score ≥ 2 SD or $Xrs5$ z-score ≤ -2 SD) in one child with a history of very low birth weight, and within normal limits in others (16) (Table 1). All except two children responded to methacholine by an increase of $Rrs5$ at least 40% having a median PD_{40} of 129 (20–920) μg . Recordings of TB were successful in all the subjects at each time point.

Agreement between measurement methods. To evaluate whether the agreement between IP and PNT signals varies with different states of respiratory function, assessments were made separately at the baseline, MIB, and BRD phases. The sample-by-sample differences, D_{SS} , for baselines 1 and 2 (BL1 and BL2), MIB, and BRD phases were (mean \pm SD) $5.7 \pm 1.2\%$, $6.7 \pm 1.9\%$, $6.9 \pm 1.4\%$, and $7.5 \pm 2.0\%$ of TPIF, respectively. When comparing D_{SS} between the phases of the study a statistically significant change in D_{SS} was obtained between the mean of BL1 and BL2 vs. BRD ($P = 0.003$), but not vs. MIB ($P = 0.277$). D_{SS} did not correlate with the degree of airway obstruction, assessed by z scores of any of the oscillometric measures ($P > 0.35$ for all).

The average deviation from linearity, D_L , for BL1, BL2, MIB, and BRD phases was (mean \pm SD) $2.4 \pm 1.0\%$, $3.0 \pm 1.3\%$, $2.6 \pm 0.9\%$, and $3.1 \pm 1.4\%$ of TPIF, respectively. When comparing D_L between all phases of the study a statis-

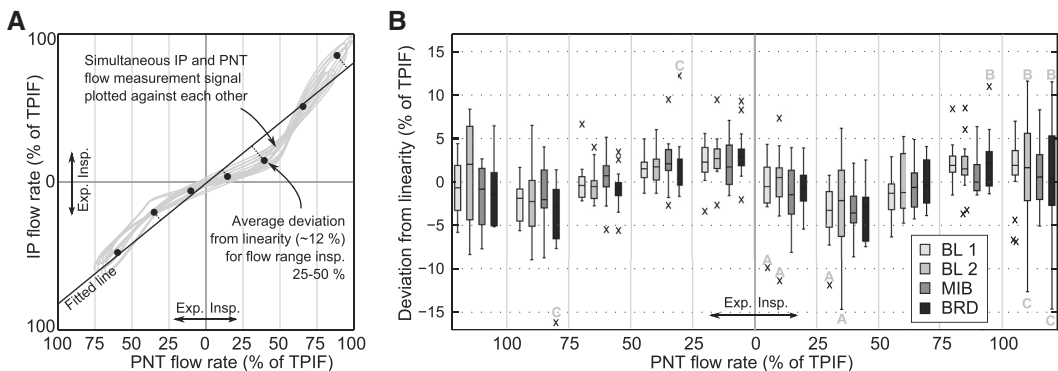


Fig. 2. A: method for estimation of linearity between pneumotachograph (PNT) and impedance pneumograph (IP) flow rate signals. For each measurement sample the distance (deviation) from a fitted line is calculated and the median value (black dots) of the deviations is provided in each 25% flow range. Each measured flow signal was normalized to 100%, representing median tidal peak inspiratory flow (TPIF). B: linearity between PNT and IP in simultaneous flow rate measurement. Each column contains results from 18–21 patients. The boxes denote the 25th–75th percentiles, the middle lines denote the median, and the whiskers extend to extreme values excluding outliers (crosses). Letters A–C next to extreme results denote results of specific patients.

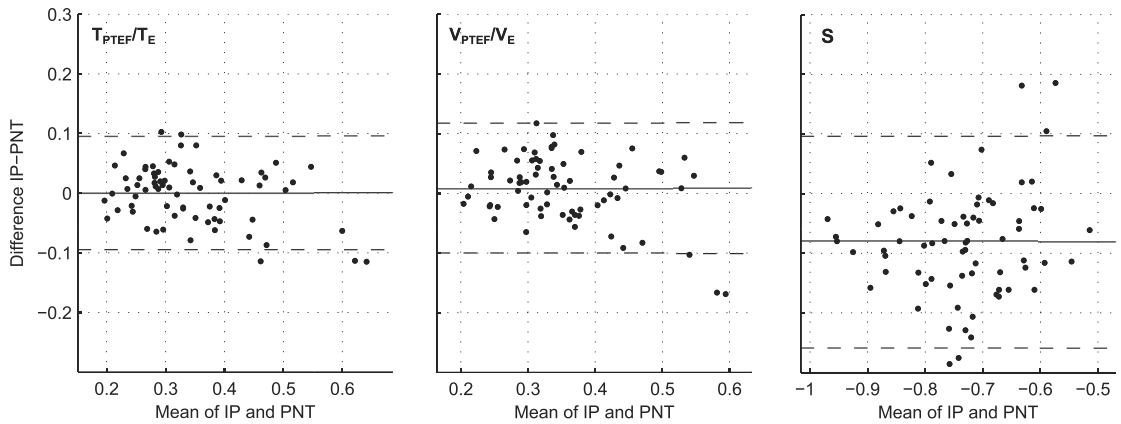


Fig. 3. Bland-Altman comparison plot of three tidal breathing parameters (T_{PTEF}/T_E , V_{PTEF}/V_E , and S) obtained simultaneously with impedance pneumograph (IP) and pneumotachograph (PNT). The solid line denotes the mean; the dashed line denotes the 95% confidence intervals of the difference between IP and PNT results.

tically significant difference was obtained only for MIB vs. BRD ($P = 0.018$), but not for the mean of BL1 and BL2 vs. MIB or BRD ($P = 0.330$ and $P = 0.210$, respectively). D_L did not correlate with the degree of airway obstruction, assessed by z scores of any of the oscillometric measures ($P > 0.6$ for all).

The distribution of the difference between PNT and IP flow signals was slightly dependent on the respiratory phase, illustrated in Fig. 2B. On average, the IP measurement showed a few percentage higher readings than PNT during the 25–50% inspiratory flow range. During expiration the IP readings were higher than PNT at low flows and lower than PNT at high flow rates. However, this behavior was not consistent for all patients. All the deviations from the linearity were rather modest, with the highest single deviation from linearity being –15% of TPIF. The most extreme results in Fig. 2B came from three individual patients denoted by letters A, B, and C. Patient A was the child with a history of very low birth weight, BPD and RDS, and highly abnormal lung function at baseline.

In TB parameters the differences between PNT and IP results were -0.002 ($-0.097 \dots 0.093$), 0.007 ($-0.102 \dots 0.116$), and -0.083 ($-0.260 \dots 0.094$), respectively for T_{PTEF}/T_E , V_{PTEF}/V_E , and S presented as mean and 95% confidence interval. The mean differences between PNT and IP as

intersubject z-scores were 0.017, 0.066, and 0.82 for T_{PTEF}/T_E , V_{PTEF}/V_E , and S , respectively, showing that the relative difference between PNT and IP was small in T_{PTEF}/T_E and V_{PTEF}/V_E but rather large in S . The ICC between PNT and IP were 0.94, 0.91, and 0.68 ($P < 0.0001$ for all), respectively for T_{PTEF}/T_E , V_{PTEF}/V_E , and S . For all parameters the difference was mostly homogeneously distributed as can be observed in the Bland-Altman plot (Fig. 3).

Tidal breathing parameter changes induced by MIB and BRD. The 1-min recordings contained 4–26 (median 11.0) acceptable respiratory cycles that were averaged to yield the TB parameter values. The repeatability of TB parameters between baseline measurements 1 and 2 was satisfactory, SD_{ws} (mean \pm SD) being 0.047 ± 0.049 , 0.048 ± 0.049 , and 0.051 ± 0.050 for T_{PTEF}/T_E , V_{PTEF}/V_E , and S , respectively, for PNT and similarly for IP 0.045 ± 0.034 , 0.053 ± 0.041 , and 0.062 ± 0.041 . There was no significant difference between IP and PNT measurements in repeatability as assessed by SD_{ws} ($P > 0.10$ for all). The absolute values for the TB parameters are presented in Table 2. For T_{PTEF}/T_E , the V_{PTEF}/V_E parameter value in most patients decreased from baseline to MIB as expected, and increased from MIB to BRD, but there were also individuals for whom this pattern was reversed. In subjects

Table 2. Values of tidal breathing parameters and oscillometric parameters

	BL1 (n = 19)		BL2 (n = 18)		MIB (n = 17)		BRD (n = 16)	
	PNT	IP	PNT	IP	PNT	IP	PNT	IP
Tidal breathing								
T_{PTEF}/T_E	0.36 ± 0.11	0.36 ± 0.10	0.36 ± 0.12	0.37 ± 0.10	$0.31 \pm 0.11^*$	$0.31 \pm 0.11^*$	0.35 ± 0.11	0.33 ± 0.08
V_{PTEF}/V_E	0.36 ± 0.11	0.36 ± 0.09	0.37 ± 0.11	0.38 ± 0.08	$0.31 \pm 0.10^*$	$0.32 \pm 0.09^*$	0.36 ± 0.10	0.36 ± 0.07
S	-0.69 ± 0.11	-0.77 ± 0.13	-0.72 ± 0.10	-0.80 ± 0.12	-0.65 ± 0.08	-0.73 ± 0.10	-0.71 ± 0.12	-0.81 ± 0.11
Oscillometry (n = 21 in all phases)								
$Rrs5$		0.82 ± 0.26				$1.26 \pm 0.31\ddagger$		$0.71 \pm 0.27\ddagger$
$Xrs5$		-0.22 ± 0.08				$-0.43 \pm 0.16\ddagger$		$-0.18 \pm 0.07\ddagger$
$Zrs5$		0.85 ± 0.27				$1.34 \pm 0.33\ddagger$		$0.73 \pm 0.27\ddagger$

Values are means \pm SD. BL1, baseline 1; BL2, baseline 2; MIB, methacholine-induced bronchoconstriction; BRD, bronchodilation; PNT, pneumotachograph; IP, impedance pneumography; $Rrs5$, respiratory resistance at 5 Hz; $Xrs5$, respiratory reactance at 5 Hz; $Zrs5$, total respiratory impedance at 5 Hz. * $P < 0.05$; † $P < 0.002$; ‡ $P < 0.00001$ between mean of BL 1 and BL2 values and the corresponding value.

with significant MIB assessed by impulse oscillometry, the change in T_{PTEF}/T_E , V_{PTEF}/V_E , and S was considered significant (exceeded 1.65 times $SD_{w(s)}$) in 6, 6, and 5 patients for PNT; and in 6, 6, and 5 patients for IP, respectively.

Table 3 shows the association between MIB- and BRD-induced changes in TB parameters and changes in lung function assessed by impulse oscillometry. The changes in all three TB parameters correlated significantly with the corresponding changes in respiratory resistance and impedance, but only T_{PTEF}/T_E and V_{PTEF}/V_E correlated with reactance. The association with lung function was evident both in PNT and IP recordings.

DISCUSSION

The two compared modes of measurement for tidal flow are based on completely different principles. PNT essentially measures air pressure variations in a tube outside the airway opening, whereas IP measures changes in the electrical conductivity of the thorax. However, the IP with novel filtering technique showed excellent agreement with PNT in the assessment of tidal flow signal in most of the young children we tested. This high agreement was modestly affected by induced bronchoconstriction. The estimated TB parameters and their association with changes in lung function were similar between IP and PNT, thereby showing that IP may be considered as a potential method for recording tidal airflow profiles in young children with wheezing disorders.

Most of our children were too young to perform conventional lung function tests such as spirometry. Therefore, in this experimental design we chose to measure lung function changes by using impulse oscillometry, which enables assessment of mechanical input impedance even in children as young as 2–3 years of age (16). The study group represented young children in need of diagnostic evaluation, and in whom the potential clinical value of IP is highlighted. Because the primary objective was to estimate the agreement of flow signals between the methods and not to test the discriminatory properties of TB parameters measured by IP, healthy subjects were not included in this study.

For assessment of TB, direct measurement of airflow and volume at the airway opening via flow sensors such as PNT is the conventional method (1), and has been successfully applied, i.e., in a prospective cohort studies of infants (11).

Noninvasive respiration measurement methods have been of research interest because they may enable ambulatory long-term assessment of tidal breathing and do not distort the spontaneous breathing pattern as PNT does (8, 23). However, literature on the accuracy of noninvasive measurement methods in respiratory flow assessment is somewhat limited. Jackson et al. (12) found good agreement between respiratory inductance plethysmography (RIP) and PNT for T_{PTEF}/T_E in healthy infants and in infants with recurrent wheeze, but concluded that the measurement of T_{PTEF}/T_E is not possible with uncalibrated RIP in all infants, particularly at ages beyond the neonatal period and in wheezing subjects. Stick et al. (29) found corresponding agreement in healthy infants. The closest comparative study to ours is that of Manczur et al. (17), who studied RIP in wheezy young children and found agreement with PNT for T_{PTEF}/T_E that was slightly less than ours between IP and PNT. They concluded that the mean T_{PTEF}/T_E was significantly lower using RIP, and thus results from RIP and PNT are not interchangeable. Having two belts that record chest wall movements, RIP enables an assessment of the degree of thoracoabdominal asynchrony (TAA), but it is questionable how accurately the differentiated sum signal of the belts can represent the air flow at the mouth. Indeed, Jackson et al. discussed that TAA could have been the major contributor to the error in the RIP-derived flow signal. TAA is not as likely a source of error for IP because with appropriately (high) placed electrodes, IP signal reflects lung aeration instead of chest wall movement or the movement of the diaphragm or the liver (13, 15, 19, 24). Two studies have also evaluated the agreement between electromagnetic inductance plethysmography and PNT in infants (33, 19). No previous study has assessed the effect of induced bronchoconstriction on the measurement accuracy or presented flow signal linearity between any noninvasive and direct method in any disease or age group.

Agreement between measurement methods. In general, the agreement in flow signal measurement between PNT and IP was excellent both in terms of sample-by-sample absolute signal difference, D_{SS} , and PNT-IP flow signal linearity, D_L (Fig. 2). Although D_{SS} is small it should not be neglected because it may have some implications for the use of IP. If the measured flow signal is noisy (high D_{SS}), more breaths need to be averaged to account for the error caused by the noise.

There was a minor increase in D_{SS} from baseline to MIB and BRD states. Notably, the signal difference between IP and PNT was not related to changes in mechanical impedance measured by the oscillometric technique, suggesting that other mechanisms than changes in airway diameter per se are more important in determining IP accuracy. Increased ventilation heterogeneity induced by methacholine (5) and changes in ventilation/perfusion distribution after inhalation of salbutamol (20) may potentially affect IP measurement. The recorded IP signal is dependent on the volume changes of the lung tissue (19) occurring within the measurement sensitivity region, which is determined by the electrode locations (10). However, such effects were not noticeable in the linearity curve (Fig. 2B). Three individuals showed larger disagreement in linearity between IP and PNT signals. One of them had a history of very low birth weight and bronchopulmonary dysplasia, and highly abnormal lung function with increased ventilation heterogeneity and asynchronous breathing pattern may explain the nonlinear behav-

Table 3. Correlation between change in tidal breathing parameters and change in oscillometric parameters due to methacholine and bronchodilation

	Rrs5	Xrs5	Zrs5
T_{PTEF}/T_E			
PNT	-0.41*	-0.49†	-0.44‡
IP	-0.45†	-0.42†	-0.46†
V_{PTEF}/V_E			
PNT	-0.53‡	-0.58‡	-0.55‡
IP	-0.53‡	-0.45†	-0.54‡
S			
PNT	0.37*	-0.28	0.36*
IP	0.40*	-0.32	0.39*

Rrs5, respiratory resistance at 5 Hz; Xrs5, respiratory reactance at 5 Hz; Zrs5, total respiratory impedance at 5 Hz; PNT, pneumotachograph; IP, impedance pneumography. * $P < 0.05$; † $P < 0.02$; ‡ $P < 0.005$.

ior of IP signal. In two subjects, no obvious reasons for higher differences between IP and PNT were found.

The agreement for T_{PTEF}/T_E , the most commonly used TB parameter, was found to be high between PNT and IP and approximately the same as in studies on healthy adults (25) and adults with varying degree of airway obstruction (27). The agreement for S was lower than those of T_{PTEF}/T_E and V_{PTEF}/V_E . A potential reason for this is the small residual cardiac distortion left after filtering the IP signal, which may cause large variation in S as each breath is normalized to the highest encountered value.

Tidal breathing parameters. Despite careful controlling of the start of the recording during steady breathing, some of the samples contained episodes of irregular breathing. Understandably, completely relaxed and unattended breathing is difficult to achieve in laboratory conditions in awake young children. However, these problems did not compromise the agreement between IP and PNT signals, or the association of TB parameters with changes in lung function.

We found slightly higher T_{PTEF}/T_E and V_{PTEF}/V_E values than Van der Ent et al. (29a) and Cutrera et al. (3), respectively, in a similar study design with children during bronchial challenge. Characteristics of the computer algorithms that derive the parameters may explain the differences with earlier results. The technical and computational aspects of TB recording, for instance—techniques for segmenting the signal into individual exhales—has been discussed by Bates et al. (1). Van der Ent found a controversial response in T_{PTEF}/T_E in 5 of 26 patients, which is similar to our findings. Due to complex physiological functions that regulate breathing, measures of TB are influenced by both respiratory mechanics and control of breathing, which may vary individually and temporarily. Although we found significant correlations between lung function assessed by impulse oscillometry and TB parameters, only some of the children showed significant changes (exceeding 1.65 times SD_{ws}) in TB parameters during MIB, suggesting that the sensitivity of TB parameters to reflect induced bronchoconstriction is less than that of the oscillometric indices.

Unlike other TB parameters, parameter S did not change significantly between the phases of the study. However, the association with changes in respiratory resistance and reactance was confirmed in the correlation analyses. In the initial study by Williams et al. (32) of parameter S on 66 adults, patients were classified into three distinct groups on the basis of visual examination of the expiratory flow curve shape and one of the groups (25% of patients) was left out from the analysis. No such selection was performed in this study, and this likely weakens the statistical significance of our findings.

Error sources in measurement devices. The small differences between the PNT and IP flow signals have many potential contributors. The PNT system is reported ambiguously by the manufacturer to have an accuracy of $\pm 5\%$. As with any instrument, it will have limited linearity. Moreover, the cardiac contraction causes a small volume displacement in the left lung, which is reflected in the PNT flow signal and not known to be accounted for in the PNT system in any way. For IP measurement, the cardiogenic oscillatory distortion is a well recognized phenomenon that is effectively attenuated by a specialized filtering algorithm (26), but in these short, somewhat irregular segments of tidal breathing the time-adaptive algorithm might not always perform optimally. Furthermore,

although care was taken in time-synchronization of IP and PNT signals, it is possible that a small time difference between the signals may contribute to the slight nonlinearity trend observed in Fig. 2B.

Potential clinical implications. The major advantage in measuring tidal flow by IP includes minor requirements for cooperation, making the recordings suitable for even young children, undisturbed without PNT. IP also enables measurement of tidal flow in an ambulatory setting (i.e., overnight), offering an interesting tool for studying changes in long-term variations in respiratory mechanics in various research designs. Longer recordings would also increase the statistical power in assessing the TB characteristics, compared with what has been previously possible in laboratory settings, such as in the current study. Further studies are needed to evaluate the clinical usefulness of such applications of IP (e.g., in the management of young children with wheezing disorders).

Conclusions. IP and PNT have high agreement in measured respiratory flow signal and derived TB parameters despite induced airway obstruction and irregular breathing in awake young children. MIB induces significant and concurrent changes in TB parameters in most but not all patients, and this can be observed in IP and PNT equally. The results indicate that IP can be considered as a valid method for recording tidal airflow profiles in young children with wheezing disorders.

GRANTS

Support for this study was provided by the Tampere Tuberculosis Foundation, the Finnish Funding Agency of Technology and Innovation (Tekes), and the Sigrid Juselius Foundation.

DISCLOSURES

No conflicts of interest, financial or otherwise, are declared by the author(s).

AUTHOR CONTRIBUTIONS

Author contributions: V.-P.S., A.S.P., A.K.-S., M.J.M., J.V., and L.P.M. conception and design of research; V.-P.S. and L.P.M. analyzed data; V.-P.S. prepared figures; V.-P.S. and L.P.M. drafted manuscript; V.-P.S., A.S.P., A.K.-S., M.J.M., J.V., and L.P.M. edited and revised manuscript; M.J.M., J.V., and L.P.M. interpreted results of experiments; L.P.M. approved final version of manuscript.

REFERENCES

- Bates J, Schmalisch G, Filbrun D, Stocks J. Tidal breath analysis for infant pulmonary function testing. ERS/ATS Task Force on Standards for Infant Respiratory Function Testing. European Respiratory Society/American Thoracic Society. *Eur Respir J* 16: 1180–1192, 2000.
- Beydon N, Davis SD, Lombardi E, Allen JL, Arets HG, Aurora P, Bisgaard H, Davis GM, Ducharme FM, Eigen H, Gappa M, Gaultier C, Gustafsson PM, Hall GL, Hantos Z, Healy MJ, Jones MH, Klug B, Lødrup Carlsen KC, McKenzie SA, Marchal F, Mayer OH, Merkus PJ, Morris MG, Oostveen E, Pillow JJ, Seddon PC, Silverman M, Sly PD, Stocks J, Tepper RS, Vilozni D, Wilson NM, on behalf of the American Thoracic Society/European Respiratory Society Working Group on Infant, and Young Children Pulmonary Function Testing. An official American Thoracic Society/European Respiratory Society statement: pulmonary function testing in preschool children. *Am J Respir Crit Care Med* 175: 1304–1345, 2007.
- Cutrera R, Filtchev SI, Merolla R, Willim G, Haluszka J, Ronchetti R. Analysis of expiratory pattern for monitoring bronchial obstruction in school-age children. *Pediatr Pulmonol* 10: 6–10, 1991.
- Davies H, Helms P, Gordon I. Effect of posture on regional ventilation in children. *Pediatr Pulmonol* 12: 227–232, 1992.
- Downie SR, Salome CM, Verbanck S, Thompson BR, Berend N, King GG. Effect of methacholine on peripheral lung mechanics and ventilation heterogeneity in asthma. *J Appl Physiol* 114: 770–777, 2013.

7. **Fiamma MN, Straus C, Thibault S, Wysocki M, Baconnier P, Similowski T.** Effects of hypercapnia and hypocapnia on ventilatory variability and the chaotic dynamics of ventilatory flow in humans. *Am J Physiol Regul Integr Comp Physiol* 292: R1985–R1993, 2007.
8. **Fleming PJ, Levine MR, Goncalves A.** Changes in respiratory pattern resulting from the use of a facemask to record respiration in newborn infants. *Pediatr Res* 16, 1031–1034: 1982.
9. **Frey U, Silverman M, Suki B.** Analysis of the harmonic content of the tidal flow waveforms in infants. *J Appl Physiol* 91: 1687–1693, 2001.
10. **Geselowitz DB.** An application of electrocardiographic lead theory to impedance plethysmography. *IEEE Trans Biomed Eng* 18: 38–41, 1971.
11. **Håland G, Lødrup-Carlson KC, Sandvik L, Devulapalli CS, Munthe-Kaas MC, Pettersen M, Carlén KH.** Reduced lung function at birth and the risk of asthma at 10 years of age. *N Engl J Med* 355: 1682–1689, 2006.
12. **Jackson E, Stocks J, Pilgrim L, Dundas I, Dezateux C.** A critical assessment of uncalibrated respiratory inductance plethysmography (RespiTrace®) for the measurement of tidal breathing parameters in newborns and infants. *Pediatr Pulmonol* 20: 119–124, 1995.
13. **Kawakami K, Watanabe A, Ikeda K, Kanno R, Kira S.** An analysis of the relationship between transthoracic impedance variations and thoracic diameter changes. *Med Biol Eng* 12: 446–453, 1974.
14. **Kotaniemi-Syrjänen A, Malmberg LP, Pelkonen AS, Malmström K, Mäkelä MJ.** Airway responsiveness: associated features in infants with recurrent respiratory symptoms. *Eur Respir J* 30: 1150–1157, 2007.
15. **Logic JL, Maksud MG, Hamilton LH.** Factors affecting transthoracic impedance signals used to measure breathing. *J Appl Physiol* 22: 251–254, 1967.
16. **Malmberg LP, Pelkonen A, Poussa T, Pohjanpalo A, Hahtela T, Turpeinen M.** Determinants of respiratory system input impedance and bronchodilator response in healthy Finnish preschool children. *Clin Physiol Funct Imaging* 22: 64–71, 2002.
17. **Manczur T, Greenough A, Hooper R, Allen K, Latham S, Price JF, Rafferty GF.** Tidal breathing parameters in young children: comparison of measurement by respiratory inductance plethysmography to a facemask pneumotachograph system. *Pediatr Pulmonol* 28: 436–441, 1999.
18. **Morris M, Madgwick R, Collyer I, Denby F, Lane D.** Analysis of expiratory tidal flow patterns as a diagnostic tool in airflow obstruction. *Eur Respir J* 12: 1113–1117, 1998.
19. **Nopp P, Harris N, Zhao TX, Brown B.** Model for the dielectric properties of human lung tissue against frequency and air content. *Med Biol Eng Comput* 35: 695–702, 1997.
20. **Orphanidou D, Hughes JM, Myers MJ, Al-Suhali AR, Henderson B.** Tomography of regional ventilation and perfusion using krypton 81m in normal subjects and asthmatic patients. *Thorax* 41: 542–551, 1986.
21. **Rodriguez-Roisin R, Ferrer A, Navajas D, Agustí AG, Wagner PD, Roca J.** Ventilation-perfusion mismatch after methacholine challenge in patients with mild bronchial asthma. *Am Rev Respir Dis* 144: 88–94, 1991.
22. **Samara Z, Raux M, Fiamma MN, Gharbi A, Gottfried SB, Poon CS, Similowski T, Straus C.** Effects of inspiratory loading on the chaotic dynamics of ventilatory flow in humans. *Respir Physiol Neurobiol* 165: 82–89, 2009.
23. **Schmalisch G, Foitzik B, Wauer RR, Stocks J.** Effect of apparatus dead space on breathing parameters in newborns: “flow-through” versus conventional techniques. *Eur Respir J* 17: 108–114, 2001.
24. **Seppä VP, Hyttinen J, Uitto M, Chrapek W, Viik J.** Novel electrode configuration for highly linear impedance pneumography. *Biomed Tech (Berl)* 58: 35–38, 2013.
25. **Seppä VP, Hyttinen J, Viik J.** Agreement between impedance pneumography and pneumotachograph in estimation of a tidal breathing parameter. *Chest* 138: 816A, 2010.
26. **Seppä VP, Hyttinen J, Viik J.** A method for suppressing cardiogenic oscillations in impedance pneumography. *Physiol Meas* 32: 337–345, 2011.
27. **Seppä VP, Kööbi T, Kähönen M, Hyttinen J, Viik J.** Impedance pneumography for assessment of a tidal breathing parameter in patients with airway obstruction. *Eur Respir J* 38: 219S, 2011.
28. **Seppä VP, Viik J, Hyttinen J.** Assessment of pulmonary flow using impedance pneumography. *IEEE Trans Biomed Eng* 57: 2277–2285, 2010.
29. **Stick SM, Ellis E, Lesouëf PN, Sly PD.** Validation of respiratory inductance plethysmography (“RespiTrace”) for the measurement of tidal breathing parameters in newborns. *Pediatr Pulmonol* 14: 187–191, 1992.
- 29a. **Van der Ent C, Brackel H, Mulder P, Bogaard J.** Improvement of tidal breathing pattern analysis in children with asthma by on-line automatic data processing. *Eur Respir J* 9: 1306–1313, 1996.
30. **Veiga J, Lopes AJ, Jansen JM, Melo PL.** Airflow pattern complexity and airway obstruction in asthma. *J Appl Physiol* 111: 412–419, 2011.
31. **Vuorela T, Seppä VP, Vanhala J, Hyttinen J.** Design and implementation of a portable long-term physiological signal recorder. *IEEE Trans Inf Technol Biomed* 14: 718–725, 2010.
32. **Williams E, Madgwick R, Morris M.** Tidal expired airflow patterns in adults with airway obstruction. *Eur Respir J* 12: 1118–1123, 1998.
33. **Williams EM, Pickerd N, Eriksen M, Øygarden K, Kotecha S.** Estimation of tidal ventilation in preterm and term newborn infants using electromagnetic inductance plethysmography. *Physiol Meas* 32: 1833–1845, 2011.
34. **Wysocki M, Fiamma MN, Straus C, Poon CS, Similowski T.** Chaotic dynamics of resting ventilatory flow in humans assessed through noise titration. *Respir Physiol Neurobiol* 153: 54–65, 2006.

Tampereen teknillinen yliopisto
PL 527
33101 Tampere

Tampere University of Technology
P.O.B. 527
FI-33101 Tampere, Finland

ISBN 978-952-15-3388-4
ISSN 1459-2045